Molecular and Biochemical Studies of the Hair Bundle

by

Hongyu Zhao

A dissertation in partial fulfillment of the requirements for the degree of

Doctor of Philosophy

Presented to the Neuroscience Graduate Program

Oregon Health & Science University

School of Medicine

March 2012

School of Medicine
Oregon Health & Science University

CERTIFICATE OF APPROVAL

This is to certify that the Ph.D. dissertation of
HONGYU ZHAO
has been approved on March 9th, 2012

Advisor, Peter Gillespie, PhD

Member and Chair, John Adelman, PhD

Member, Caroline Enns, PhD

Member, John Brigande, PhD

Member, Gary Westbrook, MD

Table of Contents

List of Figures

List of Abbreviations

AAV	Adeno-associated virus
ACCN1	Amiloride-sensitive cation channel neuronal 1
AcGFP	Aequorea coerulescens green fluorescent protein
ATP2B2	Plasma membrane calcium-transporting ATPase 2
CDH2	Cadherin 2, type 1, N-cadherin (neuronal)
CDH23	Cadherin-23
Cer	Ceramide
ChaK1	Channel-Kinase 1
CTB	Cholera toxin B subunit
Da	Dalton
DAG	Diacylglycerol
DEG	Degenerins
dEx20	Delta exon 20
DEX26	TRPM6_dEx20
DEX27	TRPM7_dEx20
DMSO	Dimethyl sulfoxide
dnTRPM7	Dominant negative TRPM7
DOPC	Dioleyl phosphatidylcholine
DPhPC	Diphytanoyl phosphatidylcholine
DRM	Detergent-resistant membrane
Efr3a	Protein EFR3 homolog A

EGFP	Enhanced green fluorescent protein
EGTA	Ethylene glycol tetraacetic acid
ENaC	Epithelial Na^+ channels
ERM	Ezrin-radixin-moesin
FITC	Fluorescein isothiocyanate
GFP	Green fluorescent protein
GLB1	β-galactosidase
GPI	Glycosylphosphatidylinositol
GSLs	Glycosphingolipids
GUVs	Giant unilamellar vesicles
HA	Hemagglutinin
HEXA	β-hexosaminidase alpha
HexCer	Hexosylceramide
HPBC	2-hydroxypropyl-beta-cyclodextrin
HRP	Horse radish peroxidase
IACUC	Institutional Animal Care and Use Committee
IHC	Inner hair cell
K2P	2-pore-domain K+ channel
KCNK	Potassium channel, subfamily K
L_d	Liquid disordered
L_o	Liquid ordered
LPM	Liters per minute

LTLD	Lower tip-link density
LTRPC7	Long transient receptor potential channel, member 7
MEC-2	Mechanosensory protein 2
MET	Mechanotransduction
MYO6	Myosin-VI
MYO7A	myosin-VIIA
MβC	Methyl-β-cyclodextrin
NAGA	N-acetylgalactosaminidase
NHERF2	Na^+/H^+ exchanger regulatory factor 2
nompC	No mechanoreceptor potential C
OCR-2	OSM-9 and capsaicin receptor-related, member 2
OHC	Outer hair cell
OSM-9	OSMotic avoidance abnormal family member 9
PA	Phosphatidic acid
PAO	Phenylarsine oxide
PC	Phosphatidylcholine
PCDH15	Protocadherin-15
PE	Phosphatidylethanolamine
PEI	Polyethyleneimine
PG	Phosphatidylglycerol
PI	Phosphatidylinositol
$PI(4,5)P_2$	Phosphatidylinositol 4,5-bisphosphate

PIK4CA	Type III alpha phosphatidylinositol 4-kinase
PIP_2	Phosphatidylinositol 4,5-bisphosphate
PIP5K1A	Type I alpha phosphatidylinositol-5-phosphate 4-kinase
PIP5K2B	Type II beta phosphatidylinositol-5-phosphate 4-kinase
PITPNA	Phosphatidylinositol transfer protein alpha
PLC	Phospholipase C
PMCA	Plasma-membrane Ca2+-ATPase
PMCA2	Plasma-membrane Ca2+-ATPase isoform 2
POPC	Palmitoyl-oleoyl phosphatidylcholine
pRDX	Phosphorylated radixin
PS	Phosphatidylserine
PTPRQ	Protein tyrosine phosphatase receptor type Q
RDX	Radixin
RHOA	Ras homolog gene family, member A
Rh-PE	Rhodamine-phosphatidylethanolamine
SATn	Sialyltransferase
SCNN1	Sodium channel, nonvoltage-gated 1
SLC9A3R2	solute carrier family 9, member 3 regulator 2
SM	Sphingomyelin
S_o	Solid gel
TfR	Transferrin receptor
TMC	Transmembrane channel-like protein

TMC1_ex1	Transmembrane channel-like protein, member 1, (start with) exon 1
TMC1_ex2	Transmembrane channel-like protein, member 1, (start with) exon 2
TRP	Transient receptor potential
TRPA1	Transient receptor potential cation channel, subfamily A, member 1
TRPC	Transient receptor potential canonical
TRPM	Transient receptor potential cation channel, melastatin subfamily
TRPML	Transient receptor potential cation channel, mucolipin subfamily
TRPN	Transient receptor potential cation channel, subfamily N
TRPN1	Transient receptor potential cation channel, subfamily N, member 1
TRPP	Transient receptor potential polycystic
TRP-PLIK	Transient receptor potential-phospholipase C interacting kinase
TRPV	Transient receptor potential cation channel, vanilloid
TRPA	Transient receptor potential cation channel, subfamily A
TRPY1	Transient receptor potential cation channel, yeast, member 1
TTC7A	Tetratricopeptide repeat domain 7A
USH1C	Usher syndrome 1C
UTLD	Upper tip-link density
Ypp1	Alpha-sYnuclein Protective Protein
YVC1	Yeast vacuolar conductance channel, member 1

Acknowledgments

Abstract

Inner ear hair cells are critical for our senses of hearing and balance. Mechanotransduction happens in the hair bundle, a unique sub-cellular organelle of the hair cells. This thesis characterizes some molecular components of the hair bundle, explores the localization of these molecules, and studies the interactions among them. Chapter 1 gives a background of the relevant literature on molecular components of hair bundle, mechanotransduction, and lipid domains, highlighting what information is lacking and how the experiments on this thesis will advance our understanding. Chapter 2 describes an improved method to transfect hair cells, as a useful tool to study localization and interaction of hair bundle proteins. Chapter 3 presents data on the lipid components of and functional lipid domains on the hair bundle. Chapter 4 presents data on the interaction of several hair bundle proteins related to mechanotransduction. Combined, this thesis characterizes molecular components of the hair bundle and provides new insights into their localization, interaction, and function.

Chapter 1 – Introduction

The Inner Ear

Our ability to hear and maintain body balance stems from the inner ear, which is consisted of six tiny organs inside the temporal bone. The six organs are all part of the fluid-filled membranous labyrinth. Five out of the six organs are responsible for the sense of balance: the sacculus, which senses vertical acceleration; the utriculus, which senses horizontal acceleration; and three ampullae of the semi-circular canals, which detect angular accelerations along the three axes that are perpendicular to each other (Figure 1.1). The other organ, called the cochlea, is responsible for hearing.

The bullfrog sacculus, a common organ used for hair cell research, has approximately 3000 hair cells (Figure 1.2) coupled to an overlying membrane composed of extracellular matrix. The membrane is named otolithic membrane, because there are calcium carbonate crystals, known as otoconia, on top of it (Marmo et al., 1983). Vertical acceleration of the bullfrog head causes movement of the otoconia relative to the surrounding structures, pulling the otolithic membrane with them and stimulating the hair cells underneath the otolithic membrane. The utriculus is very similar to the sacculus, except that it senses accelerations in the horizontal plane.

The cochlea is responsible for converting sound pressure impulses from the outer ear (mechanical stimulus) into electrical impulses, which are passed on to the brain via the auditory nerve. Structurally, it is a spiral tube that is divided (along its longitudinal axis) into three compartments, each filled with different fluid: the scala

media, the scala vestibuli, and scala tympani. The Reissner's membrane separates the scala vestibuli (above) from the scala media (middle), which is separated by the basilar membrane from the scala tympani (below). The scala vestibuli and scala tympani are continuous, both filled with perilymph, which has a composition similar to extracellular fluid; the scala media is filled with endolymph, which has a composition similar to intracellular fluid. During the process of hearing, sound vibrations from the air are transmitted through the middle ear ossicles to the oval window of the scala vestibule, displacing the perilymph fluid through the round window of the scala tympani. In the process, the basilar membrane is displaced, which stimulates the organ of Corti inside the scala media (Figure 1.3). The organ of Corti is comprised of four rows of hair cells that are parallel to the longitudinal axis of the cochlea tube. The mechanosensitive hair cells are tonotopically arranged along the same axis, with hair cells that sense high frequencies located at the base and those sensing low frequencies at the apex. Three out of the four rows of hair cells are outer hair cells (OHCs), which are innervated primarily by efferent nerves and are responsible for signal amplification; the other row of hair cells, called inner hair cells (IHCs), are innervated by afferent nerves and are responsible for sending the electrical signals, converted from the mechanical stimulus, to the brain (Figure 1.3). The tectorial membrane, a membrane composed of extracellular matrix, mechanically couples the three rows of outer hair cells on the apical side. Perilymph fluid movement in the scala tympani displaces the basilar membrane, which causes a shearing movement between the tectorial membrane and

organ of Corti, which in turn excites the outer hair cells and the inner hair cells. (Figure 1.3)

Hair Bundles

Hair cells are responsible for converting the mechanical stimuli to electrical signals, the universal language of the nervous system. Hair cells are so named because of their unique morphology: on the apical surface of each hair cell, there are 30 to 300 of hair-like stereocilia (Figure 1.4). The membrane-enclosed, actin-filled stereocilia are arranged in a highly organized fashion into the hair bundle, which is responsible for detecting the slightest mechanical stimulation (less than 1 nm; Gillespie and Müller, 2009). During hair cells development, a true cilium (composed of microtubules) called the kinocilium serves a role in patterning the hair bundle (Kelley et al., 1992; Montcouquiol et al., 2003). The 30 to 300 stereocilia are arranged in a descending fashion from the kinocilium, with the stereocilia nearest to the kinocilium being tallest. In mature hair cells, the kinocilium may or may not be present, thus its presence is not necessary for proper mechanosensation (Hudspeth and Jacobs, 1979).

Each stereocilium contains a paracrystal of actin filaments, sheathed by the hair cell's plasma membrane, which is contiguous with that of the hair cell plasma membrane (Gillespie and Müller, 2009). At the base of the stereocilium, there is an electron-dense structure called the rootlet, which inserts into the cuticular plate, a network of actin filaments beneath the hair cell apical surface (Hudspeth, 1989). During mechanosensation, the hair bundle moves as a unit, with neighboring stereocilia of different height sliding along each other (Karavitaki and Corey, 2010).

Mechanotransduction

Deflections of the hair bundle along the axis from the shortest to the longest stereocilia, or axis of mechanical sensitivity, leads to depolarization of the hair cell, which in turn triggers neurotransmitter (glutamate) release from the synapse on the basal side of the hair cell. Deflection of hair bundles toward the longest stereocilia (positive stimuli) leads to the opening of cation-selective transduction channels, depolarizing the hair cell and increasing glutamate release. Because 10-20% of the transduction channels are open at rest, movement of the hair bundle toward the shortest stereocilia (negative stimuli) closes the transduction channels, hyperpolarizes the hair cells, and inhibits release of glutamate.

In the current model of mechanotransduction, positive deflection of the hair bundle increases tension in a gating spring, which quickly increases the open probability of transduction channels (mechanotransduction channels, or MET channels). Following activation, mechanotransduction currents quickly adapt, a process called adaptation.

MET channels are located at the lower end of tip links (Beurg et al., 2009a), the extracellular filaments connecting the tip of each stereocilium to their adjacent taller neighbor (Figure 1.4). Tip links are composed of two strands that form a helix 150–200 nm in length; each strand is about 4 nm in diameter. Intracellular electron-dense areas, the lower tip-link density (LTLD) and upper tip-link density (UTLD), are juxtaposed to the lower and upper insertion site of tip links (Furness and Hackney, 1985) (Figure 1.5). Their positions relative to tip links and transduction channels suggest that these densities have important functions in mechanotransduction. The tip link is composed of

PCDH15 and CDH23 (Kazmierczak et al., 2007; Siemens et al., 2004); while the UTLD contains harmonin and myosin 7A, the LTLD contains myosin 15A. Both the UTLD and LTLD probably contain many other protein components that are yet to be identified.

The MET Channel

Functional studies of the inner ear and the mechanotransduction current has provided insight into the properties of the MET channel.

The MET channel responds best to stimuli along the axis from the shortest to the longest stereocilia. Stimuli perpendicular to the axis have little effect on channel gating (Shotwell et al., 1981). In the absence of a stimulus, MET channels flicker between the open and closed states, with an open probability, P_o, of ~0.1. Positive deflections (stimuli toward the longest stereocilia) increase the P_o, while negative deflections decrease the P_o (Shotwell et al., 1981).

The MET channels open very quickly. In hair cells of the bullfrog sacculus, MET channels can open within ~10 μs (Corey and Hudspeth, 1979b), with larger deflections gating channels much more rapidly (Corey and Hudspeth 1983). The fast speed of channel opening rules out enzymatic conversion or diffusion as mechanisms for gating (Corey and Hudspeth, 1979b).

The relationship between MET channel P_o and mechanical stimulus size can be well described by a three-state Boltzmann distribution (Corey and Hudspeth 1983). In the most common interpretation, this means that there are two closed states and one open state of the channel (Corey and Hudspeth 1983). Hair bundle deflection stretches the gating spring, a linearly elastic spring of stiffness ~1 mN/m, which in turn raises the

energy of the MET channels that are in closed states, thus favoring the open state, allowing an influx of cations to enter the hair cell. Notably, a direct gating mechanism like this allows for a reciprocal interaction of gating and stimulus. For example, MET channel gating independent of stimuli allows for reverse transduction, where a mechanical signal (sound) is sent out from the inner ear.

The MET channel is a non-selective cation channel with a preference for Ca^{2+} (Corey and Hudspeth, 1979a; Ohmori, 1985). Electrophysiological experiments suggest that there are two active channels per tip link (Beurg et al., 2006; Denk et al., 1995; Howard and Hudspeth, 1988; Ricci et al., 2003). In turtle, the MET channel pore is thought to be significantly bigger than that of other cation channels, with a minimal pore diameter of 12.5 Å (Farris et al., 2004). In rat, the channel conductance in IHCs is around 260 pS; it varies tonotopically in OHCs from 145 pS at the apex (low frequency end) and 320 pS at the base (high-frequency end) of the cochlea (Beurg et al., 2006). Similar tonotopic conductance differences are observed in turtle (Ricci et al., 2003), suggesting a conserved property of the cochlea. The conductance differences also suggest that the channel might consist of several distinct subunits with variations in subunit composition from the base to the apex of the cochlea.

Initial Ca^{2+} imaging studies suggested that MET channels are located near both ends of the tip-link (Denk et al., 1995). However, a more recent study using high-resolution imaging indicates that the MET channel is localized only near the lower end of the tip-link (Beurg et al., 2009b). The localization of the MET channel suggests a physical link to the lower end of the tip link, where PCDH15 exists. The possibility that

the MET channel is directly linked to lower end of the tip link suggests that it could interact with PCDH15 or proteins associated with PCDH15. However, the link does not have to be direct. The channels could be opened by the change in tension of the plasma membrane, as has been suggested in other mechanically gated systems (Cueva et al., 2007; Kung et al., 2010).

Searching for the MET Channel

Despite decades of study, the identity of the MET channel remains unknown. Major challenges to identification of the channel include: the limited number of hair cells and transduction channels per animal; the difficulty in culturing hair cell; the lack of a tissue-culture method to generate functional hair cells in large scale; and the difficulty of hair cell transfection. Moreover, time-consuming and expensive genetic studies are required for verification of channel candidates; currently, genetic studies are limited to mouse and fish models. Finally, pharmacological and conductance properties of the MET channel are not sufficiently distinct to suggest a strong candidate family (Farris et al., 2004).

Different strategies have been used to identify the MET channels. These strategies include candidate gene approaches, studying homologues of identified proteins in other systems (Ruvkun and Hobert, 1998), genetic screens, expression cloning (Caterina et al., 1999), imaging mechanotransduction with fluorescent dyes (Meyers et al., 2003), and using DNA microarrays to find transduction components (Shin et al., 2003).

Genetic screening has been proved to be useful in finding MET channels. For example, this approach was used to search for MET channels responsible for touch sensation in *C. elegans* (Hart et al., 1995), for bristle mechanosensation and hearing in *D. melanogaster* (Eberl et al., 1997; Kernan et al., 1994), for hearing and lateral line mechanosensation in zebrafish (Granato et al., 1996; Nicolson et al., 1998) and for hearing in mice (Brown et al., 2008; Friedman et al., 2007). In addition, many human deafness genes have also been studied (Petit, 2006). However, these approaches have not identified the mammalian MET channel in hair cells.

Although the low abundance of the hair cells and MET channels makes the use of protein purification and other classical biochemical approaches to purify transduction components very difficult, advancement in ultra-sensitive mass spectrometry technology has continuously lowered the amount of protein required for reliable identification of proteins in the hair bundle (Gillespie lab, unpublished result), providing another promising approach to identify the MET channel.

The above approaches have identified several classes of MET channel proteins that have been considered as possible mammalian MET channel candidates: DEG/ENaC (degenerin (also known as ACCN1)/epithelial Na+ channel (ENaC; also known as SCNN1)) subunits, transient receptor potential (TRP) proteins and two-pore-domain K+ channel (K2P; also known as KCNK) subunits.

The DEG/ENaC channels have been shown to transduce mechanical signals in C. elegans (Kellenberger and Schild, 2002), yet their role in mechanical signaling in other organisms is unclear (Chalfie, 2009). Early on, they were considered strong candidates

for the MET channel. However, when DEG/EnaC channel knockouts in mammals were screened for altered transduction, modest or no defects were seen in touch sensation, and no hearing defects in these knockouts were found (Drew et al., 2004; Drummond et al., 2000; Fricke et al., 2000; Garcia-Anoveros et al., 2001; Price et al., 2000).

Study of the no mechanoreceptor potential C (nompC) gene in *D. melanogaster* suggested that NOMPC was needed for transduction in fly hearing (Kernan et al., 1994; Walker et al., 2000). NOMPC falls into the TRPN subgroup within the phylogeny of the TRP superfamily. In zebrafish, reduction of the *nompC* (also known as trpn1) gene using morpholino oligonucleotides causes deafness, a circling behavior that is indicative of the loss of the vestibular sense, and a loss of microphonic potentials that result from mechanical stimulation of the lateral line hair cells (Sidi et al., 2003). These data suggest an evolutionarily conserved (but undefined) role for the NOMPC channels in mechanosensation. However, protein homologues of nompC have not been identified in mammals (Corey, 2006; Sidi et al., 2003).

Several other TRP channels have been implicated in various forms of mechanosensation. These include the TRPV genes *nanchung* and *inactive* (Gong et al., 2004), TRPA painless gene in *D. melanogaster* (Tracey et al., 2003), the TRPV proteins OSM-9 and OCR-2 in *C. elegans* (Liedtke et al., 2003; Tobin et al., 2002), and the TRP-like protein TRPY1 (also known as YVC1) in yeast (Zhou et al., 2003). Although these channels are sensitive to various forms of mechanical stimulus, their role in hearing has been unclear at best (Chalfie, 2009).

The mammalian TRPA1 had been an interesting candidate (Corey et al., 2004), but subsequent knock-out experiments ruled it out (Kwan et al., 2006). Similar results have been found for TRPA1 in zebrafish (Prober et al., 2008).

Although TRPC1 and TRPC6 have been suggested to form stretch-activated channels, mouse knock-out experiments have not revealed hearing loss (Dietrich et al., 2007).

Recently, transmembrane channel-like proteins (TMCs) have been proposed as MET channel candidates (Kawashima et al., 2011). Mutations in the gene encoding TMC1 cause hearing loss without vestibular dysfunction in both mice and humans; knocking out both TMC1 and TMC2 in mice results in vestibular dysfunction, deafness, and structurally normal hair cells that lacked all mechanotransduction activity. Expression of exogenous TMC1 or TMC2 in the knock-out mice rescued mechanotransduction, and GFP-tagged TMC proteins localized near stereocilia tips. These results suggest that TMC1 and TMC2 are necessary for hair cell mechanotransduction and may be integral components of the mechanotransduction complex. However, TMCs have not been shown to have channel-like activities, and structural prediction programs predict no pore-like structures within the proteins (Kurima et al., 2003; Labay et al., 2010).

Regulation of Mechanotransduction by Membrane Lipids

Lipid components in the membranes regulate mechanotransduction. For example, cholesterol has been shown to be a major component of hair cell stereocilia (Forge, 1991; Jacobs and Hudspeth, 1990). One of the DEG/ENaC channels in C. elegans, MEC-2, binds cholesterol and mutations that disrupt touch sensation also disrupts cholesterol binding (Huber et al., 2006). In vertebrate hair cells, phosphatidylinositol 4,5-bisphosphate ($PI(4,5)P_2$, or PIP_2) is required for mechanotransduction (Hirono et al., 2004).

Stereocilia are protrusions from apical surfaces of the hair cell, with cores primarily composed of actin. As a result, the stereocilia membrane is contiguous and part of the hair cell plasma membrane. Membrane proteins are required for mechanotransduction, overall shape, and viability of stereocilia. Much less is known about the membrane lipids in stereocilia, including their composition, precise functional role, and trafficking to and from the stereocilia.

Lipid Composition of the Cell Membrane

There are three major groups of lipids in eukaryotic cell membranes: Glycerophospholipids, sphingolipids, and cholesterol. Glycerophospholipids are the major structural lipids in eukaryotic membranes. This group contains phosphatidylcholine (PC), phosphatidylethanolamine (PE), phosphatidylserine (PS), phosphatidylinositol (PI) and phosphatidic acid (PA). Their common hydrophobic backbone is diacylglycerol (DAG), with associated fatty acyl chains of varying lengths, either saturated or cis-unsaturated.

Ceramide (Cer) is the hydrophobic backbone for sphingolipids, another class of structural lipids. This group can be further divided into sphingomyelin (SM) and the glycosphingolipids (GSLs), which contain one or more saccharides units. Gangliosides are GSLs with sialic acids as the terminal saccharides. Because of the unique structures of the above groups of lipids, membranes of different lipid composition adopt different physical properties such as thickness, diffusion rates, melting temperature, and curvature. These properties are further modified by the protein components of the membrane (van Meer et al., 2008).

Lipid Model Systems

Membranes with different lipid compositions are likely to exhibit different phase behaviors. In model systems, three phases are defined: L_d, liquid-disordered; L_o, liquid-ordered; S_o, solid gel. These phases have been investigated by physical techniques such as fluorescence microscopy, X-ray diffraction, and other spectroscopic methods (Feigenson, 2007; Veatch and Keller, 2003). Lipid mixtures can exist in different conditions, ranging from single-phased, well mixed states to states in which multiple compositionally distinct regions co-exist in immiscible phases (van Meer et al., 2008). A popular model for eukaryotic cell membrane is a three-component mixture containing cholesterol, a high-melting PC or SM, and a naturally abundant PC. At lower cholesterol concentrations, these model membranes contain co-existing L_d and S_o phases; at higher cholesterol concentrations, the phase behavior of the membrane is less clear. Whereas fluorescent images of giant unilamellar vesicles (GUVs) seems to exist in a single phase, spectroscopy results suggest co-existence of several phases (Feigenson, 2007; Feigenson

and Buboltz, 2001). In these situations, it is possible that phases coexist but are smaller than the resolution of regular fluorescent microscope (Feigenson and Buboltz, 2001). More recently, larger domains that are micrometers in size have been shown to exist in GUVs: depending on the lipid composition, nanoscopic-to-macroscopic transitions were observed in GUVs containing three PCs and cholesterol (Konyakhina et al., 2011).

In other studies, a low-melting lipid (usually naturally rare, and interacts poorly with the other two components) replaces the naturally abundant lipid (Veatch and Keller, 2003; Veatch et al., 2004). For example, both dioleoyl-PC (DOPC) and diphytanoyl-PC (DPhPC) contain two unsaturated and two methylated fatty acyl chains, conferring to a low melting temperature. These model systems have more complex behaviors, including regions with two immiscible liquids, and even regions of coexisting solid together with two immiscible liquids.

Recently, macroscopically separated liquid and gel phase domains composed of palmitoyl-oleoyl phosphatidylcholine (POPC), SM, and ceramide have been reported (Boulgaropoulos et al., 2011). Interestingly, the macro-domains were only observed in the presence of ceramide.

Membrane Domains in Cells

In the classic fluid mosaic model proposed by Singer and Nicolson (Singer and Nicolson, 1972), membrane constituents freely diffuse within the plane of the phospholipid bilayer. This model predicts that lipids and proteins, two major plasma membrane components, distribute randomly over microscopic distances. About 40 years later, our view on the plasma membrane has evolved to a more complex picture

(Lajoie et al., 2009). In particular, membrane domains, ordered structures that have distinct lipid and/or protein composition from the neighboring membrane, have received much attention. These membrane domains form because of the increased cohesion force between their protein and lipid components.

Lipid rafts, a special form of membrane domain that are enriched in sphingolipids and cholesterol, were originally defined biochemically as detergent-resistant membrane (DRM) fractions. Rafts are more tightly packed (and thus more ordered) domains than the surrounding membrane. The tighter packing is due to the saturated hydrocarbon chains in sphingolipids and phospholipids compared with the unsaturated fatty acids of phospholipids in the non-raft membrane (Simons and Vaz, 2004). Some proteins preferentially partition into these raft domains. Some proteins are anchored to the lipid raft through their lipid components, such as glycosylphosphatidylinositol (GPI)-anchored proteins (Chatterjee and Mayor, 2001), palmitoylated and myristoylated proteins (Rajendran et al., 2003), and the Src-family tyrosine kinases (Simons and Toomre, 2000); others interact with specific lipid components in the raft, such as cholesterol-binding proteins (caveolins and heterotrimeric G proteins; Kurzchalia and Parton, 1999), and phospholipid-binding proteins (annexins; Babiychuk et al., 2002).

In addition to sphingolipid and cholesterol-enriched lipid rafts, another type of domain that is highly enriched in ceramide has been described. Ceramide is capable of forming highly ordered model membranes at low cholesterol levels (Castro et al., 2009). In living cells, these ceramide-enriched, ordered domains may transiently exist, as

recently demonstrated by Babiychuk et al. (Babiychuk et al., 2008). Ceramide domains have also been shown to be important for fas signaling (Cremesti et al., 2001).

Although membrane domains in cells are generally believed to be small (10-200 nm) and transient (with half life of 100 ns or less), the small domains can aggregate to form larger and more stable domains through protein–protein and protein–lipid interactions (Bali et al., 2009; Rajendran and Simons, 2005). For example, in macrophages, macroscopic domains with marked differences in membrane packing was shown, using two-photon microscopy and 6-acyl-2-dimethylaminonaphthalene (laurdan) as a reporter probe (Gaus et al., 2003). During T-lymphocytes migration and, differentiation of large domains of the membrane is required, and this differentiation appeared to be aided by segregation of lipid phases, which partitioned the membrane proteins needed for chemotaxis into the leading edge and the uropod of the cell (Gomez-Mouton et al., 2001). During synaptic immune formation, T-cells form large specialized membrane domains enriched in cholesterol and sphingomyelin (Gomez-Mouton et al., 2001; Mossman et al., 2005). Using cholera toxin B subunit combined with fluorescent imaging, a group showed that ganglioside GM1 localized to a macrodomain in the plasma membrane in living sperm (Selvaraj et al., 2006).

Overall goals

Among techniques used to study the localizations and functions of hair bundle proteins, transient transfection of hair cells is an important strategy. However, hair cells are known for being difficult to transfect. In Chapter 2, I surveyed a variety of methods used for transiently transfect hair cells and improved an easy-to-use method, gene gun. The improved gene gun method can also be used in other systems where a deeper penetration of tissue and less damage are required.

Chapter 3 focuses on the stereocilia membrane, or hair bundle membrane, which has unique structural features and important cellular functions. Aside from membrane associated proteins, lipid is an important composition of the hair bundle membrane. Understanding the lipid composition of the hair bundle membrane, as well as the interactions between these lipid components and the protein components, may provide a deeper understanding of the hair cell function. The lipid-protein interactions are particularly interesting in the context of membrane domains, in which specific groups of lipids and proteins interact and segregate. In other cell types, the lipid domains have important functions in cell signaling and protein localization/trafficking. Do membrane domains exist in the hair bundle, and if yes, what are their functional roles?

The tip link complex (tip link, the UTLD, and LTLD) contains a variety of proteins. Many of these have not been identified, including the MET channel. Clive Morgan, a postdoctoral fellow in the Gillespie lab, has identified a MET channel candidate, TRPM7. Based on the current model of mechanotransduction, the MET channel could interact

with PCDH15, directly or indirectly. I asked several questions in Chapter 4. Does TRPM7 interact with PCDH15? If yes, what are the domains responsible for this interaction? Also, does the newly identified MET channel candidate, TMC, interact with PCDH15 and/or TRPM7?

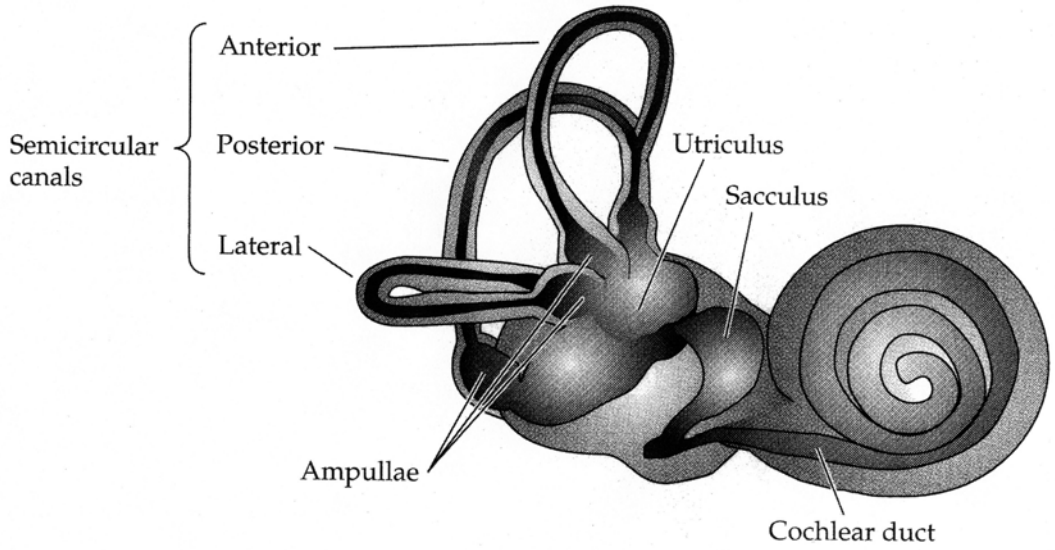

Figure 1.1 – The mammalian inner ear.

The membranous labyrinth of a mammalian inner ear is diagrammed, showing the three semicircular canals, the sacculus, the utricles, and the cochlea (from Fain, 2003).

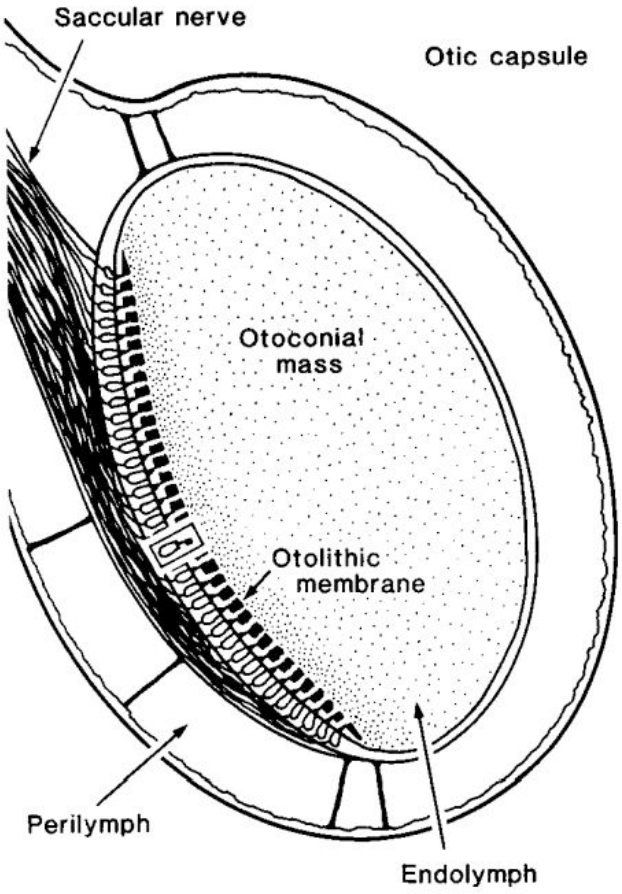

Figure 1.2 – Schematic cross section through the frog sacculus.

The otoconial mass is coupled to hair bundles by the perforated otolithic membrane. One of the roughly 3000 hair cells in the saccular macula is indicated by a box (Eatock et al., 1987)).

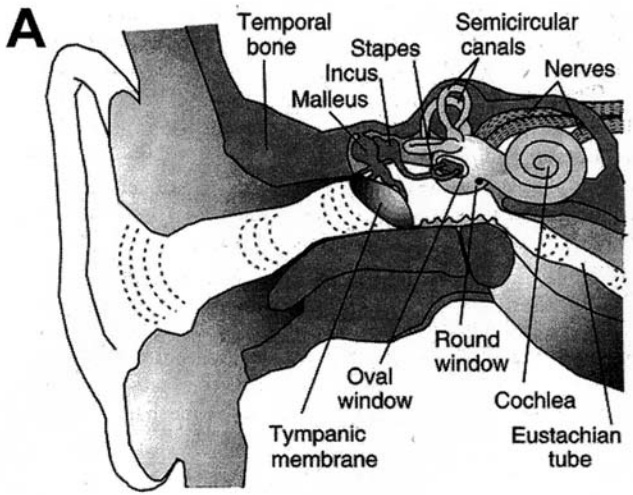
A
Temporal bone
Stapes
Incus
Malleus
Semicircular canals
Nerves
Round window
Oval window
Cochlea
Tympanic membrane
Eustachian tube

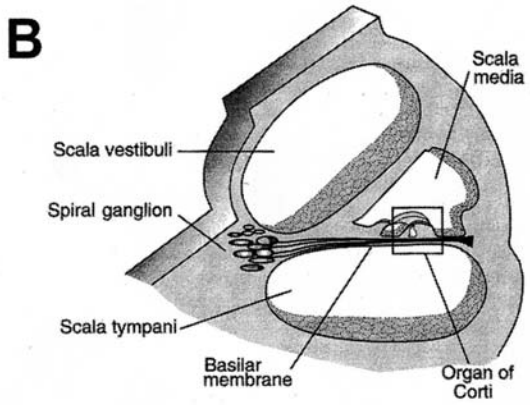
B
Scala media
Scala vestibuli
Spiral ganglion
Scala tympani
Basilar membrane
Organ of Corti

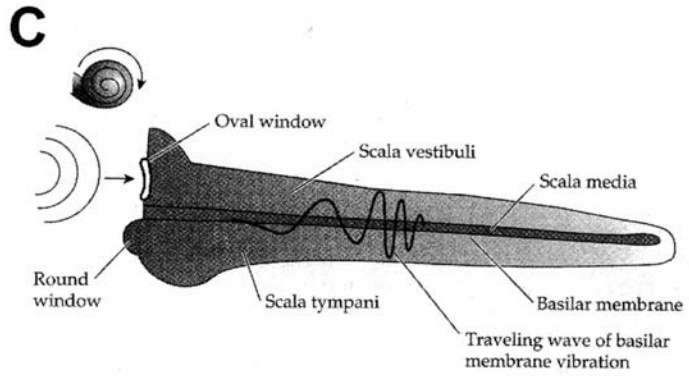
C
Oval window
Scala vestibuli
Scala media
Round window
Scala tympani
Basilar membrane
Traveling wave of basilar membrane vibration

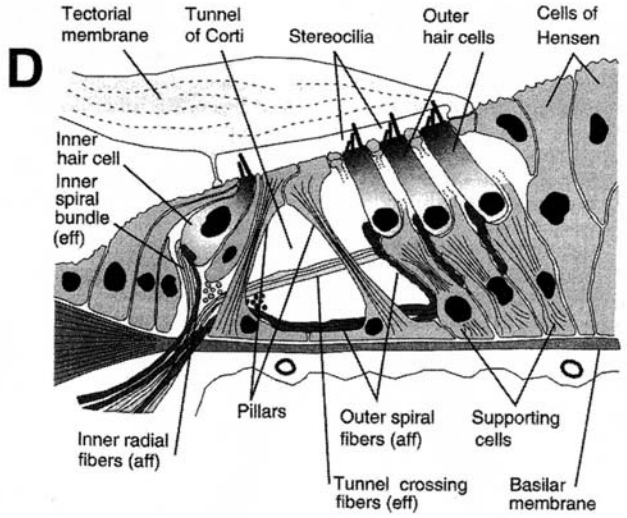
D
Tectorial membrane
Tunnel of Corti
Stereocilia
Outer hair cells
Cells of Hensen
Inner hair cell
Inner spiral bundle (eff)
Inner radial fibers (aff)
Pillars
Outer spiral fibers (aff)
Supporting cells
Tunnel crossing fibers (eff)
Basilar membrane

Figure 1.3 – Anatomy of the inner ear

A, Sound waves are transmitted to the fluid-filled inner ear through vibrations of the middle ear ossicles (malleus, incus, and stapes). B, Partial cross-section through the cochlea. The cochlea is divided into three fluid-filled chambers, the scala vestibule, scala media, and scale tympani. The hair cells are located in the organ of Corti, which sits on top of the basilar membrane. C, A uncoiled cochlea showing motions of the basilar membrane from base to apex. Vibrations of the osssicles apply pressure to the oval window, and the vibrations are propagated through the fluids of the scala vestibule and scala tympani to the round window, producing a travelling wave of basilar membrane oscillation. D, A single row of inner hair cells and three rows of outer hair cells reside in the organ of Corti. Bundles of the outer hair cells are imbedded in the overlaying tectorial membrane. Basilar membrane oscillations cause the hair cells to move relative to the tectorial membrane. Inner hair cells are primarily innervated by afferent radial fibers, while outer hair cells are contacted primarily by efferent fibers (from Fain, 2003).

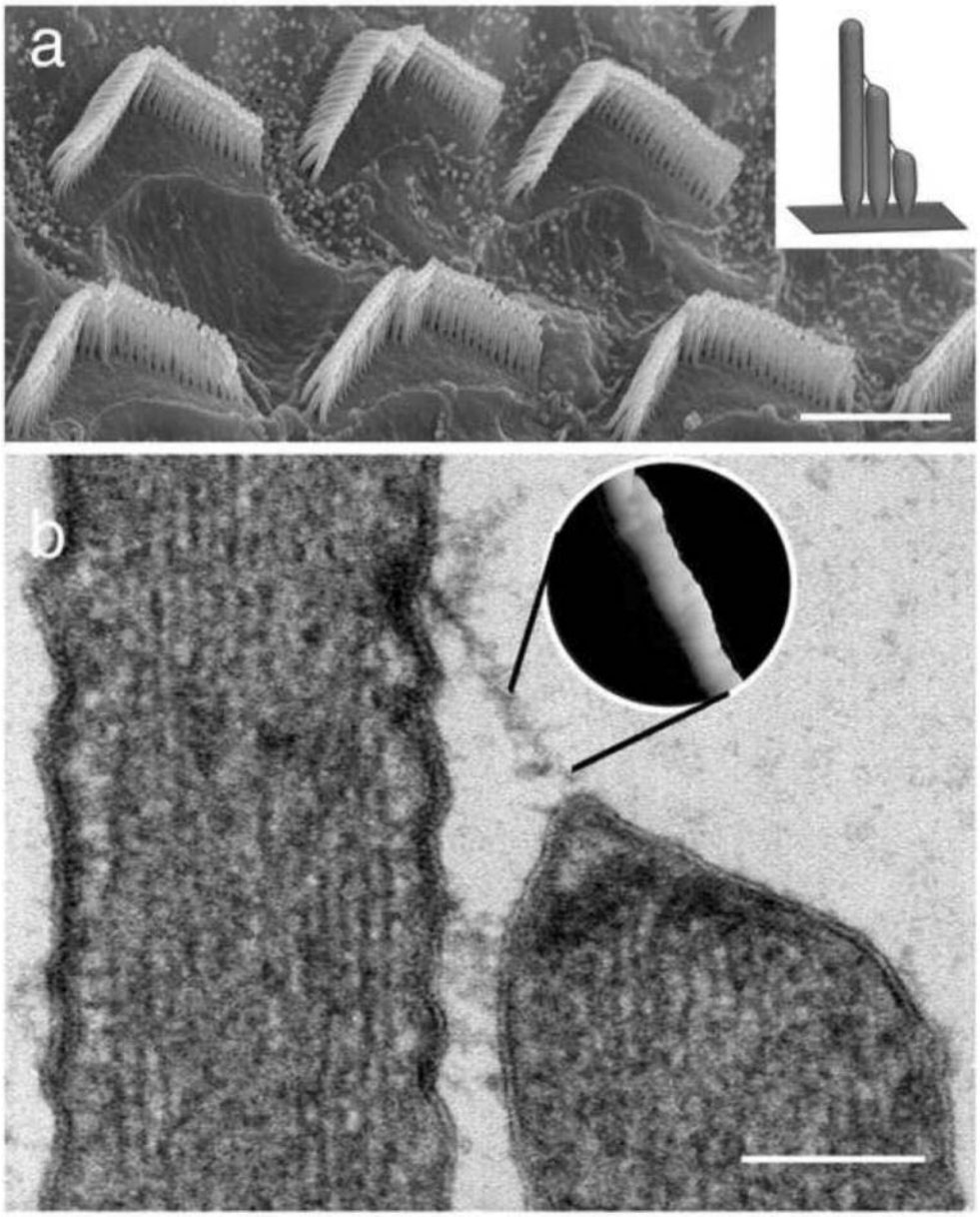

Figure 1.4 – Stereocilia of the inner ear hair cells

Stereocilia of the inner ear hair cells form organized bundles and are connected to each other by tip links. (a) Scanning electron micrograph showing stereocilia bundles on the apical surface of the outer hair cells of the rat organ of Corti. Bar = 5 μ m. (Inset in a) Model depicting a longitudinal section through a hair cell bundle. Note the staircase pattern and arrangement of tip links. (b) Thin section transmission electron micrograph showing a tip link connecting one stereocilium to an adjacent taller neighbor. Note the presence of electron dense material at the upper and lower insertion sites and that the tip of the shorter stereocilia is tented due to tip link tension (from Kachar et al., 2000). Bar = 150 nm. (Inset in b) The surface rendering of a freeze-etching image of the tip link provides a close up view of helical structure of the tip link (Sakaguchi et al., 2009).

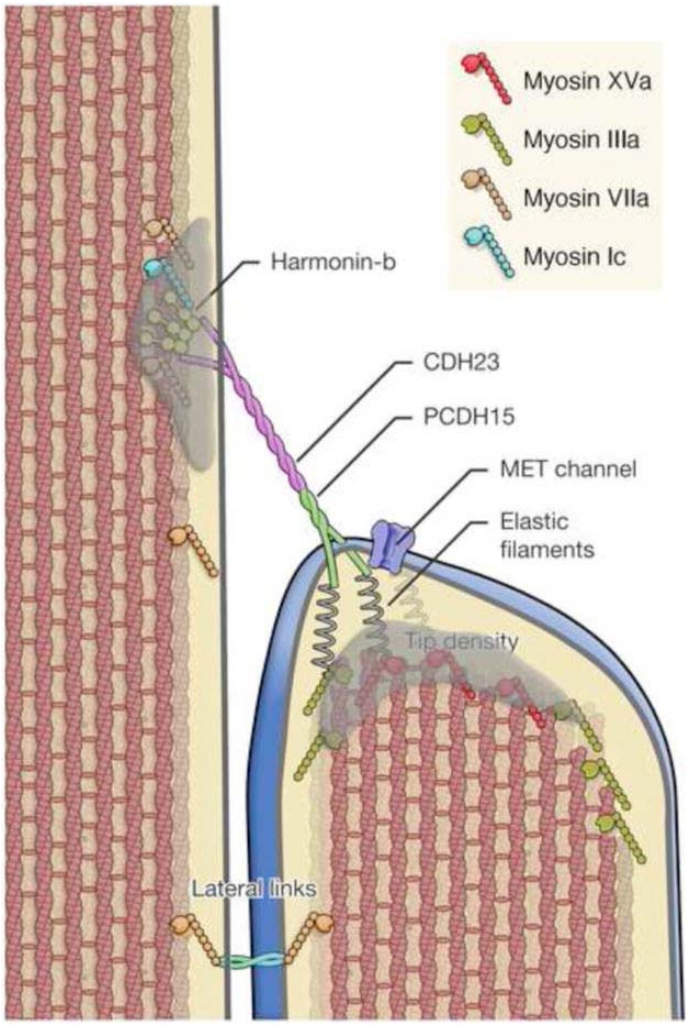

Figure 1.5 – Schematic representation of the tip link complex.

CDH23 and PCDH15 comprise the tip link, which inserts into the stereocilia membrane at the sites of the upper and lower tip densities. Tip densities are presumed to contain scaffolding proteins, which bind to the cytoplasmic domain CDH23 and PCDH15 and anchor the tip link. In addition several myosins including myosin Ic, myosin IIIa, myosin VIIa, and myosin XVa have been localized to the tip density region and proposed to participate in MET adaptation, stereocilia actin dynamics, localization of lateral links, and cargo transport. Tension on the tip link gates the mechanoelectrical transduction (MET) channel. The tip-link can exert force onto the channel either directly or indirectly by tenting the membrane. The gating mechanism is presumed to involve a gating spring element through which force is applied to the channel gate. The channel gate opens in series with this spring, thus transiently reducing the force onto this spring and increasing compliance. The coiled structure of the tip link and the properties expected of conventional cadherins suggest that the tip link is relatively stiff. The spring element should then be in series with the tip link, possible as putative “elastic filaments” between the membrane and the dense actin core (Sakaguchi et al., 2009).

Chapter 2 – Improved Biolistic Transfection of Bullfrog, Chick, and Mouse Hair Cells

---

Hongyu Zhao and Peter G. Gillespie†

Oregon Hearing Research Center and Vollum Institute, Oregon Health & Science University, 3181 SW Sam Jackson Park Road, Portland, Oregon 97239, U.S.A

Ph: 503 404 2936; Fax: 503 494 2976

†Corresponding author (gillespp@ohsu.edu)

Abstract

Transient transfection of hair cells has proven challenging. Here we describe modifications to the Bio-Rad Helios Gene Gun that, along with an optimized protocol, improves transfection of bullfrog, chick, and mouse hair cells. For example, using the improved method, we were able to transfect hair cells in the bullfrog sacculus and chick cochlea for the first time. Moreover, the increased penetrating power afforded by our method allowed us to transfect mouse hair cells from the basal side, through the basilar membrane; this configuration should protect hair bundles from damage during the procedure. Using the optimized protocol, we transfected hair cells with EGFP fusions of harmonin b (USH1C) and PMCA2 (ATP2B2; plasma-membrane Ca2+-ATPase isoform 2); while PMCA2-EGFP localization was similar to endogenous PMCA2 detected with antibodies, high levels of harmonin-EGFP were found at stereocilia tapers in bullfrog and chick, but not mouse, hair cells. By contrast, harmonin-EGFP was concentrated in stereocilia tips in mouse hair cells.

Introduction

Hair cells are specialized epithelial sensory cells in the inner ear, transducing mechanical stimuli into electrical signals in the process of hearing and balance (Hudspeth, 1989). Mechanoelectrical transduction occurs within the hair bundle, the unique organelle structure on the apical end of a hair cell. Many proteins critical for mechanotransduction, such as plasma membrane Ca2+-ATPase (PMCA) and harmonin, reside at discrete locations in the bundle that are important for their roles in mechanotransduction (Grillet et al., 2009; Yamoah et al., 1998). Although many proteins have been identified in bundles by mass spectrometry (Shin et al., 2007), precise locations of many of them remains unknown. Although in many cases, immunocytochemistry works well to show protein localization, this method depends on antibodies of high specificity and affinity, which are not always available. Transient transfection of hair cells with fluorescent fusion proteins provides an alternative method that is relatively quick and independent of antibodies. However, transfection of hair cells has proven challenging, and most transfection methods have failed for hair cells (Wang et al., 2011).

Biolistic transfection ("gene gun transfection") has resulted in successful delivery of foreign DNA to cells when other methods have failed (Karra and Dahm, 2010). In this method, gold or tungsten particles are coated with DNA, and the particulate complexes are accelerated to ultrasonic speed. The momentum of the DNA-coated particles

enables them to penetrate cell membranes and enter cell nuclei, resulting in transfection of the cell (Klimaschewski et al., 2002). This method is technically simple, requires less time for reagent generation than viral methods, and provides a quick turnaround. However, not only is the method inconsistent in its efficiency, but the shock wave and particle shower can damage the target tissue. Often, one is faced with the dilemma of sacrificing penetrating power in order to avoid excessive tissue damage.

Bullfrog and chick hair cells are useful for studying protein localization in hair bundles. These cells are easy to obtain, easy to dissect, and, in the case of bullfrog, have much larger bundles that allow better imaging. However, transient transfection of bullfrog hair cells using biolistic approaches has not been successful, probably because of the sacculus' large hair bundles and thick cuticular plate, the actin-rich structure immediately under the apical plasma membrane; both present obstacles to delivery that demand more penetrating power from the DNA-coated particles. Unfortunately, increasing penetrating power also greatly increases tissue damage.

Using an improved biolistics method with more penetrating power and minimal tissue damage, we show here transient transfection of hair cells from bullfrog sacculi and chick cochlea, each for the first time. Harmonin-EGFP localizes to unexpected locations in these hair cells. In addition, due to the increased penetration power and minimal blast effect of the method, we were also able to transfect mouse cochlea hair cells by shooting particles through the basilar membrane, on the opposite side of the hair cell from the hair bundle, thus minimizing the chance of bundle damage. Harmonin-EGFP expressed in these hair cells is transported to stereocilia tips, the endogenous

location of harmonin. Our biolistics method thus allows us to study protein localization and function in hair cells.

Results

Alternative transfection methods

While trying to transfect hair cells from the bullfrog sacculus, we tried a variety of lipid- and polymer-based methods, including Lipofectamine, branched polyethyleneimine (PEI), linear PEI, Fugene, Effectene, and Superfect; in each case, we were unable to transfect hair cells (each n=3). The lack of success may be due to physical barriers to delivery; the hair cells' basolateral side is sealed off by tight junctions with neighboring supporting cells, preventing access of DNA complexes. Unfortunately, methods designed to open tight junctions (e.g., chelating Ca2+ ions with EGTA or use of solutions with reduced osmolarity) either resulted in hair cell death or no transfection. Several unique properties of the hair cells' apical surface may have also limited transfection. First, the cuticular plate forms a rigid support under the plasma membrane. Second, surrounding this cuticular plate is a ring-shaped "pericuticular necklace" (Hasson et al. 1997), a zone of active exo- and endocytosis. However, vesicles in this region are only about 100 nm (Kachar et al., 1997), much smaller than most DNA complexes used for transfection. Because DNA complexes used in most lipid- and polymer-based transfection methods are larger than 100 nm (Ma et al., 2007; Ogris et al., 1998), they probably cannot enter hair cells by apical endocytosis. The efficiency of in vitro transfection increases with the size of DNA complex (Ogris et al., 1998; Ross and Hui, 1999; Zuidam and Barenholz, 1999); such DNA complexes usually enter cells through phagocytosis, which can accommodate much larger particles (Dalluge et al.,

2002). Although DNA complexed to polyethyleneimine (PEI) can apparently be made into particles smaller than 100 nm (Boussif et al., 1995; Finsinger et al., 2000; Ogris et al., 1998), we were unable to transfect bullfrog hair cells or COS-7 cells with PEI-DNA complexes (n=3). To specifically trigger PEI-DNA endocytosis, we also chemically crosslinked the transferrin receptor (TfR) to PEI, then formed a TfR-PEI-DNA complex (Diebold et al., 2001). Unfortunately, that strategy also did not yield any transfected bullfrog hair cells (n=3).

In vitro and in vivo electroporation methods have been successfully used to transfect developing mouse and rat hair cells or hair-cell progenitors (Driver and Kelley, 2010; Gubbels et al., 2008; Zheng and Gao, 2000). We also tried in vitro electroporation with bullfrog sacculi, which again resulted in no transfection of hair cells or indeed any cells in the epithelium (n=5). The lack of success likely arose because of the specialized apical surface of the adult hair cell; high voltages led to total destruction of the hair cell, while lower voltages did not permit entry of DNA (n=3). Finally, when we combined electroporation with loosening tight junctions with low Ca2+ and incorporation of DNA into a complex with PEI, no hair cells were transfected (n=3).

Biolistic transfection

Using standard protocols and unmodified instruments, we attempted transfection of hair cells in the bullfrog sacculus with two biolistic instruments from Bio-Rad, the PDS-1000 and the Helios Gene Gun. We were unable to transfect bullfrog hair cells with either system, although as described before, both systems permitted low-efficiency hair-cell transfection in chick utricles, mouse utricles, and mouse cochlea

(Belyantseva et al., 2003; Belyantseva, 2009). When we used conditions that resulted in higher particle speed, we occasionally saw a few cells transfected in the non-sensory region of the sacculus. Under those conditions, however, the increased shockwave generated from either system destroyed nearly all of the hair bundles. We reasoned that as we increased helium pressure, which increases gold-particle velocity, the increased shockwave destroyed the hair cells, especially their bundles, which face the direction of gold particles.

Multiple groups have tried to modify the PDS-1000 or the Helios Gene Gun to achieve better transfection efficiency. Thomas and collaborators described a modification to transfect fragile insect tissues (Thomas et al., 2001), while O'Brien's group described a modification of the Helios Gene Gun that improved penetrating power several-fold (O'Brien et al., 2001). After modifying our PDS-1000 according to Thomas et al., we were still unable to transfect bullfrog hair cells, although we occasionally saw cells transfected in the non-sensory region. Poor transfection probably resulted from insufficient penetrating power, as the method was aimed at minimizing tissue damage. We also obtained the modified Helios Gene Gun part described by O'Brien. Although the O'Brien method provided more penetrating power by directing the helium stream with a focusing nozzle, it also substantially increased shockwave damage to the tissue.

We therefore focused on reducing the shockwave from the O'Brien method while preserving its penetrating power. To reduce the shockwave, we shortened the focusing nozzle and put the sample in a semi-air-tight chamber, with porous polyester

mesh and diffusion screen with small holes on top. The sample chamber is made of: (1) a SARSTEDT 50 ml conical tube cap at the bottom, where sample to be transfected is placed; (2) a 15 mm Netwell Insert (with 74 µm mesh size polyester membrane), inverted and trimmed to fit into the tube cap; (3) a diffuser screen (5 µm pore size) placed on top of the inverted Netwell insert; and (4) a plastic ring holder to fix the diffuser screen on top of the Netwell insert. Metal adaptors that connect the Gene Gun to the sample chamber were used to precisely control the sample position relative to tip of the nozzle and distance between sample and tip of the nozzle; we used three different adaptor lengths, corresponding to three different tip-to-sample distances (Fig. 1).

The shortened nozzle tip and the semi-air-tight chamber, with a net-supported membrane on top, greatly reduced the shockwave; sacculi were not disturbed even at 200 psi, while the standard Bio-Rad and O'Brien set-ups blew the sacculi away or damaged the hair cells badly. Excessive particles also cause tissue damage (Raju et al., 2006). Because we used two layers of filters, one with a 74 µm mesh and one with 5 µm pores, we substantially reduced the particle density as compared to the standard Bio-Rad and O'Brien methods. We estimated hair-cell damage using the three methods by labeling saccular actin with phalloidin (Fig. 2). Damage to hair bundles was evident with both the Bio-Rad and O'Brien methods; bundles were missing, knocked over, or splayed (Fig. 2B-C). By contrast, using the present method, bundles remained vertical and appeared intact (Fig. 2D). With this method, particle density was dramatically reduced (Fig. 3), minimizing the damage caused by particles themselves. Because of the much

reduced particle density, we were unable to directly compare penetration power of the three methods; it is likely, however, that some particles pass through the two filters at high velocity.

Using this modified setup, we were able to transfect hair cells in bullfrog sacculus, chick utricle, and chick cochlea with proteins that localize to hair bundles. To estimate transfection efficiency, we transfected bullfrog sacculus with EGFP fused to harmonin b (harmonin-EGFP) and observed on average three transfected hair cells in each sacculus, and many more cells outside the sensory epithelium (Fig. 4).

Location of harmonin-EGFP and PMCA2-EGFP in hair cells using biolistic transfection

With the modified setup, we were able to transfect hair cells from frog sacculus, chick utricle, and chick cochlea with harmonin-EGFP (Fig. 5). In all three types of hair cells, harmonin-EGFP was concentrated at the hair bundle's base, in the taper region of the stereocilia. We also often saw harmonin-EGFP in ring-like structure that surrounded the cuticular plate (Fig. 5B,G,H). When the image gain was increased, small, discrete clusters of harmonin-EGFP were sometimes seen along stereocilia shafts (Fig. 5F); this result suggests that harmonin is transported to the upper part of the stereocilia in a cluster and is consistent with the observation that harmonin interacts with the molecular motor myosin-VIIA harmonin and is transported towards stereocilia tips (Bahloul et al., 2010; Reiners et al., 2003). In chick cochlea, we saw several transfected hair cells with what appeared to be fused stereocilia (Fig. 5H); this result is consistent with the previous finding that harmonin b can bundle actin (Boeda et al., 2002).

Localization of EGFP-harmonin differed significantly from that of endogenous harmonin detected by a specific antibody, however (Fig. 5E, J).

We also transfected frog and chick hair cells with frog PMCA2 fused to EGFP. PMCA2-EGFP was concentrated in the hair bundle, uniformly distributed along the stereocilia (Fig. 5K,L). We also observed PMCA2-EGFP in the cell body and apical surface of the hair cell. These observations are consistent with previous immunocytochemical and transfection reports (Dumont et al., 2001; Hill et al., 2006). We also transfected frog and chick hair cells with rat PMCA2-EGFP and saw similar localization. Immunoreactivity of PMCA2 in frog and chick hair cells is characterized by reduced staining at the stereocilia taper region compared to the stereocilia shaft (Yamoah et al., 1998), seen in Fig. 5M. Although we did not clearly observe this pattern in transfected hair cells, we analyzed only a few cells; none of their hair bundles were visible in profile, optimal for viewing this staining pattern (Yamoah et al., 1998).

Location of harmonin-EGFP in mouse cochlea hair cells using biolistic transfection

Because of increased penetrating power, we suspected that DNA-coated gold particles might be capable of accessing cochlear hair cells from the back side of the basilar membrane. With a coarser diffuser membrane (12 µm pore size instead of 5 µm), we were able to transfect mouse cochlea hair cells through the basilar membrane. Since the gold particles enter the hair cells from the basal side, damage to the hair bundle by the gold particles and blast was minimized (Fig. 6). Removal of the tectorial membrane for transfection is unnecessary, leaving hair bundles protected from mechanical damage, including liquid surface tension during transfer of the organs. The transfection

efficiency was about 8 hair cells/cochlea (n=6). Unlike in frog and chick hair cells, harmonin-EGFP was located in the upper part of the stereocilia, usually only near the tips (Fig. 6A, C-E). Our harmonin b cDNA construct was from mouse, suggesting why harmonin-GFP was poorly transported in other species but in mouse hair cells, the harmonin b is efficiently transported toward the tip.

Discussion

Transient transfection is useful for studying protein localization in cells. Unfortunately, hair cells have been proved especially difficult to transfect both because hair cells are post-mitotic, limiting nuclear entry of exogenous DNA, and because entry of DNA into hair cells is strictly limited. Hair cells are surrounded by supporting cells on their basolateral sides, with tight junctions sealing the borders, such that only the apical surface is accessible. Furthermore, while the apical surface is a site of active endocytosis, only very small vesicles, about 100 nm in size, are involved; this size is too small for typical DNA complexes. Moreover, the plasma membrane of the apical surface is supported by a dense actin network and is thus much more rigid.

Hair cells have been successfully transfected using in utero electroporation (Gubbels et al., 2008), electroporation of organotypic cultures (Driver and Kelley, 2010; Zheng and Gao, 2000), adenovirus (Holt, 2002), lentivirus (Bedrosian et al., 2006), adeno-associated virus (AAV) (Bedrosian et al., 2006), and biolistics (Rzadzinska et al., 2004). In utero electroporation in mice at E12.5 is very efficient, as more than 50% of hair cells can be transfected with GFP (Gubbels et al., 2008); however, this is a very

challenging technique and is not practical for most labs. Although virus-based techniques also work, all viruses have some hair-cell toxicity (Dazert et al., 2001; Ishimoto et al., 2002; Liu et al., 2005; Luebke et al., 2001), making them less suitable for studying protein localization patterns. AAV causes the least toxicity of all tested viruses but has a small packing limit (4.5 kb total) and thus can only deliver small proteins. Because DNA solutions can only access the apical surface, where hair bundles reside, successful electroporation of hair cells with little damage to the hair bundle in organotypic cultures has only been reported in young mouse cochlea (earlier than P5, before hair bundles mature) and has low efficiency (Driver and Kelley, 2010).

Biolistic transfection with the Gene Gun is effective for transiently transfecting hair cells of some preparations, including mouse cochlea (Belyantseva, 2009), yet for hair cells in other preparations, especially bullfrog sacculus and chick cochlea, a high particle speed with low shockwave is necessary to transfect them. By including a focusing nozzle, the modification of Helios Gene Gun described in O'Brien et al. (O'Brien et al., 2001) resulted in a dramatic increase in penetrating power but also in more tissue damage, presumably from the stronger shockwave that come with the focused nozzle. Reducing the shockwave from the Helios Gene Gun while preserving the particle speed and hence penetrating power is challenging, as it is hard to separate the particle speed from its driving force, the shockwave. To reduce the shockwave, we shortened the nozzle and put the sample in a semi-airtight chamber, with a coarse mesh and a fine diffuser screen on top. The semi-airtight nature of the sample chamber, together with the two layers of filters and screens (74 μm and 5 μm pores). The filters stop >90% of

the particles, yet because the focusing nozzle concentrates the particles, enough particles reach the sample.

When expressed in tissue-culture cells, harmonin b bundles actin (Boeda et al., 2002), which likely occurs because harmonin b contains an actin-binding site (Boeda et al., 2002) and can oligomerize (Siemens et al., 2002). Harmonin initially localizes in tissue culture cells to focal adhesions, sites of clustered actin filament barbed ends. Harmonin clustering in transfected bullfrog and chick hair cells at stereocilia tapers was thus surprising; most stereocilia actin filaments' pointed ends are found at the tapers. The extent of harmonin clustering at tapers varied from cell to cell, probably reflecting differences in expression levels. In many cells we could detect much smaller clusters of harmonin in stereocilia shafts; these clusters were usually asymmetric, with the longitudinal axis (relative to the stereocilia shaft) being 1.5 - to 2-fold longer than the horizontal axis. We presume that these are small clusters in transit towards stereocilia tips; their size may reflect geometric considerations of the transport mechanism or stereocilia structure. Regardless, endogenous harmonin was only seen clearly at stereocilia tips in bullfrog hair cells, located at the tip link's upper end (Grillet et al., 2009).

In contrast to results with bullfrog and chick hair bundles, in mouse bundles harmonin-EGFP was located near stereocilia tips and was absent from tapers. The difference between the species could reflect inefficient transport of the mouse harmonin fusion protein in bullfrog and chick bundles, or it could indicate differences in structure of the taper region. Adult bullfrog and E20-E21 chick hair cells are more

mature than P4 mouse hair cells; the difference in harmonin-EGFP localization may also represent developmental differences in bundle structure.

High levels of harmonin-GFP expression led to distorted harmonin- and actin-containing structures that appeared to consist of fused stereocilia (Fig. 5H,I; Fig. 6B). Large apical rings were also seen (Fig. 5B,H,I). Both of these structures were reminiscent of the wavy actin bundles seen in tissue-culture cells (Boeda et al., 2002).

In conclusion, we modified the Helios Gene Gun and developed a protocol to transfect hair cells from bullfrog sacculus and chick cochlea, previously recalcitrant to transfection. With simple optimization steps, the protocol can be easily adapted to transfect hair cells from other species and organs and should result in increased transfection efficiency with minimal damage to hair cells. Moreover, the combination of increased penetration power and reduced shockwave will be of general applicability for transfection of many other cell types and tissues for which standard methods for foreign DNA introduction are unsuccessful. The improved gene-gun transfection method should facilitate studies examining protein localization, interaction, and function in hair cells and many other cell types.

Experimental Procedures

Ethics statement. Animal experiments reported here were approved by the Oregon Health & Science University Institutional Animal Care and Use Committee (IACUC); the approval number was A684. All experiments began with euthanasia of the animal, carried out using methods approved by American Veterinary Medical Association Panel on Euthanasia.

Materials. The Helios Gene Gun, PDS-1000, gold particles, and Tefzel tubing were from Bio-Rad; TreffLab microcentrifuge tubes were from Scidynamics LLC; the 15 mm Netwell Insert with 74 µm mesh size polyester membrane was from Corning; the diffuser screen was from Millipore (5 µm pore size, TMTP 025000) and SPI supplies (12 µm pore size, E12025-MB); the plastic ring holder was made from the cap of Fisher culture test tube (#14-956-1J); and the 50 ml conical tube cap was from SARSTEDT. The modified Gene Gun barrel was purchased from Dr. John O'Brien, and the tip of the focusing barrel were shortened by 5 mm in a local machine shop.

Preparation of tubing loaded with DNA-coated gold particles. A total of 2 mg of 1.6 µm diameter gold particles (Bio-Rad) were transferred to a 1.5 ml microfuge tube and then add 25 µl spermidine (0.05 M in dH2O, pH 10.5). The spermidine-gold mixture was sonicated in a bath sonicator for 20 seconds. Mix 4 µg DNA, dH2O, and 5 µl 25% glycerol in 12.5 µl total volume in a microcentrifuge tube. The DNA solution was then mixed with the spermidine-gold mixture and vortexed. While still vortexing, 25 µl of 1 M CaCl2 is added dropwise. This suspension is sonicated briefly and incubated at room

temperature for 10 min. The suspension was then washed three times with 0.5 ml 100% ethanol, with brief sonication in between. The DNA coated gold particles were then resuspended in 0.6 ml of 100% ethanol.

Bullet preparation. To prepare the bullets, a piece of 6-inch Tefzel tubing was with a flow of nitrogen (0.3–0.4 LPM for 10 min); the tubing was then attached to a 2 ml syringe. After a brief sonication, the suspended DNA-gold particles were drawn into the tubing. The gold particles were allowed to settle for 10 min, before the supernatant was slowly removed using the syringe. The tubing was rotated for 30–40 sec, dried with a flow of nitrogen, cut, and stored desiccated at 4°C until use.

Dissection, biolistics, and organotypic cultures. Sacculi from adult bullfrogs (mixed sexes, 2-5 inch bodies) were dissected; the otolithic membrane was loosened with a 20 min treatment with 65 μg/ml protease XXIV (Sigma) at room temperature, then was then carefully removed with forceps. After shooting at 200 psi, the sacculi were washed 2x with culture medium 0.75x DMEM/F12 with HEPES (Invitrogen #11039), supplemented with 10% FBS and 20 μg/ml carbenicillin. Sacculi were then cultured for 16-24 hours at 27ºC with 5% CO2.

Utricles and cochleas were dissected from E20-E21 chicks; otolithic or tectorial membranes were removed before shooting at 200 psi. Organs were then cultured for 16-24 hours at 37ºC with 5% CO2 in DMEM/F12 with HEPES containing 2% FBS, 5 μg/ml carbenicillin, 0.002% ciprofloxacin.

Cochleas were dissected from CD1 mice in ice-cold PBS supplemented with 100 μM CaCl2 and 1 mM MgCl2. After exposing the cochlea by removal of the temporal

bone, the organ of Corti, together with the lateral wall and Reissner's membrane, was removed from the rest of the inner ear. To carry out this step, we grasped the base of the lateral wall and organ of Corti with forceps and unwound them together as one piece from the core structures of the cochlea. The tissue was oriented so that the basilar membrane faced up before being shot at 200 psi. Instead of using the standard 5 µm pore size diffuser, we use a 12 µm SPI-Pore polycarbonate membrane filter. Organs were cultured in the culture medium for 48 hours in DMEM/F12 containing 5 µg/ml carbenicillin at 37ºC with 5% CO2.

Confocal microscopy. After culturing, the organs were fixed with 4% formaldehyde for 30 min at room temperature, and counter-stained for 1 hr with TRITC-phalloidin or Alexa Fluor 488-phalloidin (in PBS containing 0.2% saponin), washed, and mounted. In some cases, cells were stained for harmonin using an antibody (H3) directed against the C-terminal PDZ domain [3] or with an antibody (F2a) directed against the "a" splice form of PMCA2 [28]. All samples except that of Fig. 5E were observed with an Olympus FV1000 confocal microscope equipped with a 60x, 1.42 NA oil-immersion plan apochromat objective. The image of Fig. 5E was obtained using structured-illumination microscopy with an Applied Precision OMX system.

Acknowledgements

We thank Peter S. Steyger, PhD for advice on bullfrog sacculus organ culture.

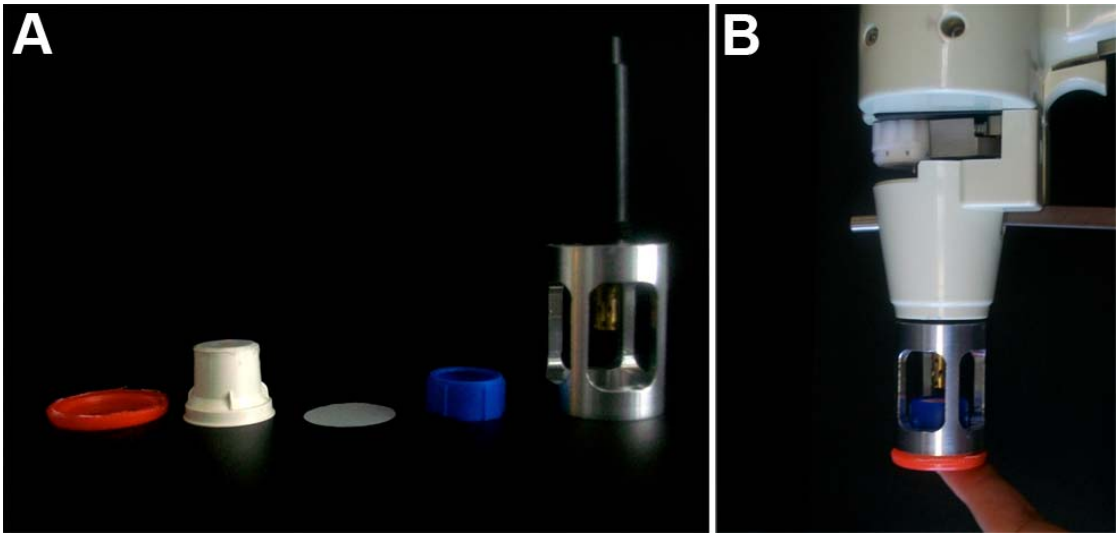

Figure 2.1 - Diagram of modifications to the Helios Gene Gun.

A, components of the modified setup. From left to right, SARSTEDT 50 ml conical tube cap, with sides cut; 15 mm Netwell Insert (with 74 µm mesh size polyester membrane); diffuser screen; plastic ring holder to fix the diffuser screen on top of the Netwell insert; metal adaptor that connects the Gene Gun to the sample chamber. B, assembled setup.

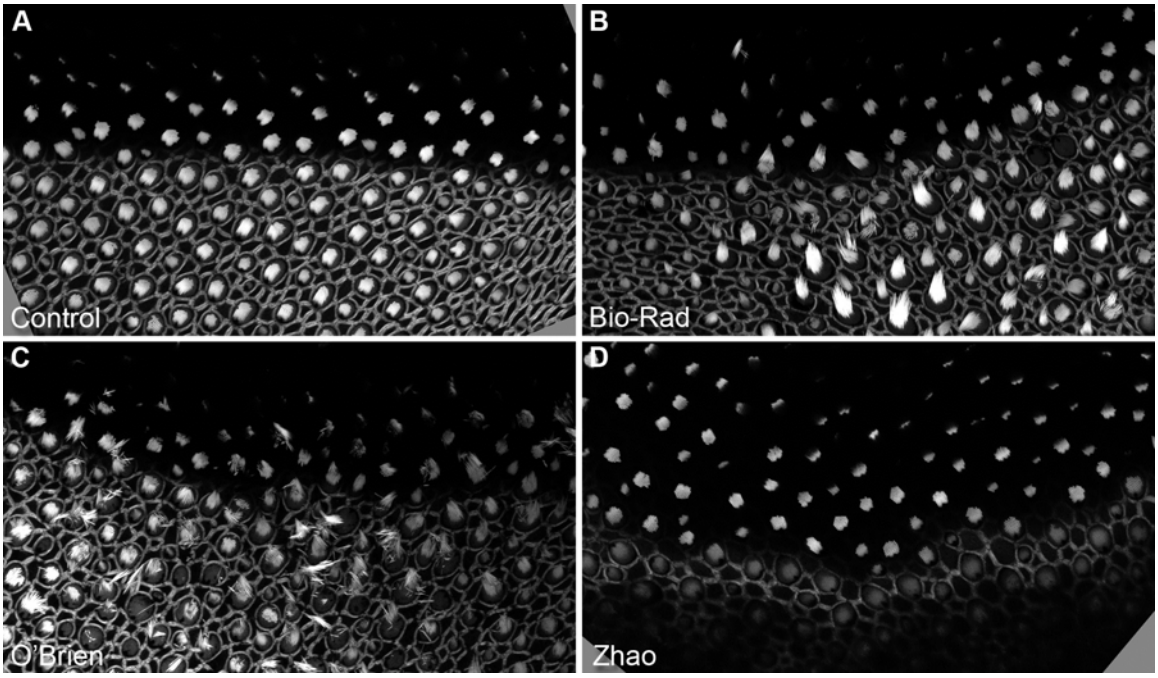

Figure 2.2 – Shockwave damage from biolistics transfection methods.

Bullfrog sacculi were dissected, shot with different Gene Gun setups, immediately fixed, and stained with Alexa Fluor 488-phalloidin. A, control (not shot); B, standard Bio-Rad setup, at 200 psi; C, O'Brien setup, 75 psi; D, Zhao setup, 200 psi. Panels are 950 µm wide.

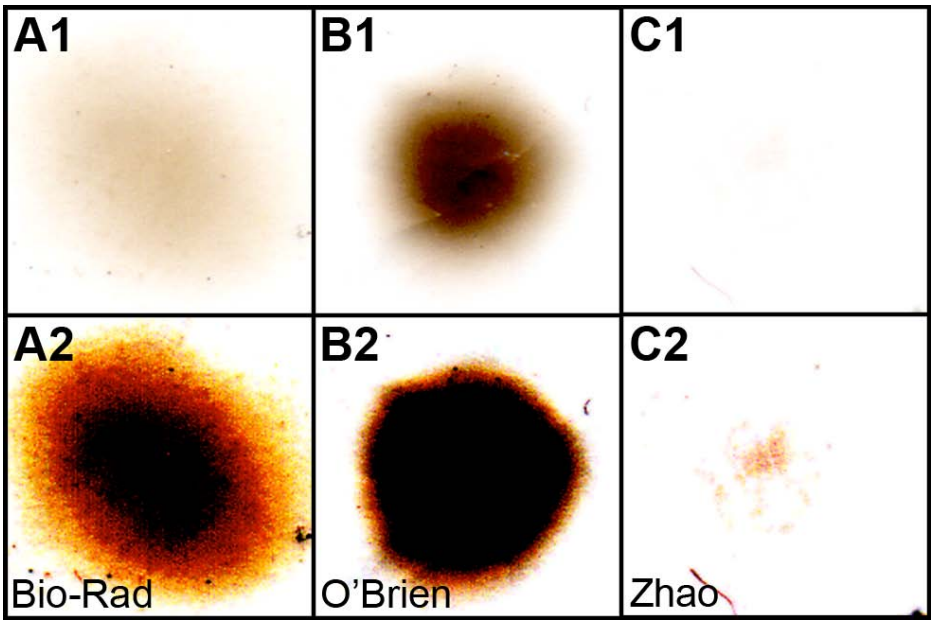

Figure 2.3 – Particle pattern of different biolistics transfection methods.

Millipore diffuser membranes (3 µm) were placed at the sample target position for shooting. After shooting, the diffuser membranes were scanned using a regular flatbed scanner. A1-C1, particle patterns of standard Bio-Rad setup, O'Brien setup, and Zhao setup, respectively. A2-C2, images with increased digital gain showing the much-reduced particle density in Zhao setup (C2). Panels are 6.9 mm wide.

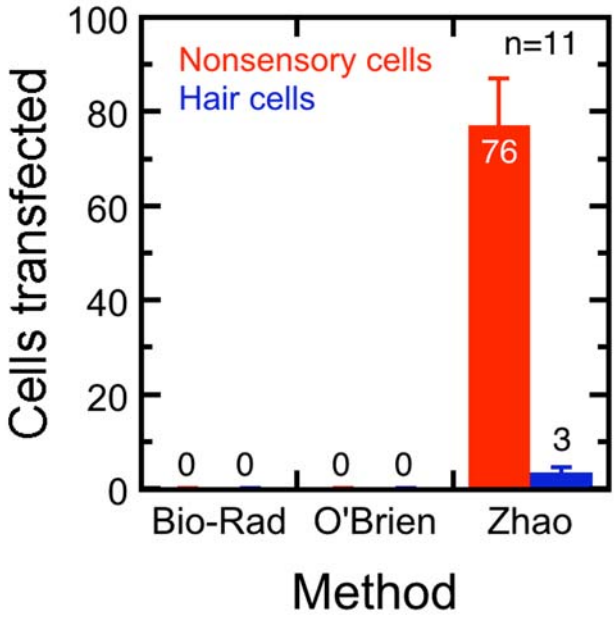

Figure 2.4 – Efficiency of biolistics transfection methods.

Bullfrog sacculi were transfected using the standard Bio-Rad setup, O'Brien setup, and Zhao setup. Sacculi were cultured, fixed and stained, then imaged. Harmonin-EGFP positive cells were counted. The average number of transfected nonsensory cells were shown in red, while the number of transfected hair cells were shown in blue. Error bars represent SEM. Approximate numbers of transfected cells per epithelium are indicated by bars, as is the total number of epithelia analyzed.

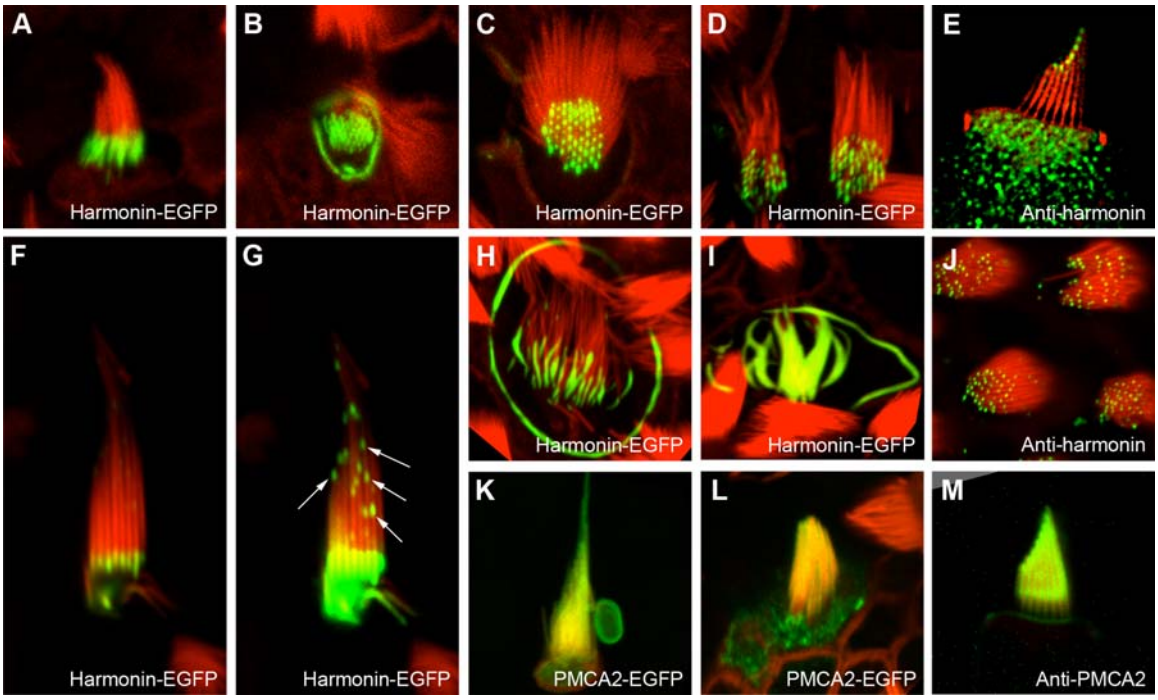

Figure 2.5 – Localization of harmonin-EGFP and PMCA2-EGFP in transfected bullfrog and chick hair cells.

Mouse harmonin b fused with EGFP on the C-terminus (harmonin-EGFP) and frog PMCA2 fused with EGFP on the C-terminus (PMCA2-EGFP) were transfected into frog and chick hair cells using the modified setup. Harmonin-EGFP and PMCA2-EGFP are pseudo-colored green, and phalloidin-stained actin is shown in red, except in panel K, in which co-transfected mCherry-actin is shown in red. A-D, Frog sacculus hair cells transfected with harmonin-EGFP. E, Frog sacculus hair cells labeled with anti-harmonin antibody H3. Structured-illumination image. F, Chick utricle hair cell transfected with harmonin-EGFP; G, Higher digital gain image of E, showing clusters of harmonin-EGFP along the stereocilia (arrows). H-I, chick cochlea hair cells transfected with harmonin-EGFP. J, Frog sacculus hair cells labeled with anti-harmonin antibody H3. K, Live-cell imaging of a chick utricle hair cell transfected with PMCA2-EGFP and mCherry-actin (red). L, Frog sacculus hair cell transfected with PMCA2-EGFP. M, Frog sacculus hair cell labeled with anti-PMCA2a antibody F2a. Panels are 18.4 µm wide.

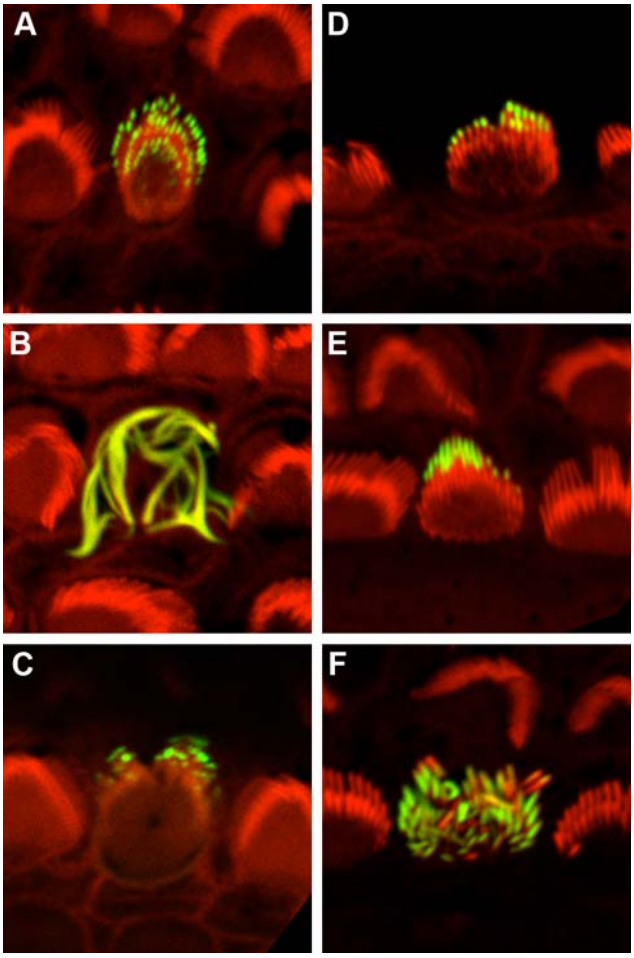

Figure 2.6 – Localization of harmonin-EGFP in transfected mouse cochlea hair cells.

Harmonin-EGFP was transfected into cochlear hair cells of CD1 mice at P4 using the modified biolistics setup. Harmonin-EGFP was localized close to the tips of the stereocilia of both outer (A,C) and inner (D-E) hair cells. In some cases, we saw fused stereocilia in outer hair cells, similar to harmonin-EGFP transfected hair cells in chick cochlea. Panels are 17.6 µm wide.

Chapter 3 – Large Membrane Domains in Hair Bundles Specify Spatially Constricted Radixin Activation

---

Hongyu Zhao[1], Diane E. Williams[1], Jung-Bum Shin[1], Britta Brügger[2], and Peter G. Gillespie[1]

[1]Oregon Hearing Research Center & Vollum Institute, Oregon Health & Science University, Portland, OR 97239, USA

[2]University of Heidelberg, D-69120 Heidelberg, Germany

Corresponding author: Peter G. Gillespie

Oregon Hearing Research Center

L335A / 3181 SW Sam Jackson Pk. Rd.

Portland OR 97239

503-494-2936

gillespp@ohsu.eduGillespie

Abstract

The plasma membrane of vertebrate hair bundles interacts intimately with the bundle cytoskeleton to support mechanotransduction and homeostasis. To determine the membrane composition of bundles, we used lipid mass spectrometry with purified chick vestibular bundles. While the bundle glycerophospholipids and acyl chains resemble those of other endomembranes, bundle ceramide and sphingomyelin nearly exclusively contain short-chain, saturated acyl chains. Confocal imaging of isolated bullfrog vestibular hair cells shows that the bundle membrane segregates spatially into at least three large structural and functional domains. One membrane domain, including the stereocilia basal tapers and ~1 μm of the shaft, the location of the ankle links, is enriched in the lipid phosphatase PTPRQ (protein tyrosine phosphatase Q) and polysialylated gangliosides. The taper domain forms a sharp boundary with the shaft domain, which contains the plasma-membrane Ca2+-ATPase PMCA2 and phosphatidylinositol 4,5-bisphosphate ($PI(4,5)P_2$); moreover, a tip domain has elevated levels of cholesterol, PMCA2, and $PI(4,5)P_2$. Protein mass spectrometry shows that bundles from chick vestibular hair cells contain a complete set of proteins that transport, synthesize, and degrade $PI(4,5)P_2$. The membrane domains have functional significance; radixin, essential for hair-bundle stability, is activated at the taper-shaft boundary in a $PI(4,5)P_2$-dependent manner, allowing assembly of protein complexes at that site. Membrane domains within stereocilia thus define regions within hair bundles

that allow compartmentalization of Ca2+ extrusion and assembly of protein complexes at discrete locations.

Introduction

Extracellular Hair cells, neuroepithelial cells in the inner ear that transduce auditory and vestibular stimuli to electrical currents, provide a remarkable example of correlation of structure with function. Transduction takes place in a dedicated subcellular organelle, the hair bundle, which is composed of 30-300 stereocilia arranged in a precise staircase; each stereocilium contains a paracrystal of actin filaments, sheathed by the hair cell's plasma membrane (Gillespie and Müller, 2009). Mechanical stimuli deflect the bundle and open transduction channels, which admit K+ and Ca2+ from the apical extracellular fluid, endolymph, that bathes the bundle. Bundles remove Ca2+ using the plasma membrane Ca2+-ATPase isoform 2 (PMCA2), a calcium pump that is highly concentrated in stereocilia (Lumpkin and Hudspeth, 1998; Yamoah et al., 1998; Dumont et al., 2001). Phosphatidylinositol 4,5-bisphosphate ($PI(4,5)P_2$), a known regulator of PMCA2 (Hilgemann et al., 2001), also controls transduction and adaptation by hair cells (Hirono et al., 2004).

$PI(4,5)P_2$ is localized in hair cell plasma membranes in a strikingly non-uniform pattern; it is present in stereocilia shafts and concentrated at tips, but is absent from the taper region at stereocilia bases and from the soma's apical surface (Hirono et al., 2004). Protein tyrosine phosphatase receptor type Q (PTPRQ), a phosphatidylinositol phosphatase (Oganesian et al., 2003), presents a near-perfect reciprocal localization pattern to $PI(4,5)P_2$ (Hirono et al., 2004); PTPRQ may therefore maintain low levels of $PI(4,5)P_2$ in the apical surface and basal taper region. Steady-state degradation of

$PI(4,5)P_2$ at tapers by PTPRQ would be a very inefficient way to maintain $PI(4,5)P_2$ distribution in stereocilia; more likely $PI(4,5)P_2$ is segregated into a separate membrane domain (McLaughlin et al., 2002).

In many circumstances, members of the ezrin-radixin-moesin (ERM) family depend on $PI(4,5)P_2$ for triggering a conformation that allows activating phosphorylation (Fehon et al., 2010). Radixin is required for normal hearing in mice (Kitajiri et al., 2004) and humans (Khan et al., 2007). Although radixin has been localized to the taper region in stereocilia (Pataky et al., 2004) and potentially interacts with many functionally significant proteins present in stereocilia (J.B. Shin and P.G. Gillespie, unpublished observations), little is known about the mechanism of activation in stereocilia.

We show here that the lipid composition of the hair bundle's membrane resembles most cellular endomembranes, except that ceramide lipids are unusually rich in N-palmitoyl (16:0) chains. Strikingly, polysialylated gangliosides are found in a micrometer-scale membrane domain at the stereocilia basal tapers that is physically segregated from the shaft/tip $PI(4,5)P_2$ domain; this domain is stable even when cholesterol is extracted. These membrane domains are coextensive with protein domains; PTPRQ and PMCA2 are found respectively in the ganglioside and $PI(4,5)P_2$ domains. Moreover, radixin, essential for hair-cell function, is poised at the taper-shaft boundary and is activated at the border of the $PI(4,5)P_2$ domain. These experiments show that hair bundles have two large membrane domains, at least one of which may

contain additional lipid microdomains, which are likely responsible for compartmentalization of actin dynamics, protein targeting, and mechanotransduction.

Results

Lipid composition of hair-bundle membranes

To determine the lipid composition of hair bundles, purified bundles from E20-21 chick utricles (Gillespie and Hudspeth, 1991; Shin et al., 2007) were subjected to quantitative lipid analysis using nano-electrospray ionization tandem mass spectrometry (Fig. 1). Despite the high sensitivity of mass spectrometry analysis, only by pooling hair bundles from many dissections were we able to readily detect bundle lipids. Each analysis (n=6) used bundles from 100 chicken ears (~1 μg protein for each preparation); given the average size of a chick utricle stereocilium (0.25 x 5 μm), number of stereocilia per cell (~60), and bundles recovered per ear (~8000, or 40%), we calculated a theoretical amount of 10 pmol/ear, which is in good agreement with the experimentally determined value of ~8 pmol/ear. Phosphatidylcholine (PC), cholesterol, and phosphatidylethanolamine (PE) accounted for 86% of the lipid detected; phosphatidylserine (PS), sphingomyelin (SM), and phosphatidylinositol (PI) together made up 12%. Phosphatidylglycerol (PG), ceramide (Cer), and hexosylceramide (HexCer) were also detected as minor species. We detected 182 lipid species, 76 of which accounted for 96% of the total lipid species (Figure 3.1).

Comparison with lipids of utricular epithelia revealed that the overall lipid class composition of hair bundles did not differ significantly from the whole organs, except for PI, which was higher in the epithelium (Figure 3.1B). However, individual lipid classes, significant differences were observed in the species distributions for

sphingolipids and glycerophospholipids. In hair bundles, SM and Cer species nearly exclusively contained short chain, saturated N-palmitoyl (16:0) acyl chains. For example, the 16:0 species of Cer accounted for 73% of all Cer in bundles, 33% in epithelium, but only 2% in porcine brain (B. Brügger, unpublished observations). Moreover, epithelial lipids show an unusual broad distribution of sphingolipid species. For PC and PE, hair bundles were enriched in arachidonoyl-containing species (36:4, 38:4 and 40:4), while docosahexaenoic-containing species (38:6 and 40:6) of PS were elevated in bundles as compared to epithelium.

Membrane domains in hair bundles

We localized lipid domains of hair bundles using isolated bullfrog hair cells; the stereocilia of these cells have a large diameter (~0.4 μm), permitting unusually clear visualization of individual stereocilia, basal stereocilia tapers, and other structures. We confirmed that $PI(4,5)P_2$ segregates within hair bundles, as we previously reported (Hirono et al., 2004); because bullfrog hair cells are recalcitrant to transfection, we used immunostaining to show that $PI(4,5)P_2$ was absent from the basal taper region but found throughout the remainder of the hair bundle (Figure 3.2C).

Gangliosides, which are sialic acid-modified, ceramide-based glycosphingolipids, have often been associated with cell signaling and membrane domains (Sonnino et al., 2007) (see Figure 3.4D). To probe for gangliosides in stereocilia, we used cholera toxin B subunit (CTB), which binds to many gangliosides but particularly tightly to GM1 (Kuziemko et al., 1996). Under standard conditions, CTB binding sites were absent from hair bundles (Figure 3.2A); however, pretreatment of isolated hair cells with

neuraminidase, which converts polysialylated gangliosides to GM1 (Rauvala, 1979), markedly increased the ability of CTB to label bundles (Figure 3.2B). Neuraminidase-dependent labeling extended from the apical surface of the hair cell, through the stereocilia taper region, and terminating a micrometer or so above the tapers in the region of the ankle links; the region labeled with CTB was exactly reciprocal of the $PI(4,5)P_2$ domain. This pattern was observed in at least 95% of isolated hair cells, in more than 15 separate experiments. The lateral membrane, segregated from the apical membrane by the remnants of the tight junctions, had much lower levels of neuraminidase-dependent CTB labeling.

Both boiling the CTB and preincubation with excess GM1 ganglioside eliminated labeling in bundles. While not labeling as strongly as CTB, an antibody specific for GM1 ganglioside gave a similar pattern after neuraminidase treatment (Figure 3.3A). We were unable to identify the specific ganglioside species responsible for the taper labeling. Although antibodies against GD1a and GT1a, two polysialylated GM1 relatives, gave no hair-bundle signal, cells potentially have many polysialylated gangliosides that can be converted into GM1 (Figure 3.4D). Methyl-β-cyclodextrin (MβC), which extracts cholesterol and often disrupts ganglioside-containing lipid domains (Simons and Sampaio, 2011), did not disrupt the basal ganglioside domain (Figure 3.3E).

We usually detected gangliosides with a two-step procedure, first labeling with CTB, then amplifying the signal with an anti-CTB antibody (Fra et al., 1994; Harder et al., 1998). While useful for its sensitivity, the method can generate artificially large ganglioside domains due to antibody crosslinking (Harder et al., 1998). The taper-region

ganglioside domain was readily detected, however, when live (or fixed; not shown) hair cells were labeled with CTB modified with Alexa 488, without anti-CTB antibody (Figure 3.3B). Crosslinking CTB molecules with anti-CTB had little effect on the taper ganglioside domain, although some increase in punctate labeling was seen in stereocilia shafts (Figure 3. 3C).

Stereocilia tips also show lipid segregation. We used the antibiotic filipin, a fluorescent cholesterol-binding molecule, to localize cholesterol within hair cells (Bornig and Geyer, 1974). As seen in a previous electron microscopy study (Jacobs and Hudspeth, 1990), filipin strongly stained stereocilia tips (Figure 3.2D,G). Filipin-detected cholesterol was present in stereocilia shafts, but appeared more abundant in the soma's apical surface.

PI(4,5)P_2 pathway in hair-bundle membranes

As PI(4,5)P_2 is usually synthesized locally within cells, we used protein mass spectrometry to identify membrane proteins, as well as proteins involved in membrane trafficking and lipid synthesis in hair bundles (Figure 3.4A). As with lipid mass spectrometry, we used bundles purified from E20-E21 chick utricles. Using intensity-weighted spectral counting (Shin et al., 2007; Spinelli et al., 2012), we estimated that the 4 μm-2 plasma membrane of each stereocilium contained ~7,000 transmembrane proteins, ~10,000 peripheral membrane proteins, and ~1,000 lipid transfer molecules.

Proteins associated with PI(4,5)P_2 metabolism were readily detected in hair bundles (Figure 3.4B-C,E). Lipid transfer proteins included ~120 molecules/stereocilium of phosphatidylinositol transfer protein alpha (PITPNA), which is thought to shuttle PI within cells. We also detected ~10 molecules/stereocilium each of type III alpha phosphatidylinositol 4-kinase (PIK4CA) and type II beta phosphatidylinositol-5-phosphate 4-kinase (PIP5K2B), kinases that sequentially transform PI to PI(4,5)P_2; type I alpha phosphatidylinositol-5-phosphate 4-kinase (PIP5K1A) was also detected. In yeast, the PIK4CA ortholog

Stt4 is anchored to the membrane by the scaffolding protein Ypp1 and the integral membrane protein Efr3a (Baird et al., 2008); we detected the orthologs TTC7A (by SEQUEST only) and EFR3A (by both search algorithms) in bundles. Finally, stereocilia contained ~3000 molecules of PTPRQ, the principal PI(4,5)P_2 phosphatase in hair bundles. The relative abundances of these proteins was also reflected by the spectral count tally for each in the complete dataset (Figure 3.4B). Although antibodies against PIK4CA and PIP5K2B were insufficiently sensitive to detect these proteins by immunocytochemistry, we readily detected PIPTNA, present in a punctate pattern throughout stereocilia (data not shown), and PTPRQ (Figure 3.5). Thus a complete pathway for transport, synthesis, and hydrolysis of PI(4,5)P_2 is present in hair bundles (Figure 3.4C).

Although we did not detect any glycosphingolipid synthetic enzymes in stereocilia using mass spectrometry, these glycolipids are usually synthesized in the ER and Golgi, then transported to plasma membrane. While glycosphingolipids are usually degraded in lysosomes, we detected several enzymes of the pathway for metabolizing polysialylated gangliosides, including GLB1 (β-galactosidase), HEXA (β-hexosaminidase alpha), and NAGA (N-acetylgalactosaminidase) (Figure 3.4D-E).

Membrane proteins respect the glycosphingolipid domain

The stereocilia transmembrane proteins PMCA2 and PTPRQ localized respectively to the PI(4,5)P_2 and glycosphingolipid domains. In isolated bullfrog hair cells, PMCA2 labeling extended through the upper part of stereocilia shafts, but was reduced substantially in the glycosphingolipid zone, the bottom 2 μm of the stereocilia (Figure 3.5A, C). This PMCA2 localization was not an artifact of cell isolation, as cells in wholemount bullfrog sacculus tissue, folded to allow high-resolution imaging, displayed similar localization (Figure 3.5B). When cells were co-labeled with the PMCA2 antibody and CTB, PMCA2 and gangliosides did not overlap significantly (Figure 3.5C).

While PMCA2 was always excluded from the glycosphingolipid domain, the pattern of labeling seen in the upper domain varied remarkably. Stereocilia tip labeling

was usually stronger than that of shafts; labeling often diminished ~1 µm below stereocilia tips, then increased near the taper region. This pattern was seen with monoclonal and polyclonal antibodies against PMCA2, and was not seen with antibody against NHE9, another stereocilia membrane protein (Hill et al., 2006). Remarkably, the PMCA2 labeling pattern appeared continuous between adjacent stereocilia, as if localization was coordinated across the gap.

As reported previously (Hirono et al., 2004), PTPRQ was located at the base of the stereocilia; PTPRQ and CTB labeling overlapped extensively (Figure 3.5D), although CTB punctae seen in upper parts of stereocilia shafts apparently contained little or no PTPRQ.

$PI(4,5)P_2$ at the taper-shaft boundary activates radixin

The membrane-to-actin crosslinker radixin, a member of the ezrin-radixin-moesin (ERM) family, is concentrated at basal tapers (Pataky et al., 2004), although not as exclusively as is PTPRQ (Figure 3.6A). Mass spectrometry indicates that the ~6000 molecules of radixin per stereocilium accounts for >97% of total bundle ERM proteins (J.B. Shin and P.G. Gillespie, unpublished observations). As shown previously (Pataky et al., 2004), starting at the base of a hair bundle, radixin rose in concentration to a point ~1 µm from the apical surface, then fell exponentially towards stereociliary tips (Figure 3.6D-E).

Radixin interacts with membranes and membrane proteins only after activation, which requires sequential $PI(4,5)P_2$ binding and phosphorylation on T564 (Fehon et al., 2010). Once activated, radixin not only links membrane and cytoskeleton, but coordinates

cellular activities by scaffolding signaling components (Neisch and Fehon, 2011). In hair bundles, radixin may interact with a large network of candidate partners identified by network analysis, including overlapping interaction with SLC9A3R2 (NHERF2) and RHOA networks (J.B. Shin and P.G. Gillespie, unpublished observations).

To examine phosphoradixin distribution in stereocilia, we used a phosphospecific antibody selective for ERM proteins phosphorylated on the activating threonine (T564 for radixin). Remarkably, phosphorylated radixin was only detected above the basal tapers (Figure 3.6B-D). The boundary was sharp and corresponded to the taper-shaft membrane-domain boundary. Above the boundary, phosphorylated radixin was elevated in a band about ~0.5 μm wide, then declined exponentially towards stereocilia tips; taller stereocilia had more intense, more extensive labeling (Figure 3.6B-D). Notably, this band was located near the ankle links and a concentration of myosin-VIIA (MYO7A) (Hasson et al., 1997), although the phosphoradixin band only partially overlapped with the MYO7A band (Figure 3.6D).

To demonstrate the dependence of the phosphoradixin zone on $PI(4,5)P_2$, we depleted $PI(4,5)P_2$ using the PI(4)P kinase inhibitor phenylarsine oxide (PAO). As previously reported (Hirono et al., 2004), PAO effectively reduced $PI(4,5)P_2$ levels in hair bundles (Figure 3.7G-I). Likewise, PAO reduced the level of phosphoradixin by almost 60% (Figure 3.7A-B,I). Although PAO also affects enzymes other than PI(4)P kinase, our result is consistent with the hypothesis that localized phosphoradixin formation depends on $PI(4,5)P_2$. In addition, PAO treatment destabilized radixin, as total radixin in bundles declined by ~50%. This result suggests that a substantial fraction of radixin in bundles is

phosphorylated, and when dephosphorylated, it exits bundles. PAO had no effect on the distribution or abundance of PMCA2 or PTPRQ (Figure 3.7C-F).

Discussion

Hair bundle lipid composition

The lipid composition of stereocilia membranes is similar to that of other cellular membranes; PC and cholesterol make up the bulk of the lipids, with PE, PS, SM, and PI each contributing 3% or more to the total. Acyl chains are mixed between the relatively short and saturated 34:1 PC and 16:0 SM chains, and longer unsaturated chains predominant in PE, PS, and PI. Although mass spectrometry cannot determine the leaflet distribution of each component, stereocilia devote substantial effort to properly maintaining phospholipid asymmetry (Shi et al., 2007; Goodyear et al., 2008). Indeed, the ATP8B1 P type transporter, proposed to be responsible for translocating lipids from the extracellular to intracellular leaflet, is essential for hearing (Stapelbroek et al., 2009) and is readily detected by mass spectrometry in chick utricle hair bundles (J.B. Shin and P.G. Gillespie, unpublished observations).

Several key lipids were not detected in our analysis. $PI(4,5)P_2$ is typically present at much lower levels than PI; moreover, isolated hair bundles likely deplete ATP rapidly, preventing synthesis of $PI(4,5)P_2$, and PTPRQ may exhaust remaining $PI(4,5)P_2$ before bundles can be isolated and degradation stopped. Thus the concentration of PI measured likely reflects the total PI + PI(4)P + $PI(4,5)P_2$ in intact bundles. Glycosphingolipids are not readily detected by mass spectrometry because of their scarcity and diversity; together, they account for only a few percent of all lipids, and over 100 distinct glycosphingolipid species have been identified (Hakomori, 2004).

Although lipidomics with high-resolution mass spectrometers allows direct detection of gangliosides (Sampaio et al., 2011), the total amount of lipid in bundles and levels of gangliosides are too low for detection at present.

Two membrane domains in stereocilia

We show here that stereocilia membranes are divided into at least three large domains, each containing specific lipids and proteins. Glycosphingolipids and PTPRQ are enriched in the taper domain, which extends from a micrometer or so above the stereocilia tapers to the apical surface of the hair cell. While glycosphingolipids are prominent in so-called membrane rafts (Edidin, 2003; Simons and Sampaio, 2011), insensitivity of the taper domain to cyclodextrins suggests that cholesterol is not necessary for its stability. Although cholesterol is typically a component of rafts, gangliosides can form separate domains with sphingomyelin but without cholesterol (Ferraretto et al., 1997). Above basal tapers, $PI(4,5)P_2$ and PMCA2 are enriched in the shaft domain; however, $PI(4,5)P_2$ and PMCA2 both appear clustered within stereocilia shafts and are further concentrated at stereocilia tips along with cholesterol, suggesting that additional segregation of membrane components occurs. Distribution of PMCA2 and PTPRQ into shaft and taper domains did not depend on CTB, CTB antibody, neuraminidase, or cell dissociation.

The membrane domains reported here are unusually large. Although lipid domains have long been detected in artificial vesicles and in native cells (Klausner et al., 1980), stable lipid clustering on a micrometer scale is not typically seen in native cells (Simons and Sampaio, 2011). The extent and appearance of the stereocilia membrane

domains could have been affected by our detection techniques, as the two-step detection could cluster CTB pentamers by antibody crosslinking. However, the glycosphingolipid domain was readily visible using CTB alone, with fixed or live cells, which demonstrates that glycosphingolipids were clustered prior to CTB treatment. If preexisting ganglioside domains were not present, CTB could not induce formation of a continuous, large-scale phase in stereocilia (Lingwood et al., 2008).

Physical basis of membrane domains

Lateral lipid segregation can occur due to structural dissimilarity of domains' lipid acyl chains. Hair-bundle gangliosides consist of an unusually high fraction of N-palmitoyl (16:0) species; both ceramide, the precursor for all gangliosides, and its metabolite sphingomyelin predominantly have a 16:0 N-acyl chain (Fig. 1). By contrast, brain ceramide lipids are predominantly composed of 18:0 or longer N-acyl chains (Ben-David and Futerman, 2010). Strikingly, the utricular epithelium as a whole is far more enriched than bundles in long-chain species of ceramide and sphingomyelin (Figure 3.1B). Sphingolipids (e.g., sphingomyelin, ceramide, and gangliosides) readily form segregated membrane domains due to ceramide-moiety hydrogen bonding, polar headgroup interaction, and acyl chain mismatch with glycerophospholipids (Masserini and Ravasi, 2001); the preponderance of N-palmitoyl species in bundles would enhance this latter effect (Holopainen et al., 2001). Together these physical features may promote lateral membrane segregation of gangliosides in hair bundles, presumably along with ceramide and sphingomyelin.

Extensive on the apical surface, it is curious that gangliosides do not extend fully throughout the stereocilia, as shown with CTB labeling. Some mechanism must control the balance of sphingolipids and glycerophospholipids in the apical membrane. Gangliosides are typically thought to be localized on convex surfaces, as their bulky headgroup and compact acyl chains gives them a wedge-like shape. Although the stereocilia external leaflet is highly concave where the taper enters the apical surface of the hair cell, this highly concave region is quite small and likely cannot be resolved by light microscopy. Localization of PTPRQ to stereocilia bases has been proposed to depend on active transport by myosin-VI (MYO6) (Sakaguchi et al., 2008), so presence of glycosphingolipids within the basal taper region could plausibly depend on PTPRQ, particularly if the structure of PTPRQ's transmembrane domain favored binding of short, saturated acyl chains. The glycosphingolipid domain remained even when PTPRQ was internalized, however, suggesting that once the domain formed, it was relatively stable.

Spatial constriction of radixin activation

A primary role for the hair-bundle membrane domains may be to allow precise spatial activation of radixin at the position where the ganglioside and $PI(4,5)P_2$ domains meet. While total radixin was abundant in the stereocilia taper region, we only saw phosphoradixin beginning at the ganglioside-$PI(4,5)P_2$ boundary; only there should $PI(4,5)P_2$ be present at high enough levels to preactivate radixin, allowing activating phosphorylation by an unknown kinase. Indeed, the phosphoradixin profile seen in bundles can be modeled accurately as the $[pRDX] = [RDX]2 \bullet [PI(4,5)P_2]2$ (Figure 3.8A), suggesting that phosphoradixin formation depends steeply on the concentrations of

radixin and PI(4,5)P_2 . Moreover, the presence of ceramide in the taper domain could also promote radixin dephosphorylation, as is the case for ezrin (Canals et al., 2010). This phosphoradixin activation zone recalls the concentration of phospho-ERM proteins towards microvillar tips, despite the presence of total ERM proteins throughout a microvillus (Hanono et al., 2006).

Based on recruitment of the PDZ-domain protein SLC9A3R1 by ERM proteins in microvilli (Reczek et al., 1997), once stereocilia radixin is activated, we speculate that it recruits the paralog SLC9A3R2, which is present at a concentration close to that of radixin (J.B. Shin and P.G. Gillespie, unpublished observations). SLC9A3R2, in turn, may bind to many important stereocilia proteins (J.B. Shin and P.G. Gillespie, unpublished observations). In addition, as in other systems (Fehon et al., 2010), activated radixin may bind directly to other membrane proteins, serving as a actin-membrane connector. The role of ERM proteins is so important that in radixin's absence, hair cells upregulate the paralog ezrin, partially compensating for radixin's loss (Kitajiri et al., 2004).

Corralling PI(4,5)P_2 with glycosphingolipids

The bundle contains far more PTPRQ, which degrades PI(4,5)P_2 , than it does the PI(4,5)P_2 synthetic enzymes PIK4CA, PIP5K2B, and PIP5K1A. While turnover numbers for these enzymes are not known, if PI(4,5)P_2 freely interacted with PTPRQ, present at a concentration >100-fold greater than the synthetic enzymes, it would be readily hydrolyzed. The glycosphingolipid domain may therefore act as a physical barrier to prevent PI(4,5)P_2 exchange between the hair bundle and apical surface; PI(4,5)P_2 might enter the domain infrequently because of structural mismatch with glycosphingolipid

domain, but PTPRQ would be present to mop up those $PI(4,5)P_2$ molecules that did manage to penetrate the basal taper compartment.

Are there reasons for compartmentalization of $PI(4,5)P_2$ in stereocilia beyond phosphoradixin activation? $PI(4,5)P_2$ levels in the apical surface may fluctuate as exocytosis occurs, as fusion of vesicles with the plasma membrane is associated with $PI(4,5)P_2$ synthesis. By contrast, $PI(4,5)P_2$ controls transduction and adaptation (Hirono et al., 2004), as well as other critical molecules such as PMCA2. Formation of a discrete stereocilia $PI(4,5)P_2$ domain using the glycosphingolipid physical barrier thus allows precise activity control through $PI(4,5)P_2$ levels.

Gangliosides play an essential role in the inner ear; mice with a null mutation in GM3 synthase (SATI), which is essential for formation of most ganglioside species, transiently show some responses in an auditory brainstem response (ABR) assay; however, all knockout mice are deaf by P17 (Yoshikawa et al., 2009). The ganglioside defect could be in stereocilia; likewise, PTPRQ null mice show progressive hearing loss that is complete by several weeks of age (Goodyear et al., 2003). We thus suggest that the basal taper domain, consisting of glycosphingolipids and PTPRQ (Fig. 8B), is essential for hair-cell function, presumably by segregating $PI(4,5)P_2$, PMCA2, and other stereocilia components away from the soma's apical surface and allowing radixin activation in a spatially precise manner.

Experimental Procedures

Materials. Sigma-Aldrich (St. Louis, MO) was the source for: protease type XXIV, cholera toxin B subunit (#C9903), neuraminidase (#N2876), DNase I, carbenicillin, BSA, FITC-phalloidin, TRITC-phalloidin, filipin (type III), methyl-b-cyclodextrin, and phenylarsine oxide (#P3075). The mouse anti-cholera toxin B antibody was from AbD Serotec (Raleigh, NC; #9540-0108). Formaldehyde (16% stock, in sealed ampules) and glutaraldehyde (8% stock in sealed ampules) was obtained from Electron Microscopy Sciences (Hatfield, PA). DME/F12 medium was from Thermo Scientific HyClone (Logan, UT; #SH30023.01). Buffers, salts, and other solution components were of the highest quality available. The PTPRQ antibody was a gift of Guy Richardson, University of Sussex, UK); PMCA2a was detected using antibody F2a (Dumont et al., 2001). Radixin was detected with #H00005962-M06 mouse monoclonal antibody from Abnova (Walnut, CA); phospho-ERM was detected using #3149 from Cell Signaling Technology (Danvers, MA).

Lipid mass spectrometry. Lipid and protein mass spectrometry used E20-21 chick utricles of either sex. Hair bundles were purified from utricles by the twist-off technique (Gillespie and Hudspeth, 1991; Shin et al., 2007). To obtain utricular sensory epithelia, otoconia and otolithic membranes were removed from dissected utricles; the epithelium was then peeled off the basement membrane using an eyelash.

Lipids were extracted from hair bundles and epithelial fractions using an acidic organic phase (Bligh and Dyer, 1959) in all cases except for plasmalogens, which were

extracted under neutral conditions. Quantitative analyses of lipids by nano-electrospray ionization tandem mass spectrometry (nano-ESI-MS/MS) were performed as described (Brügger et al., 2006). Lipid analysis was done in positive ion mode on a QII triple quadrupole mass spectrometer (Waters), equipped with a nano Z-spray. Cone voltage was set to 30 V. Phosphatidylcholine and sphingomyelin detection was performed by precursor ion scanning for fragment ion 184 Da at a collision energy of 32 eV. Neutral loss scanning of m/z 141 Da, 185 Da, 189 Da or 277 Da, respectively, was applied for the analyses of phosphatidylethanolamine, phosphatidylserine, or phosphatidylinositol, employing a collision energy of 20 eV, except for phosphatidylinositol where a collision energy of 30 eV was applied. Precursor ion scanning of m/z 364, 390 and 392 was used for detection of plasmalogen species, employing a collision energy of 20 eV. Hexosylceramide and ceramide were detected by precursor ion scanning for fragment ion 264 Da at a collision energy of 35 eV and 30 eV, respectively. Cholesterol was analyzed as an acetate derivate as described (Liebisch et al., 2006).

Protein mass spectrometry. Purified hair bundles were analyzed by mass spectrometry as described (Shin et al., 2010). Label-free protein quantitation used MS2 intensities (Spinelli et al., 2012) divided by molecular mass, normalized to the sum of all intensity/molecular mass; these normalized molar intensities (im) are proportional to the mole fraction of each protein (J.B. Shin and P.G. Gillespie, unpublished observations). Data analyzed here were from a SEQUEST-X! Tandem analysis (J.B. Shin and P.G. Gillespie, unpublished observations).

Hair cell isolation and immunocytochemistry. Hair cells were isolated from saccular epithelia of bullfrogs of either sex using previously described methods (Hirono et al., 2004) in low-Ca2+ saline: 112 mM NaCl, 2 mM KCl, 2 mM MgCl2, 100 µM CaCl2, 3 mM D-glucose, and 10 mM HEPES at pH 7.4. Briefly, sacculi were treated with 1 mM EGTA for 15 min, then 75 µg/ml protease XXIV (Sigma) for 30 min. After a 5 min treatment with 100 µg/ml DNase I, the cells were isolated from the epithelium using an eyelash.

For standard immunocytochemistry, cells were fixed with 4% formaldehyde in low-Ca2+ saline, washed, blocked in PBS with 1% normal donkey serum, 1% BSA, and 0.2% saponin, then incubated overnight at 4°C with primary antibodies in the blocking solution. Cells were washed, then treated with secondary antibodies (7.5 µg/ml) and 0.25 µM FITC-phalloidin. All samples were observed with an Olympus FV1000 confocal microscope equipped with a 60x, 1.42 NA oil plan apochromat objective.

The rabbit anti-PTPRQ antibody (affinity purified, against the C-terminus) was used at 1:250; PMCA2a was detected using 10 µg/ml F2a, generated in rabbit. Radixin was detected with 5 µg/ml #H00005962-M06 mouse monoclonal antibody; phospho-ERM was detected using 0.65 µg/ml Cell Signaling #3149, generated in rabbit.

Cholera toxin B subunit labeling and neuraminidase treatment. Isolated cells were fixed with 4% formaldehyde in low-Ca2+ saline, washed thoroughly with low-Ca2+ saline, then treated with neuraminidase for 30 min. Neuraminidase was diluted to 0.8 U/ml with 0.1 M potassium acetate pH 4.5, then mixed 1:1 with low-Ca2+ saline bathing the hair cells so the final concentration was ~0.4 U/ml and the final pH was ~4.6. After

washing cells, they were treated with 10 μg/ml cholera toxin B subunit (CTB) in PBS for 15 min. The cells were washed, then incubated with a mouse anti-CTB antibody in PBS for 15 min. The cells were washed, post-fixed with 4% formaldehyde in PBS for 15 min, washed again, then blocked, permeabilized, and treated with secondary reagents as above.

Other methods. Labeling of $PI(4,5)P_2$ in bullfrog hair cells was carried out as described (Hirono et al., 2004). For phenylarsine oxide (PAO) treatment, hair cells were isolated in low-Ca2+ saline. After letting cells settle for 15-20 min at RT, cells were washed with 75% DME/F12 medium with 18.75 μg/ml carbenicillin. Hair cells were treated with 30 μM PAO in the same medium for 1.5 hr at RT (21-22°C), then washed three times with PBS and fixed. PAO was stored as a 20 mM stock solution in DMSO. Control cells were treated with 0.15% DMSO.

Filipin was made as a 5 mg/ml stock in DMSO. Hair cells were isolated as usual, then fixed with 0.75% glutaraldehyde, 2.25% formaldehyde in PBS. After washing 3x with PBS, cells were stained for 2 hr with 25 μg/ml filipin and TRITC-phalloidin. Filipin was excited using a 405 nm laser. Methyl-β-cyclodextrin (MβC) was diluted from a 2 M stock in water to a final concentration of 10 mM.

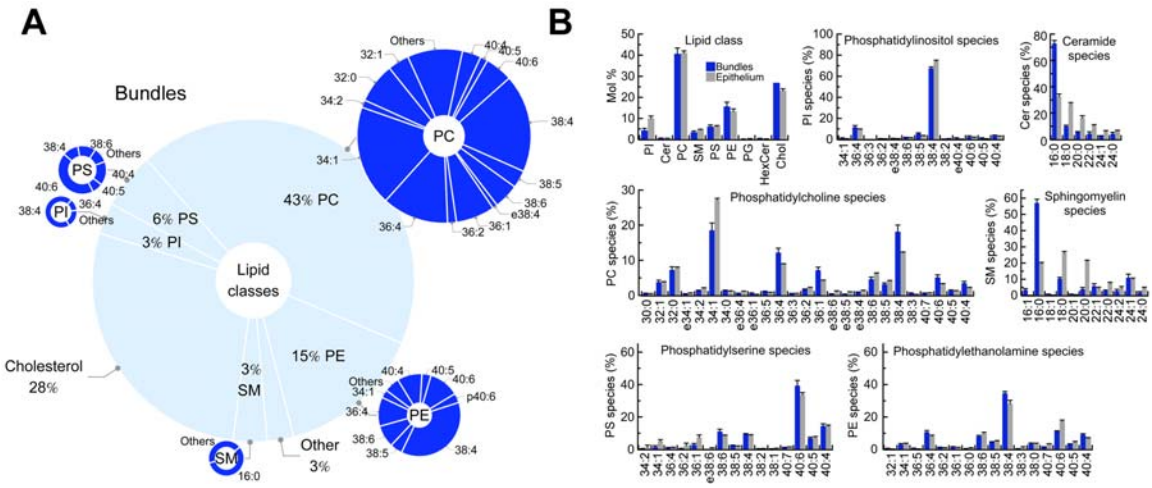

Figure 3.1 – Hair-bundle structural domains and lipid composition.

A, Lipid composition of chick utricle hair bundles. Inner light blue pie graph indicates distribution of phospholipids, sphingomyelin, and cholesterol (mol% indicated); "Other" includes ceramide, hexosylceramide, and phosphatidylglycerol. Dark blue pie graphs indicate acyl chain compositions for the indicated lipid species (for phospholipids, the sum of the two acyl chains (denoted by number of total C atoms in both fatty acids : number of total double bonds in both fatty acids). In addition to the indicated acyl chain, sphingolipids also contain a C18 sphingosine backbone. B, Species distributions for hair bundles and utricular epithelium. Mol% in "Lipid Class" panel is calculated as moles of indicated lipid divided by moles of all lipids analyzed; % in individual lipid panels refers to moles of indicated acyl-chain species divided by total moles of that lipid class. Abbreviations: PC, phosphatidylcholine; PI, phosphatidylinositol; PS, phosphatidylserine; PE, phosphatidylethanolamine; and SM, sphingomyelin. Mean ± SEM (n=6 for each) are indicated.

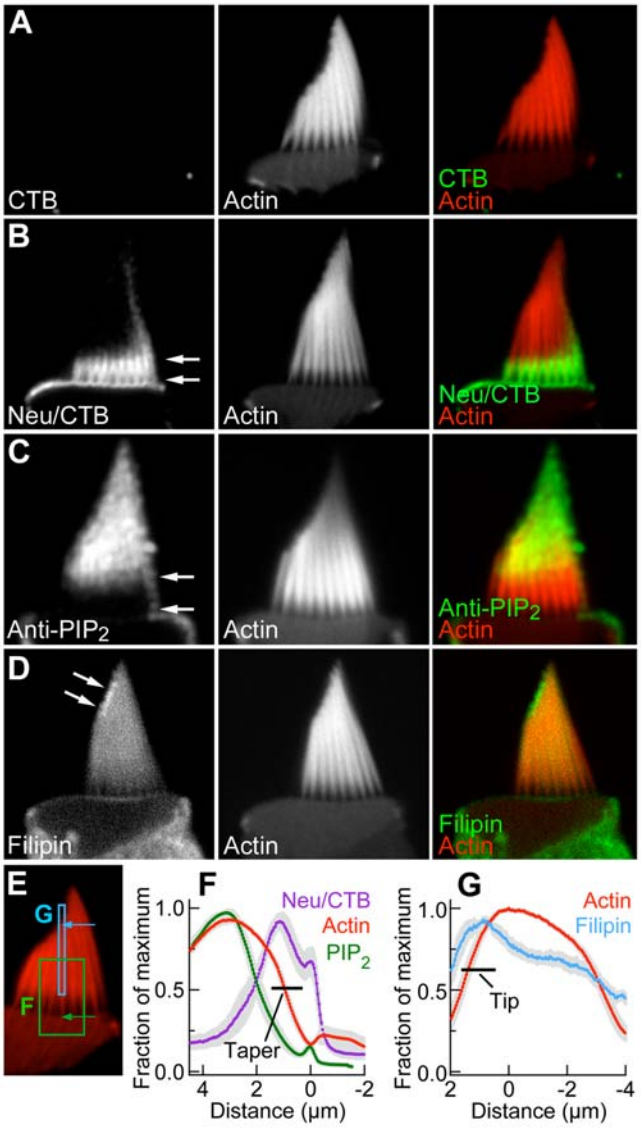

Figure 3.2 – Membrane domains in bullfrog hair bundles.

A, Little CTB labeling without neuraminidase treatment. B, Pretreatment with neuraminidase greatly enhances CTB labeling, particularly in basal taper region (delineated by arrows); hair-cell apical surface labeling was also enhanced. CTB antibody used for detection in A-B. C, PI(4,5)P_2 antibody labeling. In this and other figures PI(4,5)P_2 is abbreviated PIP_2. D, Filipin labeling. Panels A-D show isolated bullfrog hair cells; panel widths are all 12.5 μm. E, Approximate positions of regions used for profile averaging. F, Profile averages for CTB (n=7), actin (n=7), and PI(4,5)P_2 (n=6). Colored points indicate mean, gray shading is ± SEM. Profiles of individual cells were aligned to the dip in actin staining at the taper; this point was defined to be zero on the abscissa. G, Profile averages for filipin-stained cells (n=11). Profiles were aligned to the peak of actin staining, which is near stereocilia tips; this point was defined to be zero on the abscissa.

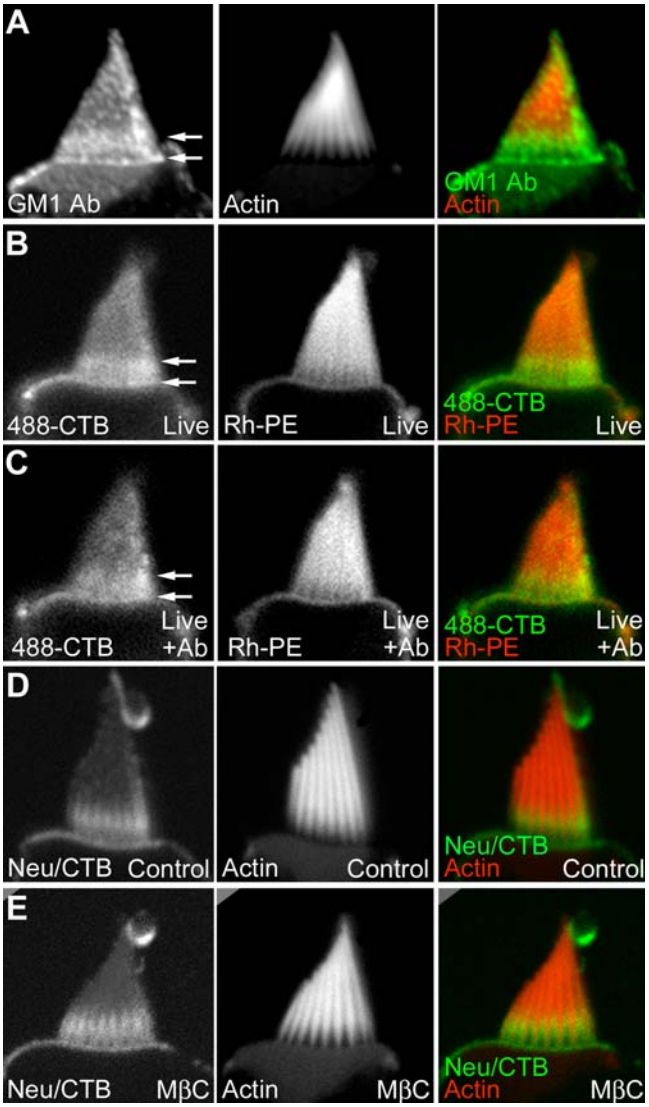

Figure 3.3 –Ganglioside domain controls.

A, Taper domain is visible with antibody against GM1 ganglioside (after neuraminidase treatment). As seen with some cells labeled with CTB (e.g., panels D and E), the lower half of the kinociliary bulb was labeled. B, After neuraminidase treatment, the taper ganglioside domain is visible in live hair cells treated with rhodamine-phosphatidylethanolamine (Rh-PE) to label membranes and Alexa 488-cholera toxin B chain (488-CTB) to label gangliosides. C, Additional treatment of cell in (B) with anti-cholera toxin antibody does not change the 488-CTB pattern appreciably. D, Control hair cell labeled with CTB after neuraminidase treatment. CTB antibody used for detection. E, Hair cell treated with 10 mM MβC for 40 minutes to extract cholesterol. The taper ganglioside domain is not disrupted. As seen occasionally, the lower halves of the kinociliary bulbs of the cells in D and E were also labeled with CTB.

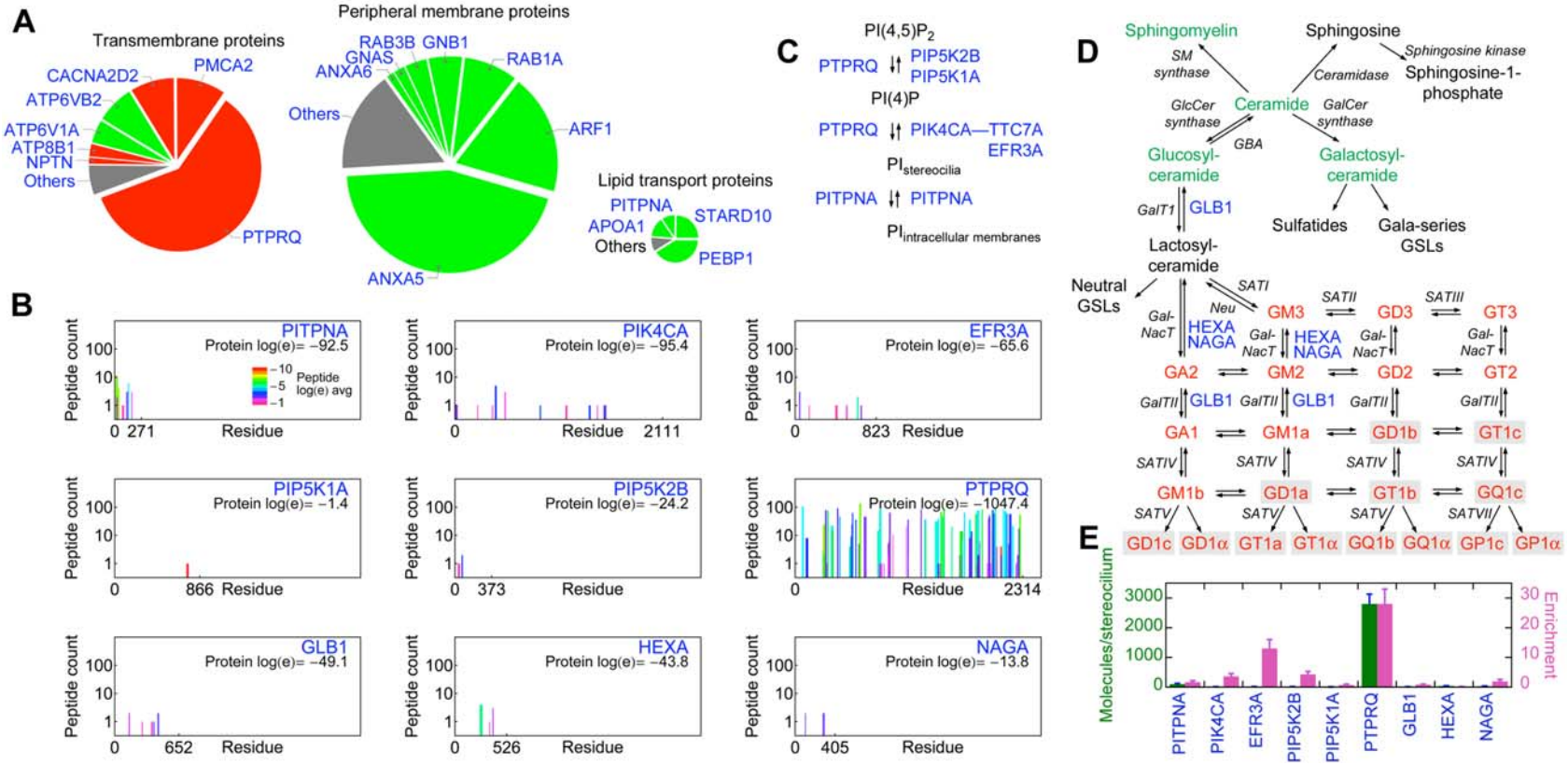
A
Transmembrane proteins
PMCA2
CACNA2D2
ATP6VB2
ATP6V1A
ATP8B1
NPTN
Others
PTPRQ
Peripheral membrane proteins
RAB3B
GNB1
GNAS
ANXA6
RAB1A
Others
ARF1
ANXA5
Lipid transport proteins
PITPNA
STARD10
APOA1
Others
PEBP1
B
PITPNA
Protein log(e)= −92.5
Peptide log(e) avg
−10
−5
−1
PIK4CA
Protein log(e)= −95.4
EFR3A
Protein log(e)= −65.6
PIP5K1A
Protein log(e)= −1.4
PIP5K2B
Protein log(e)= −24.2
PTPRQ
Protein log(e)= −1047.4
GLB1
Protein log(e)= −49.1
HEXA
Protein log(e)= −43.8
NAGA
Protein log(e)= −13.8
Peptide count
Residue
C
PI(4,5)P2
PTPRQ
PIP5K2B
PIP5K1A
PI(4)P
PTPRQ
PIK4CA—TTC7A
EFR3A
PIstereocilia
PITPNA
PITPNA
PIintracellular membranes
D
Sphingomyelin
Sphingosine
SM synthase
Ceramidase
Sphingosine kinase
Sphingosine-1-phosphate
GlcCer synthase
Ceramide
GalCer synthase
GBA
Glucosyl-ceramide
Galactosyl-ceramide
GalT1
GLB1
Sulfatides
Gala-series GSLs
Lactosyl-ceramide
Neutral GSLs
SATI
Neu
SATII
SATIII
Gal-NacT
HEXA
NAGA
GM3
GD3
GT3
GA2
GM2
GD2
GT2
GalTII
GLB1
GA1
GM1a
GD1b
GT1c
SATIV
GM1b
GD1a
GT1b
GQ1c
SATV
SATVII
GD1c
GD1α
GT1a
GT1α
GQ1b
GQ1α
GP1c
GP1α
E
Molecules/stereocilium
Enrichment
PITPNA
PIK4CA
EFR3A
PIP5K2B
PIP5K1A
PTPRQ
GLB1
HEXA
NAGA

Figure 3.4 – Hair bundle membrane proteins and $PI(4,5)P_2$ pathway.

In all panels, proteins indicated by blue-colored short names were detected in purified hair bundles by mass spectrometry. A, Chick hair-bundle membrane proteins. Proteins detected by LC-MS/MS were quantified using intensity-weighted spectral counting. The size of each slice is proportional to molar abundance. Red, proteins enriched in bundles over epithelium >5-fold; green, <5-fold. Only proteins enriched 0.1-fold or greater are plotted. B, Peptide coverage of $PI(4,5)P_2$ -transport and metabolizing proteins in LC-MS/MS of chick hair bundles. Peptides detected by X! Tandem analysis of the complete dataset of chick bundles were plotted against residue number. Height of plotted boxes corresponds to number of identical peptides detected; width corresponds to peptide length, plotted at position in sequence. Gray shading indicates peptide log(e) (log of expectation) score, indicating statistical confidence in protein identification (key in PITPNA panel). C, PI pathway in hair bundles. D, Ceramide, sphingolipid, and ganglioside pathways. Green indicates lipids analyzed by mass spectrometry (Fig. 1); glucosylceramide and galactosylceramide are analyzed together as hexosylceramide. Italicized enzyme short names correspond to proteins not detected in bundles. All sialyltransferase (SATn) reactions can be reversed by endogenous or exogenous neuraminidase. Polysialyated gangliosides that could be converted to GM1 ganglioside with neuraminidase treatment are indicated with gray shading. E, Bundle abundance (green) and bundle-to-epithelium enrichment (magenta) of $PI(4,5)P_2$ and ganglioside metabolic proteins.

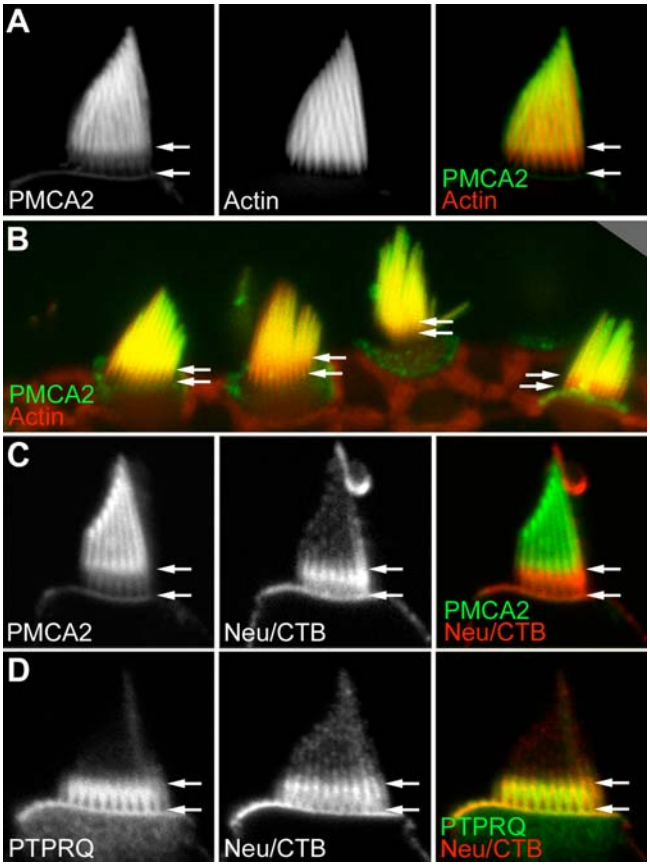

Figure 3.5 – PMCA2 and PTPRQ segregate to distinct domains delineated by CTB labeling.

PMCA2 localization in isolated cell labeled with F2a antibody. Note near-absence of PMCA2 in basal taper region (arrows), which appears red in the color merge panel. No neuraminidase, CTB, or CTB antibody were used. B, PMCA2 absence from basal taper region is also clear in wholemount tissue (arrows). C, Reciprocal PMCA2 and CTB labeling. D, PTPRQ and CTB labeling overlap. CTB antibody used for detection in C-D. Panel widths for A, C, and D are 12.5 µm; panel width for B is 65 µm.

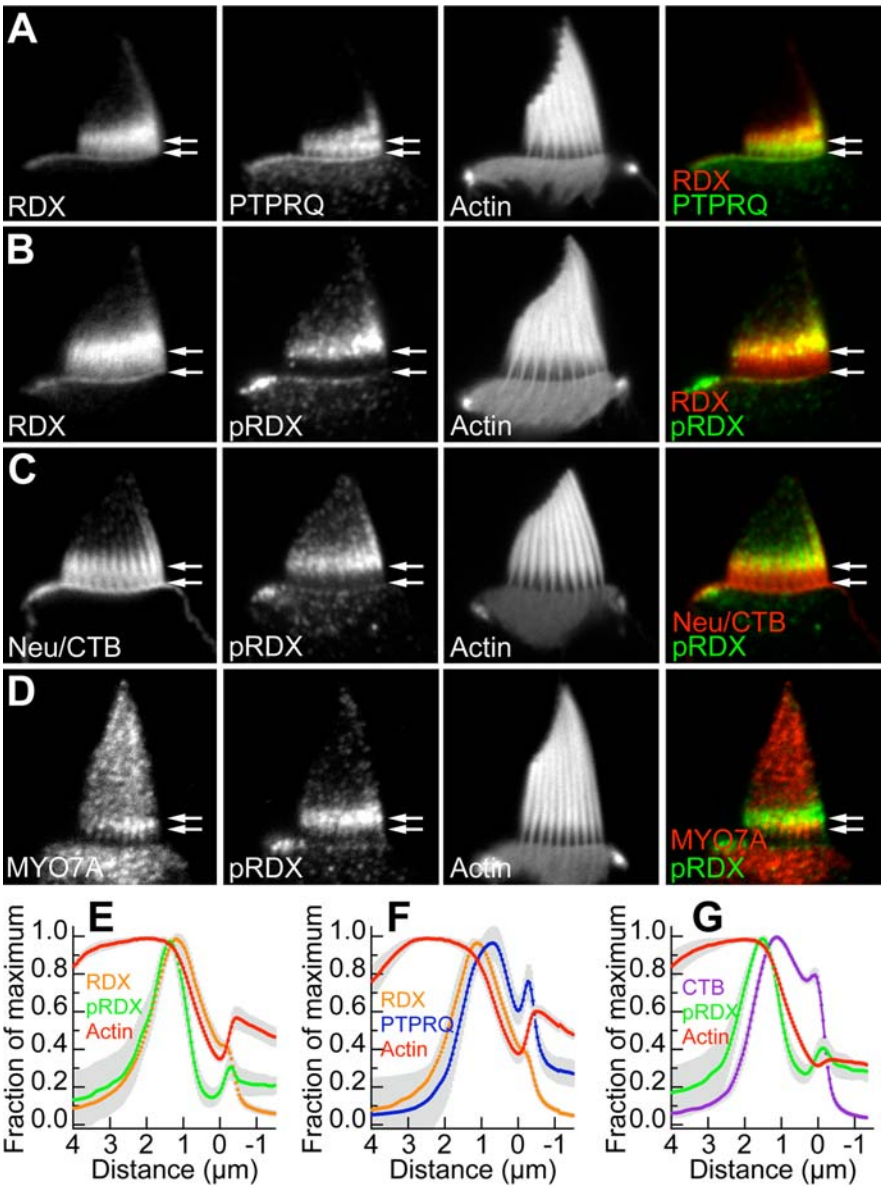

Figure 3.6 – Radixin is activated at the PI(4,5)P_2 -PTPRQ boundary.

A, Radixin and PTPRQ are located in similar, but not entirely coextensive patterns at the base of the hair bundle. B, Antibody for activated ERM proteins (including pRDX) only labels above the stereocilia tapers. Note pRDX punctae throughout bundle. Arrows indicate pRDX-free taper region. C, pRDX labeling is shifted towards stereocilia tips from CTB labeling. Arrows indicate pRDX-free taper region. D, The MYO7A band is more basal than the pRDX band. Arrows indicate basal MYO7A band. E-G, Intensity profiles for RDX/pRDX (n=5), RDX/PTPRQ (n=5), and CTB/pRDX (n=5) averaged from individual cells aligned at the apical-surface actin dip. Panel widths in A-C are 12.5 μm.

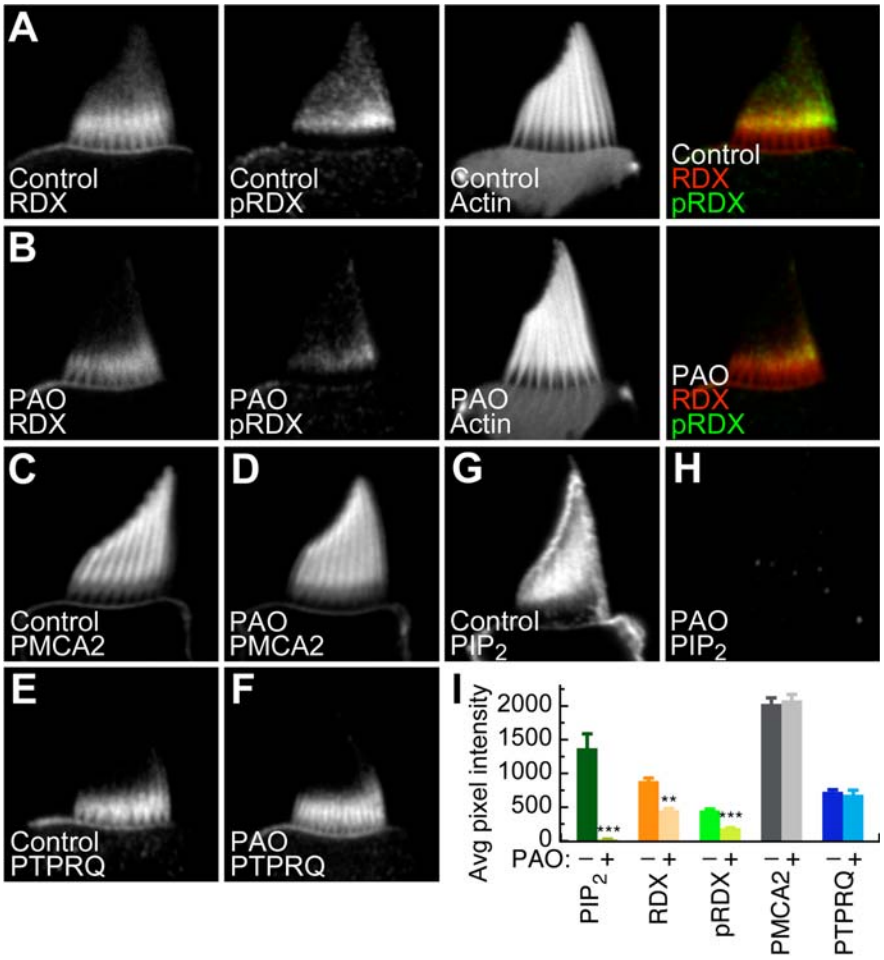

Figure 3.7 – Radixin activation depends on polyphosphatidylinositols.

A-B, RDX and pRDX (detected with anti-pERM antibody) immunolabeling without (A) and with (B) 30 µM PAO for 1 hr. pRDX and RDX both decline after PAO treatment. C-F, PMCA2 and PTPRQ distribution and intensity are not affected by PAO treatment. G-H, PI(4,5)P_2 immunolabeling ± 30 µM PAO (1 hr). PAO completely abolishes PI(4,5)P_2 immunoreactivity. I, Mean ± SEM for whole-bundle pixel intensity; regions of interest used for measurement included the entire bundle. Panel widths in A-H are 12.5 µm.

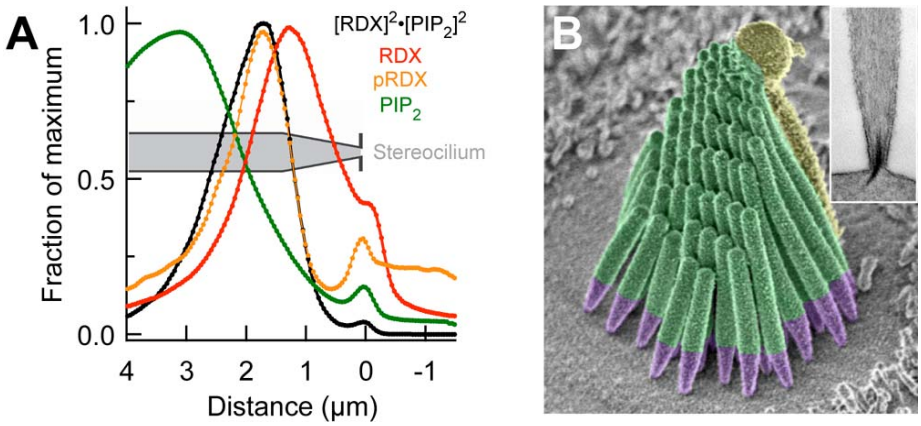

Figure 3.8 – Membrane domains in hair bundles.

A, Relationship between radixin, phosphoradixin, and PI(4,5)P_2 profiles; data are from different sets of cells, aligned at the apical surface (small peak in each profile). Black curve is obtained by multiplying the square of the relative radixin concentration times the square of the relative PI(4,5)P_2 concentration, then normalizing to a peak of 1.0. Approximate stereocilia profile is indicated by cartoon. B, Scanning electron micrograph of bullfrog hair bundle pseudocolored to indicate structural and functional domains. Purple, taper domain; Green, shaft/tip domain; yellow, kinocilium domain. Inset, transmission electron micrograph of taper region.

Chapter 4 – Protein-protein Interactions between PCDH15, TRPM6/7, and TMCs

Hongyu Zhao and Peter G. Gillespie

Introduction

Despite decades of research, the identity of the MET channel remains unknown. One approach to obtain candidates for MET channel is biochemically purifying the hair bundles followed by protein identification with mass spectrometry. Clive Morgan, a postdoctoral fellow in the Gillespie lab, further developed this approach. He dissected thousands of chicken ears and subjected these ears to a multi-step purification procedure, which includes an affinity step with a monoclonal antibody against chicken PCDH15. Using this procedure, he purified the tip link complex and identified some of its components with mass spectrometry (Figure 4.1). One of the ion channel proteins he identified was transient receptor potential melastatin type 7 (TRPM7).

TRP channels are Ca^{2+} permeable ion channels expressed in many cell types and tissues in mammals. There are three main subfamilies of TRP channels: canonical (TRPC), melastatin-related (TRPM), and vanilloid-receptor-related (TRPV). In addition, several more distantly related subfamilies exist: polycystins (TRPP), mucolipins (TRPML), ankyrin transmembrane protein 1 (TRPA), and no mechanoreceptor potential C (NOMPC), TRP channels have a wide variety of biophysical properties and gating mechanisms and play critical roles in sensory physiology. Within the TRPM family, there are eight genes in human. These family members can be further divided into four groups, based on their sequence homology: TRPM 1 and TRPM3, TRPM2 and TRPM8, TRPM4 and TRPM5, TRPM6 and TRPM7 (Fleig and Penner, 2004). In addition, because of a putative

dimerization helix in the coiled coil domain, TRPM1, TRPM3, TRPM6, and TRPM7 may form one subgroup, as can the remainder (Fujiwara and Minor, 2008).

Structurally, the TRPM channels contain N- and C-terminal intracellular domains, six transmembrane segments (S1-S6), and a pore region that lies between S5 and S6. The N-terminal domain includes a conserved region having four stretches of amino acids (TRPM homology region); the C-terminal domain includes a TRP motif, coiled coil domain, and an enzymatic domain.

Splice variants of TRPM have altered cellular localization and channel properties as compared to wild-type TRPMs (Farooqi et al., 2011). For example, two splice variants of TRPM3, TRPM3α1 and TRPM3α2, have drastically different permeability to divalent cations Ca^{2+} and Mg^{2+}. Similarly, extracellular monovalent cations block TRPM3α2 current, but not current from TRPM3α1 (Oberwinkler et al., 2005).

TRPM7 (also known as TRP-PLIK, ChaK1, and LTRPC7) is a 1,863 amino acid ion channel with a C-terminal α-kinase domain (Runnels et al., 2001). TRPM7 is a nonselective cation channel ubiquitously expressed in both human and mouse (Fonfria et al., 2006; Jin et al., 2008). In adult mice, TRPM7 expression is strongest in heart, kidney and brain (Jin et al., 2008). TRPM6, a closely related member o the TRPM family, shares 52% overall identity with TRPM7 (Schlingmann et al., 2002).

While the complete crystal structure of TRPM7 is not available, amino acid sequence analysis predicts a channel with six transmembrane domains (Runnels et al., 2001). A portion of the rat TRPM7 C-terminus has recently been crystallized, and the solved high resolution structure reveals a coiled-coil domain localized between the ion

channel and kinase domains. The coiled-coil domain of TRPM7 is predicted to form antiparallel tetramers both with itself and with the coiled-coil domain of TRPM6 (Fujiwara and Minor, 2008).

Although one study combining electrophysiology and FRET-based approaches proposed that TRPM6 was unable to form functional channels independently of TRPM7 (Chubanov et al., 2004), the result was contradicted by a later study, in which heterologously expressed TRPM6 (without TRPM7) produced functional channels (Li et al., 2006).

Single channel conductance of TRPM6, TRPM7, and TRPM6/7 has been shown to be 84 pS, 40 pS, and 57 pS, respectively (Li et al., 2006; Runnels et al., 2001; Voets et al., 2004). These conductances are significantly smaller than the reported conductance of MET channel of 145-320 pS (Beurg et al., 2006; Farris et al., 2004). The different single channel conductances suggest that TRPM6, TRPM7, and TRPM6/7 channels have distinct pore structures (Li et al., 2006). It is possible that TRPM7 forms heteromeric channels with other members of TRPM family, or different splice variants of TRPM6/7 may exist, as in the case for TRPM3 (Oberwinkler et al., 2005). These variants might have larger single channel conductances.

At physiological magnesium concentrations, TRPM7 current is small; removal of extracellular magnesium results in large outwardly rectifying currents (Kozak and Cahalan, 2003). In addition, TRPM7 current is potentiated by low extracellular pH and blocked by trivalent ions (Cherny et al., 1997; Numata and Okada, 2008; Runnels et al., 2001). The kinase domain of TRPM7 directly interacts with several phospholipase C

(PLC) family members including PLC-β_1, PLC-β_2, PLC-β_3 and PLC-γ_1, and depletion of phosphatidylinositol 4,5-bisphosphate (PIP_2) inhibit TRPM7 current (Runnels et al., 2002; Takezawa et al., 2004). Interestingly, the MET channel may also be down regulated by depleting PIP_2, since PIP_2 is required for mechanotransduction and adaptation (Hirono et al., 2004).

TRPM7 is involved in a variety of fundamental cellular processes including magnesium homeostasis, cell survival, proliferation, cell cycle progression, and responses to shear stress and oxidative stress (Bates-Withers et al., 2011; Trzeciakiewicz et al., 2005). TRPM7 knockout mice die during embryogenesis; a conditional knockout of thymocyte-restricted TRPM7 exhibits defective thymopoeisis, suggesting that TRPM7 is involved in development and organogenesis (Jin et al., 2008). Using tamoxifen-inducible disruption of TRPM7 and multiple Cre recombinase lines, a group recently showed a temporal requirement for the TRPM7 during embryogenesis (Jin et al., 2012). Whether TRPM7 is required for hair cell function or mechanotransduction is not known, and would require a conditional knockout that is restricted to hair cells.

Since the MET channel is localized near the lower end of the tip link (Beurg et al., 2009), it might interact with PCDH15, directly or indirectly. Using a heterologous expression system and in utero electroporation technique, I report here the interaction between TRPM7 (and TRPM6) and PCDH15, as well as their interactions with another MET channel candidate, TMCs. I also report the discovery of two splice variants of TRPM6 and TRPM7, which might confer different channel properties than the canonical channels.

Results

TRPM7 Co-immunoprecipitates with PCDH15 in HEK293T Cells

I expressed native mouse PCDH15 and HA-tagged TRPM7 in HEK293T cells and performed co-immunoprecipitation experiments. First, I used anti-HA agarose to pull down TRPM7, and detected PCDH15 in the complex (Figure 4.2). Anti-V5 agarose did not pull down either TRPM7 or PCDH15. Also, HA-tagged TRPC6, a TRP channel outside TRPM family, did not immunoprecipate PCDH15 (Figure 4.2 A, lane 4). Because co-expression of TRPM6 and TRPM7 resulted in higher PCDH15 protein expression and more precipitated PCDH15 than with either channel expressed alone (data not shown), I often used the heteromeric channels to further characterize the TRPM-PCDH15 interaction.

Next, I immunoprecipated PCDH15 using PB811, a PCDH15 specific antibody. HA tagged TRPM7 was detected in the complex (Figure 4.2 B, lane 4). As a control, antibody against horse radish peroxidase (HRP) did not pull down TRPM7 (Figure 4.2 B, lane 6). I also performed a control experiment in which two different populations of cells, one with over-expressed TRPM6/7, and the other over-expressed with PCDH15, were lysed independently and then mixed. Under these conditions, I did not see any interaction between the PCDH15 and TRPM6/7, suggesting that the interaction between the TRPM6/7 and PCDH15 is specific (Figure 4.3 A, lane 3). Furthermore, N-cadherin (CDH2), a classical cadherin expressed in neurons, did not interact with TRPM6/7 (Figure 4.3 B).

Domains in PCDH15 and TRPM6/7 Responsible for the Interaction

I was not able to map out the domains in TRPM6/7 that are responsible for the interaction with PCDH15, since constructs encoding the N and C terminal domains of TRPM6 and TRPM7 did not express in HEK293T cells. Because CDH2 did not interact with TRPM6/7, I generated chimeras between CDH2 and PCDH15. I also generated C terminal deletion constructs of PCDH15. All these constructs expressed well in HEK293T cells, allowing me to map out the interacting domains in PCDH15 (Figure 4.4).

Two splice variants of PCDH15, PCDH15_CD1 and PCDH15_CD3, have been shown to be components of tip links. Knocking out either variant alone in mice resulted in normal tip links and hearing, indicating that neither variant is uniquely required for tip link formation and mechanotransduction (Webb et al., 2011). The two splice variants shared the same extracellular domains, a single transmembrane domain, two juxtamembrane domains on the extracellular and intracellular side, and part of the C terminal intracellular domain (Figure 4.4 A). CDH2 has a similar general structure with PCDH15, yet all components of the protein are significantly different.

I generated two C terminal deletions of PCDH15, D1 and D2. D1 has all the structural components shared between PCDH15_CD1 and PCDH15_CD3; D2 has a stop codon at the end of the intracellular juxtamembrane domain. I also generated chimeras of PCDH15 and CDH2; 2152 is a chimera in which the transmembrane domain and the juxtamembrane domains of CDH2 were replaced with the counterparts of PCDH15; 15215 is a chimera in which the transmembrane domain and the juxtamembrane domains of PCDH15 were replaced with the counterparts of CDH2; 1522 is a chimera in

which extracellular domains of CDH2 were replaced with those of PCDH15. Because PCDH15 contains C-terminal PDZ binding domains (Webb et al., 2011), I also generated C terminal deletion constructs of PCDH15_CD1 and PCDH15_CD3, in which the C-terminal 12 amino acids were deleted. Deleting the PDZ-binding domain did not change the TRPM6/7-PCDH15 interaction (data not shown), indicating that the PDZ binding domains are not required.

D1 and D2 did not interact with TRPM6/7, suggesting that the C terminal intracellular domain is required for the interaction; however, chimera 1522, in which the transmembrane domains, juxta-membrane domains, and C terminal intracellular domains of PCDH15 were replaced with those of CDH2, interacted strongly with TRPM6/7, indicating that the C terminal domains of PCDH15 are not required for the interaction. Another chimera, 15215, in which the transmembrane domains and juxta-membrane domains of PCDH15 were replaced with those of CDH2, also interacted strongly with TRPM6/7. Furthermore, chimera 2152, in which the transmembrane domains and juxta-membrane domains of CDH2 were replaced with those of PCDH15, did not interact with TRPM6/7, indicating that these domains of PCDH15 are not required for the interaction. These results strongly suggest that the extracellular domains of PCDH15 are responsible for the PCDH15-TRPM6/7 interaction.

Two New Splice Variant of TRPM6 and TRPM7

In the process of cloning the TRPM6 and TRPM7 cDNAs from mouse inner ear, I discovered two new splice variants, one for TRPM6 and one for TRPM7. Both splice variants skipped exon 20 of TRPM6 and TRPM7 genes. Interestingly, the predicted

protein products of both splice variants lack transmembrane segment 2 (S2). The comparison between canonical and the variant of mouse TRPM7 is shown in Figure 4.5 A. Tissue expression profile of the two variants is shown in Figure 4.5 B. The predicted topology of the transmembrane segments is shown in (Figure 4.6). The delta exon 20 variants of TRPM6 (TRPM6_dEx20, or DEX26) and TRPM7 (TRPM7_dEx20, or DEX27) can be expressed at the cell surface in HEK293T cells, as shown by a surface-biotinylation experiment (Figure 4.7 A). They associate with the canonical TRPM6 and TRPM7 channels (Figure 4.8), and bind to PCDH15, similar to the canonical channels (Figure 4.7 B).

CDH23 Interacts with TRPM6/7 in HEK293T Cells

Surprisingly, co-immunoprecipitation experiments showed that CDH23 also interacts with TRPM6/7 (Figure 4.9 A). In addition, CDH23 immunoprecipitated co-expressed TRPM6_dEx20 and TRPM7_dEx20 (Figure 4.9 B). This result suggests that CDH23 interacts with TRPM6/7, possibly through the extracellular domains.

TMCs Interact with TRPM6/7, PCDH15, and CDH23 in HEK293T Cells

Because TMCs have been shown to be involved in mechanotransduction, they might interact with TRPM7 and/or PCDH15. Three TMC constructs, TMC1_ex1, TMC1_ex2, and TMC2, all in the form of C terminal AcGFP fusion proteins, were used in co-immunoprecipitation experiments (Figure 4.10). All three TMCs were associated with the TRPM-PCDH15 complex (Figure 4.10 A). Because TMC1_ex1 expressed better than the other two constructs, I used it to test if TMC interact with TRPM7. As shown in Figure 4.10 B, TMC1_ex1 binds to TRPM7, independent of PCDH15 or CDH23.

Over-expressed dnTRPM7 Interacts with PCDH15 and Localize to the Stereocilia Tips

Because a pore mutant of TRPM7, dnTRPM7, has been shown to inhibit wild type TRPM7 current (Krapivinsky et al., 2006), we over-expressed this dnTRPM7 in HEK293T cells and were able to repeat the reported results (Figure 4.11 A). dnTRPM7 also inhibited current from co-expressed TRPM6 and TRPM7, suggesting that it inhibits current from TRPM6/7 heteromeric channels (data not shown). dnTRPM7 associated with TRPM7 (Figure 4.8), and dnTRPM7_dEx20 associated with both TRPM7 and dnTRPM7_dEx20 (Figure 4.8). As shown in Figure 4.11 B, dnTRPM7 bound to PCDH15, similar to wild type TRPM7. We reasoned that if TRPM7 is the MET channel, then dnTRPM7 could block the MET current in the inner ear.

I then engineered a 3X myc tag on the c terminal end of dnTRPM7, and in collaboration with Dr. John Brigande's lab, transfected mouse hair cell progenitors with this dnTRPM7_3Xmyc construct, using in utero electroporation technique. We co-transfected EGFP with dnTRPM7_3Xmyc at E12.5 and harvested mice at P6.5. We then stained the cochlea with anti-myc antibody. Interestingly, all the inner hair cells with cell body staining of myc (myc positive) appeared to have thinner and bent stereocilia than their untransfected neighbors. This was not a result of general over-expression, as many hair cells had much stronger EGFP expression but were not myc positive, and these cells had normal stereocilia (Figure 4.12 A). The correlation between myc staining and thinner stereocilia of inner hair cells was very strong – in three independent experiments, we observed at least 20 inner hair cells that were myc positive, and all of them had thinner stereocilia. In myc positive outer hair cells, we did not observe an

obvious difference in hair bundle morphology (data not shown). These myc-positive inner hair cells also had myc labeling near the tips of stereocilia (n=20, three independent experiments), as shown in Figure 4.12 B. The myc positive outer hair cells also had elevated myc labeling in the hair bundle, yet we could not tell if these labeling were at the tips of stereocilia, due to the resolution of the microscope (data not shown).

Discussion

Our results show that in HEK293T cells, PCDH15 interacts with TRPM7, a transduction channel candidate identified by Clive Morgan, a postdoc in the Gillespie lab. Our data also indicate that heteromeric TRPM6/7 channels interact with PCDH15, although the data that suggest the presence of TRPM6 in the tip link complex is weaker than those of TRPM7. Because I over-expressed PCDH15 and TRPM channels in a heterologous system, I performed a number of control experiments to test the possibility of non-specific interaction between PCDH15 and TRPM6/7. We showed that HA tagged TRPM6/7 immunoprecipated PCDH15, and vice-versa; CDH2, another cadherin expressed in the nervous system, did not immunoprecipate TRPM6/7; TRPC6, another TRP channel, did not immunoprecipate PCDH15; and TRPM6/7, when expressed in a separate cell population from PCDH15, did not immunoprecipate PCDH15. We are in the process of testing TRPM8, a member of TRPM channel family outside the TRPM6 and TRPM7 subgroup, for its interaction with PCDH15. This experiment will provide more information about the specificity of the PCDH15-TRPM6/7 interaction.

Extracellular Domains of PCDH15 Are Responsible for Its Interaction with TRPM6/7

Because truncation of intracellular domain of PCDH15 resulted in loss of interaction, we initially thought that the intracellular domain is required. Since both PCDH15 splice variants that are believed to be tip-link components in mouse hair cells (CD1 and CD3) have c terminal PDZ binding domains, I deleted the C terminal 12 amino

acids from CD1 and CD3. These C terminal deletions, CD1_deltaC12 and CD3_deltaC12, immunoprecipated with TRPM6/7 similarly to their wild type proteins (data not shown). This result was surprising to us. Subsequently, we generated 1522, a chimera protein with the transmembrane domain, juxtamembrane domains, and the entire C terminal intracellular domains all replaced with those of CDH2. Immunoprecipitation experiments showed that 1522 interacted more strongly with TRPM6/7 than PCDH15. This result, together with the result that CDH2 and chimera 2152 (in which CDH2 transmembrane domains and juxtamembrane domains are exchanged with those of PCDH15) did not immunoprecipate with TRPM6/7, indicates that the extracellular domains of PCDH15 are necessary and sufficient for the interaction.

However, the question remains as to why the D1 and D2 deletion constructs of PCDH15 fail to interact with TRPM6/7. We suspect that the intracellular domains of PCDH15 plays a regulatory role, and removing part of this domain (in D1 and D2) could affect the dimerization of PCDH15 and/or cause conformational changes across the plasma membrane. In addition, membrane proteins are inserted cotranslationally into the lipid bilayer, with positively charged residues flanking the transmembrane segments as topological determinants. A recent report indicates that there is unanticipated plasticity in membrane protein insertion mechanisms. In this report, the authors demonstrated that a single positively charged amino acid, even at the very C terminus of the membrane protein, can act globally, affecting the topology of the entire protein (Seppala et al., 2010). If this is the case, the presence of transmembrane domains and

intracellular domains of CDH2 are probably necessary for the proper topology formation and folding of the PCDH15 extracellular domains in the 1522 chimera.

CDH23 and TMCs also Interact with TRPM6/7 in HEK293T Cells

Our results showed that CDH23, like PCDH15, interacts with TRPM6/7. It is possible that TRPM6/7 is located at the upper end of the tip link, where CDH23 exists. Further experiments, similar to deletion and chimera constructs of PCDH15, are necessary to test if this interaction is specific. The recently reported transduction channel candidate TMCs also interact with TRPM6/7 in HEK293T cells, independent of PCDH15 or CDH23. This result is consistent with the idea that the tip link complex is composed of multiple proteins with functional importance. It is clear that we are far away from completely understanding the components of the tip link complex, as well as the protein-protein interactions among these components.

dEx20 Versions of TRPM6 and TRPM7 Might Be Alternative MET Channel Candidates

A few important biophysical differences between TRPM6, TRPM7, and TRPM6/7 channels and the MET channel exist. These differences include: the TRPM6/7 channels have smaller single channel conductances comparing to the MET channel; TRPM6/7 channels are blocked by extracellular Mg^{2+}, but the MET channels are not; MET channels are gated mechanically, while TRPM6/7 channels are not. It is possible that the two newly-identified splice variants of TRPM6 and TRPM7 have different biophysical properties than their wild type counterparts, as shown to be a case in TRPM3. For example, we were not able to detect current similar to TRPM6/7 channels when we over-expressed dEX20 versions of these channels. Further electrophysiological

experiments are necessary to provide more insights into these splice variants, regarding their single channel conductances and gating mechanisms.

Over-expressed dnTRPM7 in Mouse Hair Cells Results in Thinner Stereocilia

When dnTRPM7 (with or without C terminal 3Xmyc tag) was co-expressed in HEK293T cells, it inhibited current of both TRPM7 and TRPM6/7 channels. When we over-expressed dnTRPM7 tagged with 3X myc in mouse inner hair cells, we observed myc staining near the tip of the stereocilia, and stereocilia of these myc-positive hair cells become thinner and bent. It is possible that TRPM7 and other members of the TRPM family are the MET channels, and dnTRPM7, expressed and targeted to the tip of the stereocilia, blocked or reduced the MET current. Because the MET current is probably required for normal hair bundle development and stereocilia F-actin polymerization, acting either directly or through Ca^{2+} dependent mechanisms (Caberlotto et al., 2011), reduction of the MET current at the stereocilia tips could cause the thinner and bent stereocilia. Alternatively, TRPM channels, expressed at locations other than the stereocilia tips, could be responsible for maintaining the Ca^{2+} concentration inside the stereocilia, and expression of the dnTRPM7 resulted in abnormal F-actin polymerization by reducing the intra-stereocilia Ca^{2+} concentration. Another possibility is that expression of dnTRPM7 disturbed some other aspects of the hair cell function in a non-specific manner.

We were not able to express wild type TRPM7_3Xmyc using the same in utero electroporation technique, despite multiple trials. It is possible that the wild type TRPM7 is toxic to the hair cells, or its expression was selectively inhibited by the hosting

hair cells. These possibilities will need to be tested with further experiments. Without a control of a similar channel expressed in hair cells without a phenotype, we are not sure if the stereocilia phenotype is caused by the pore mutation in dnTRPM7. To address the functional roles of TRPM7 in mouse hair cells, a conditional knock-out of TRPM7 that is restricted to hair cells is necessary. This experiment is being performed, in collaboration with Dr. Uli Mueller at Scripps Institute.

Experimental Procedures

Cell culture, transfection, and immunoprecipitation: In the coimmunoprecipitation assays we used HEK293T cells grown in 6 well tissue culture plates. HEK293T cells were passed to 6-well plates on day 1 in the morning (from a confluent 100mm dish, I passed the cells 1:4, such that by the end of the day, the cells were 50-80% confluent). The cells were incubated for at least 6 hours (important for cell health) in the incubator at 37°C, then transfected with Effectene transfection reagent (Qiagen, 301425). For simplicity, I did not change medium or wash with PBS; instead, I just prepared the DNA complex according to the manufacturer suggested protocol in PCR tubes, then added the DNA complex to the cells. After mixing the DNA complex with the medium by swirling the plate, I returned the plate to the incubator.

On Day 3 in the afternoon, I harvested the cells by aspirating the medium. For 6-well plates, I removed medium from each well, then added 500 µl of PBS. The plate were rocked back and forth and knocked against the bench side to detach the cells. The cells were then transferred to a centrifuge tube. Remaining cells in the well were washed once with another 500 µl of PBS. The cells were centrifuged briefly (16,000g for 5 sec) and supernatant removed. 300ul of cold lysis buffer (containing PBS, 1% Tx100, 0.5% NP-40, and protease inhibitor cocktail (Sigma, P8340)) were added to the cells, and the mixture were placed on ice. The mixtures were then sonicated using a tip sonicator (ultracell sonicator, Sonics) set at 25% power. Two bursts of 5 sec were used, with cell

lysate sitting on ice in between for 15-30 sec. The lysate was then centrifuged at 16,000g for 20 min at 4°C, and the supernatant (lysate) was separated from the pellet. 20 µl of the lysate were saved for loading control, and to the rest of lysate, 10 µl of HA agarose (Sigma, A2095, 20 µl slurry) was added. The mixture was incubated on a rotating incubator (for centrifuge tubes) overnight at 4°C.

On the next morning, the immunoprecipitate mixture was centrifuged at 16,000g for 1 sec, then washed 2X with 300ul lysis buffer and 1X with PBS. After the washes, 32 µl of 2X SDS sample buffer (Invitrogen) was added to the agarose beads, and the mixture was incubated for 10 min at 70°C, with mixing by slow vortexing every 1-2 min during the last 5 min of the incubation. The agarose beads were removed using a spin filter (Costar 8163), and 5ul of 10X reducing agent (Invitrogen, NP0007) were added to the protein solution. The mixture was again incubated at 70°C for 10 min. For the loading control, 4 µl 10X reducing agent (Invitrogen, NP0009) and 8ul of 4X sample buffer were added to 20 µl of lysate and incubated at 70°C for 10 min (using PCR tubes and a thermocycler).

The protein samples were separated on a 3-8% Tris-acetate gel (Invitrogen, EA03755BOX) for 30-40 min. Proteins in the gel were then transferred to PVDF membrane (Millipore, IPVH00010) using a semi-dry setup (Bio-Rad, Transbot SD). Towbin buffer with 10% MeOH, without SDS were used as transfer buffer. For 7.5X10 cm blot, voltage limit of 20V and current limit of 250mA were used. After transferring for 40-50 min, the blot was washed 1X in PBS and blocked in blocking buffer (PBS containing 10% FBS, 0.1% Tween) for 30 min, during which primary antibody were

diluted in blocking buffer (1:1000) and incubated at room temperature for 10-20 min. The blot was incubated with primary antibody for 2 hours at room temperature. Before Primary incubation is done, HRP coupled secondary antibody was diluted in blocking buffer (1:5000) and incubated for 10-20 min, before incubating with blot for 30 min. Wash between primary and secondary antibody: 2 quick rinses followed by 3 X 2min washes. Wash after secondary antibody: 2 quick rinses followed by 5 X 5min washes. SuperSignal West Pico Chemiluminescent Substrate (Pierce, 34077) was used for detection.

Anti-HA agarose or anti-V5 agarose (Sigma, A7345) were used to pull down the HA-tagged TRP channels. In the case of PCDH15 pull down, we used 10µg of PB811, a rabbit antibody against PCDH15 (gift from Dr. Uli Mueller) or 10µg of anti-HRP antibody (Jackson Immunoresearch) in 10µl of Ultralink immobilized protein A (Pierce, 53139). For western blot assays, PCDH15 was detected with PB811, TRP channels were detected with monoclonal anti-HA antibody (Applied Biological Materials, G036) or monoclonal anti-myc antibody (Genscript, A00704), and CDH23 was detected with a mouse monoclonal antibody raised against the cytoplasmic domain of CDH23 (gift from Dr. Uli Mueller).

In utero electroporation and cochlea imaging. EGFP and dnTRPM7_3Xmyc DNA (at a molar ratio of 1:5) were injected into otocysts of CD1/C57BL6 mice at E12.5 followed by Electroporation. At P6.5, ears were dissected from the mice pups. The cochlea was dissected in PBS, without removing the tectorial membrane. The organ of Corti was separated from the lateral wall, arranged to a flat disk on an uncoated plastic

petri-dish (Falcon 393003) by sticking the Reissner's membrane to the dish. The flattened cochlea was then fixed with 4% PFA for 20 min at room temperature, after which tectorial membrane was removed. The cochlea was then blocked in PBS containing 0.1% BSA, 1% normal donkey serum, and 0.2% saponin for 30-60 min at room temperature. The cochlea was then stained with mouse monoclonal anti-myc antibody (9E10, ascites fluid, 1:100) overnight at 4°C. The cochlea were then washed 3 times in PBS and incubated with goat anti-mouse antibodies coupled to Alexa Fluor 555 (Invitrogen, A21422) and TRITC-phalloidin (Sigma, P1951). After incubating at room temperature for 2 hours, the cochlea was washed 5 times (5 min each) in PBS. To mount, the cochlea was transferred to a glass slide and oriented such that hair cells were facing up. Excessive PBS was removed with a gel-loading pipette tip and a kimwipe. 30 µl of EverBrite mounting medium (Biotium, 23001) was added to the center of a cover glass, which was inverted and carefully laid on top of the cochlea, with the drop of mounting medium touching the cochlea first. The mounted cochlea was then imaged with Olympus FV-1000 confocal microscope using 60x, 1.42 NA oil-immersion plan apochromat objective.

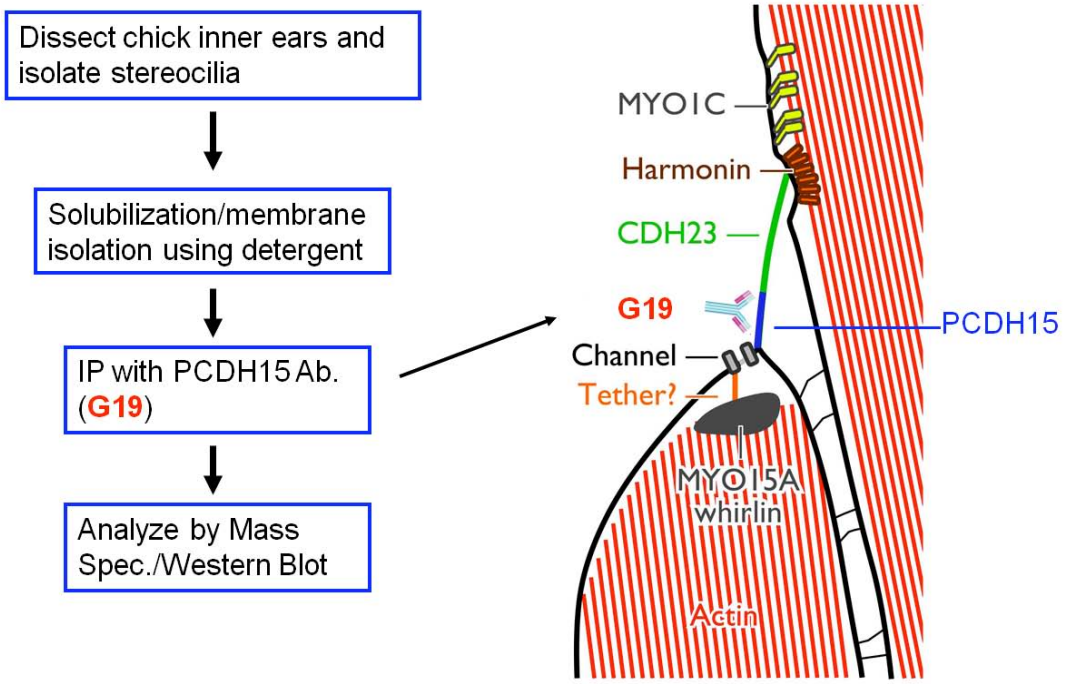

Figure 4.1 – Approach taken by Clive Morgan to identify the MET channel in chicken ear. Hundreds of chicken ears were dissected and subject to a robust purification procedure, including an affinity-purification step with the monoclonal antibody, G19, against PCDh15. The purified tip link complexes were analyzed by mass spectrometry.

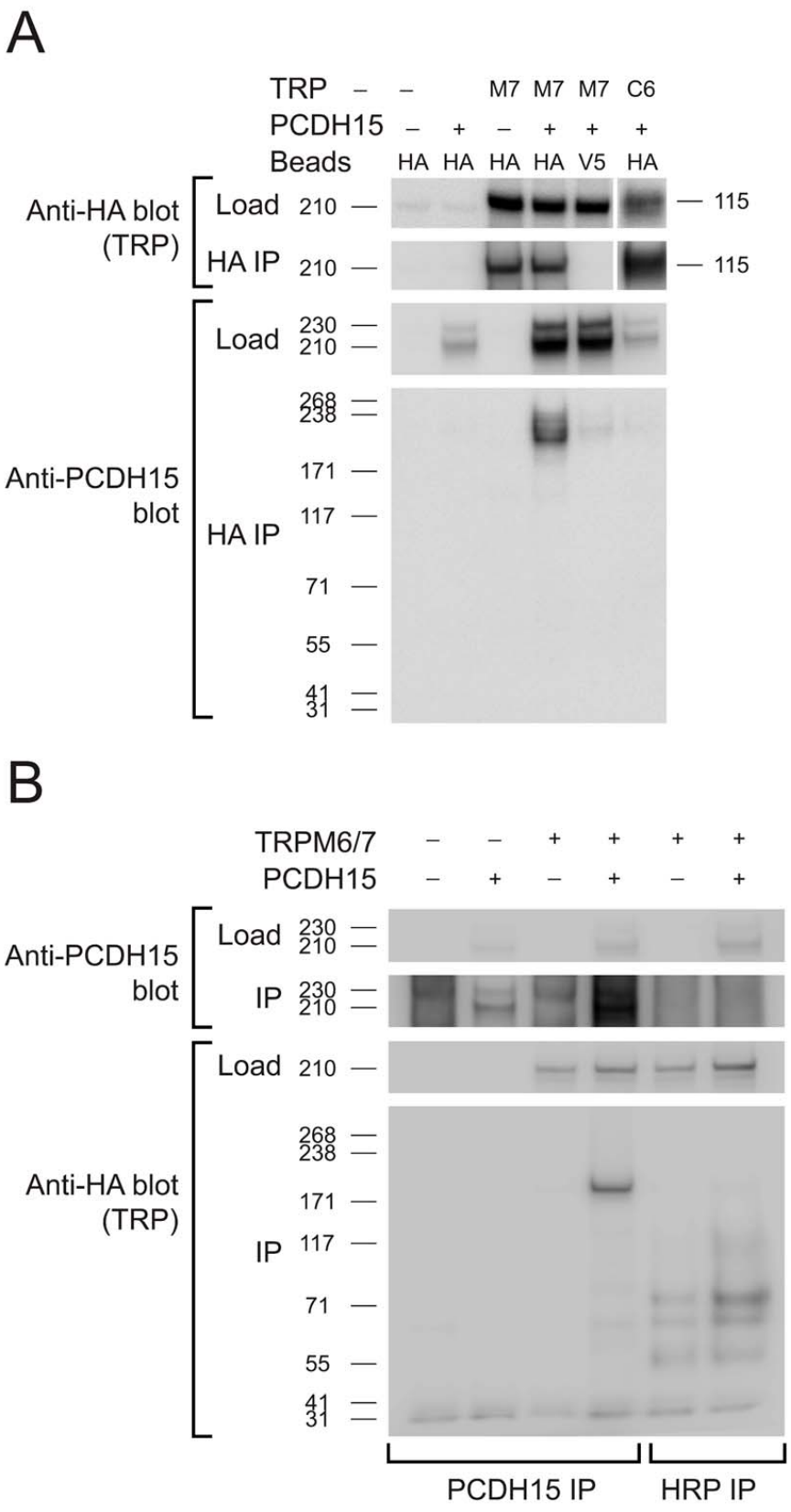
A
TRP – – M7 M7 M7 C6
PCDH15 – + – + + +
Beads HA HA HA HA V5 HA
Anti-HA blot (TRP)
Load
HA IP
210
115
Anti-PCDH15 blot
230
268
238
171
117
71
55
41
31
B
TRPM6/7 – – + + + +
PCDH15 – + – + – +
Anti-PCDH15 blot
IP
Anti-HA blot (TRP)
PCDH15 IP
HRP IP

Figure 4.2 – TRPM7 co-immunoprecipates with PCDH15 in HEK293T cells
HEK293T cells were transiently transfected with PCDH15 and TRP channels with C terminal HA tags. A, harvested lysates were immunoprecipated with anti-HA agarose and probed with an anti-PCDH15 antibody (PB811). The last two lanes are two controls: anti V5 agarose as a control for non-specific binding of the agarose with PCDH15; TRPC6 as a TRP channel outside the TRPM family. Both controls have much lower levels of PCDH15 immunoprecipated. B, lysates were immunoprecipated with protein A/G agarose and either PB811 antibody (for PCDH15) or HRP antibody (control), then probed for TRP channels with anti-HA antibody.

A

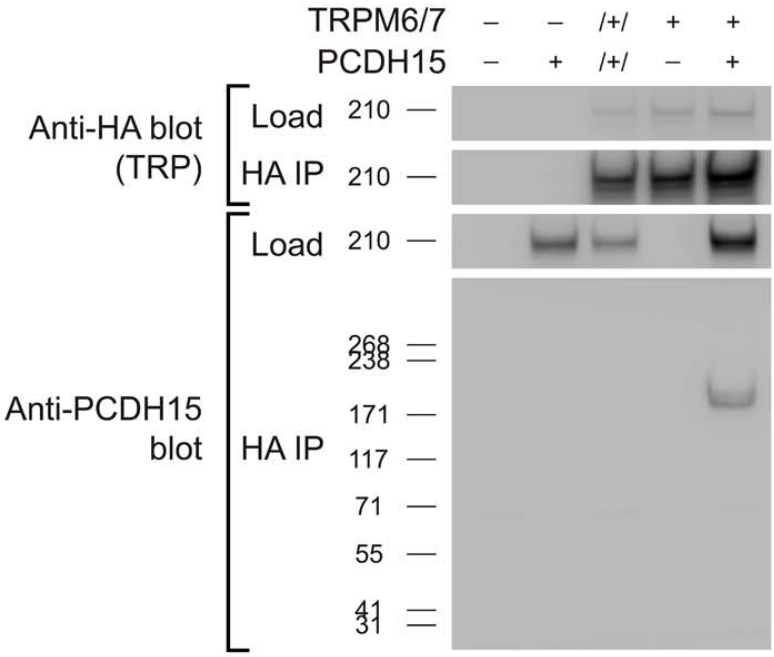
TRPM6/7 – – /+/ + +
PCDH15 – + /+/ – +
Anti-HA blot (TRP)
Load
HA IP
Anti-PCDH15 blot
Load
HA IP
210
210
210
268
238
171
117
71
55
41
31

B

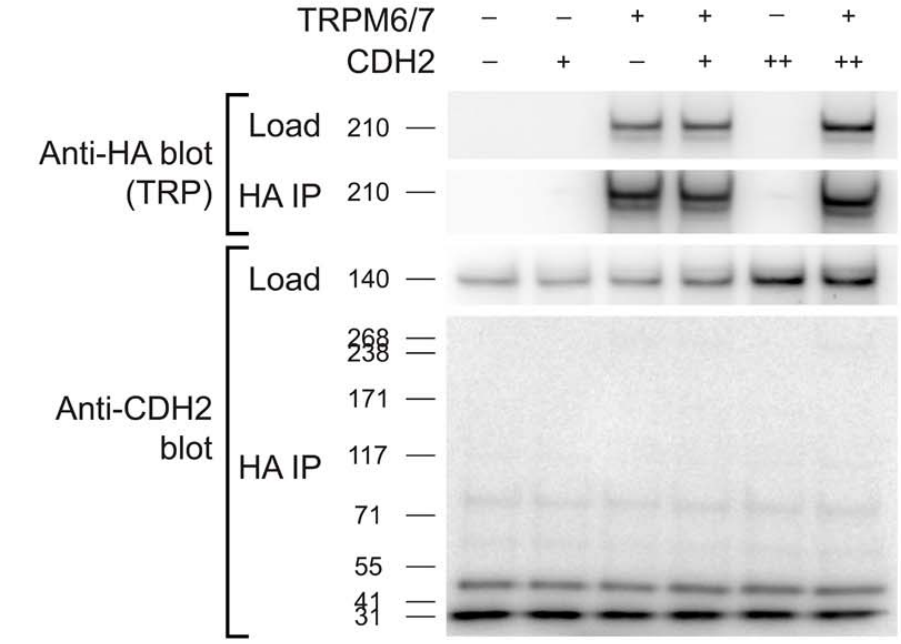
TRPM6/7 – – + + – +
CDH2 – + – + ++ ++
Anti-HA blot (TRP)
Load
HA IP
Anti-CDH2 blot
Load
HA IP
210
210
140
268
238
171
117
71
55
41
31

Figure 4.3 – Two control experiments for PCDH15-TRPM6/7 interaction.
A, TRPM6/7 and PCDH15 were expressed in two separate cell populations, harvested, and lysates mixed before immunoprecipitation. Under this condition (lane 3, in which TRPMs and PCDH15's presence is marked by "/+/"), TRPM6/7 did not co-immunoprecipate with PCDH15. B, CDH2 did not co-immunoprecipate with TRPM6/7. Because CDH2 is endogenously expressed in HEK293T cells (first lane on the left), I used two concentrations of DNA for it: "+" indicates that 0.1ug DNA were used in transfection, while "++" indicates 0.2ug DNA were used.

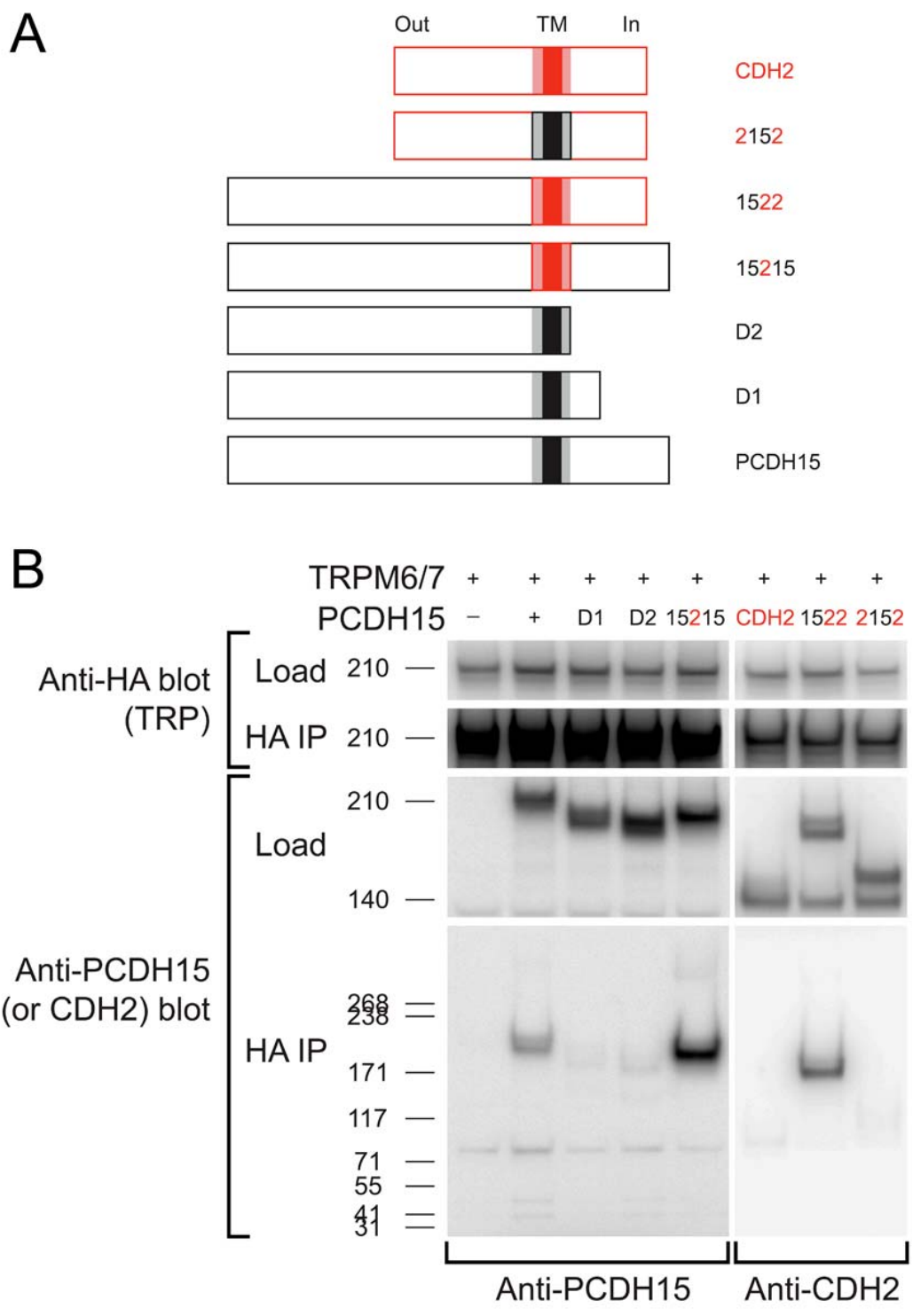
A
Out
TM
In
CDH2
2152
1522
15215
D2
D1
PCDH15
B
TRPM6/7 + + + + + + + +
PCDH15 – + D1 D2 15215 CDH2 1522 2152
Anti-HA blot (TRP)
Load
HA IP
210
210
Load
210
140
Anti-PCDH15 (or CDH2) blot
HA IP
268
238
171
117
71
55
41
31
Anti-PCDH15
Anti-CDH2

Figure 4.4 – PCDH15 domains responsible for its interaction with TRPM6/7
A, diagram of all the constructs used. Transmemrbane domains are in solid black (PCDH15) or red (CDH2); juxtamembrane domains are in grey (PCDH15) or light red (CDH2). B, lysates were immunoprecipitated with anti-HA agarose, and probed with anti-PCDH15 antibody (left) or CDH2 antibody (right). Two C terminal deletion proteins of PCDH15, D1 and D2, do not immunoprecipate with TRPM6/7; chimeras that have N terminal extracellular domains of PCDH15 (15215 and 1522) immunoprecipitate with TRPM6/7 more strongly than PCDH15; 2152, a chimera that do not contain extracellular domains of PCDH15, do not immunoprecipitate with TRPM6/7. For generation of CHD2-PCDD15 chimeras, PCDH15_CD3 was used as the starting sequence.

A

```
                                                                S1 Uniprot
mmTRPM7                 CLKLAVSSRLRPFVAHTCTQMLLSDMWMGRLNMRKNSWYKVILSILVPPAILMLEYKTKA 780
delta-Ex20_mmTRPM7      CLKLAVSSRLRPFVAHTCTQMLLSDMWMGRLNMRKNSWYKVILSILVPPAILMLEYKTKA 780
                        ************************************************************

mmTRPM7                 EMSHIPQSQDAHQMTMEDSENNFHNITEEIPMEVFKEVKILDSSDGKNEMEIHIKSKKLP 840
delta-Ex20_mmTRPM7      EMSHIPQSQDAHQMTMEDSENNFHNITEEIPMEVFKEVKILDSSDGKNEMEIHIKSKKLP 840
                        ************************************************************
                                    S2 Uniprot
mmTRPM7                 ITRKFYAFYHAPIVKFWFNTLAYLGFLMLYTFVVLVKMEQLPSVQEWIVIAYIFTYAIEK 900
delta-Ex20_mmTRPM7      ITRKFYAFYHAPIVKFWFN------------------------------------------ 859
                        ****************************----------------
                                          S3 Uniprot
mmTRPM7                 VREVFMSEAGKISQKIKVWFSDYFNVSDTIAIISFFVGFGLRFGAKWNYINAYDNHVFVA 960
delta-Ex20_mmTRPM7      --TVFMSEAGKISQKIKVWFSDYFNVSDTIAIISFFVGFGLRFGAKWNYINAYDNHVFVA 917
                          ************************************************************
                             S4 Uniprot                                   S5 Uniprot
mmTRPM7                 GRLIYCLNIIFWYVRLLDFLAVNQQAGPYVMMIGKMVANMFYIVVIMALVLLSFGVPRKA 1020
delta-Ex20_mmTRPM7      GRLIYCLNIIFWYVRLLDFLAVNQQAGPYVMMIGKMVANMFYIVVIMALVLLSFGVPRKA 977
                        ************************************************************
                                          P-loop Uniprot
mmTRPM7                 ILYPHEEPSWSLAKDIVFHPYWMIFGEVYAYEIDVCANDSTLPTICGPGTWLTPFLQAVY 1080
delta-Ex20_mmTRPM7      ILYPHEEPSWSLAKDIVFHPYWMIFGEVYAYEIDVCANDSTLPTICGPGTWLTPFLQAVY 1037
                        ************************************************************
                           S6 Uniprot
mmTRPM7                 LFVQYIIMVNLLIAFFNNVYLQVKAISNIVWKYQRYHFIMAYHEKPVLPPPLIILSHIVS 1140
delta-Ex20_mmTRPM7      LFVQYIIMVNLLIAFFNNVYLQVKAISNIVWKYQRYHFIMAYHEKPVLPPPLIILSHIVS 1097
                        ************************************************************

mmTRPM7                 LFCCVCKRRKKDKTSDGPKLFLTEEDQKKLHDFEEQCVEMYFDEKDDKFNSGSEERIRVT 1200
delta-Ex20_mmTRPM7      LFCCVCKRRKKDKTSDGPKLFLTEEDQKKLHDFEEQCVEMYFDEKDDKFNSGSEERIRVT 1157
                        ************************************************************
```

B

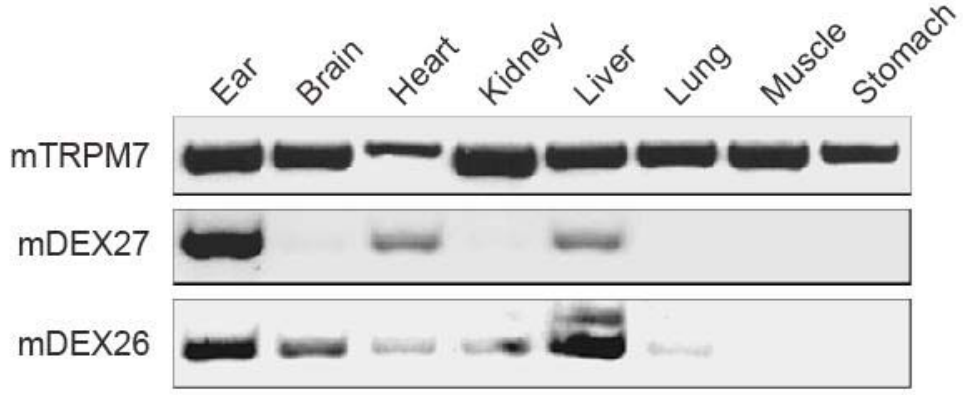

Figure 4.5 – Two new splice variants of TRPM7 and TRPM6.
A, amino acid sequence of canonical TRPM7 and DEX27. Transmembrane segments that are predicted to start from inside the cell and end on the outside are highlighted in yellow; Outside to inside ones are highlighted in green. Glycosylation sites are highlighted in red. Predictions were made by the TOPCONs SCAMPI-msa model (TOPCONS; http://topcons.net/index.php). B, tissue expression profiles of mouse TRPM7, DEX27, and DEX26. Primer sets DEX27 and DEX26 were designed such that they bind to the junction of exon 19 and exon 21. Both DEX27 and DEX26 are highly expressed in the ear (first lane on the left).

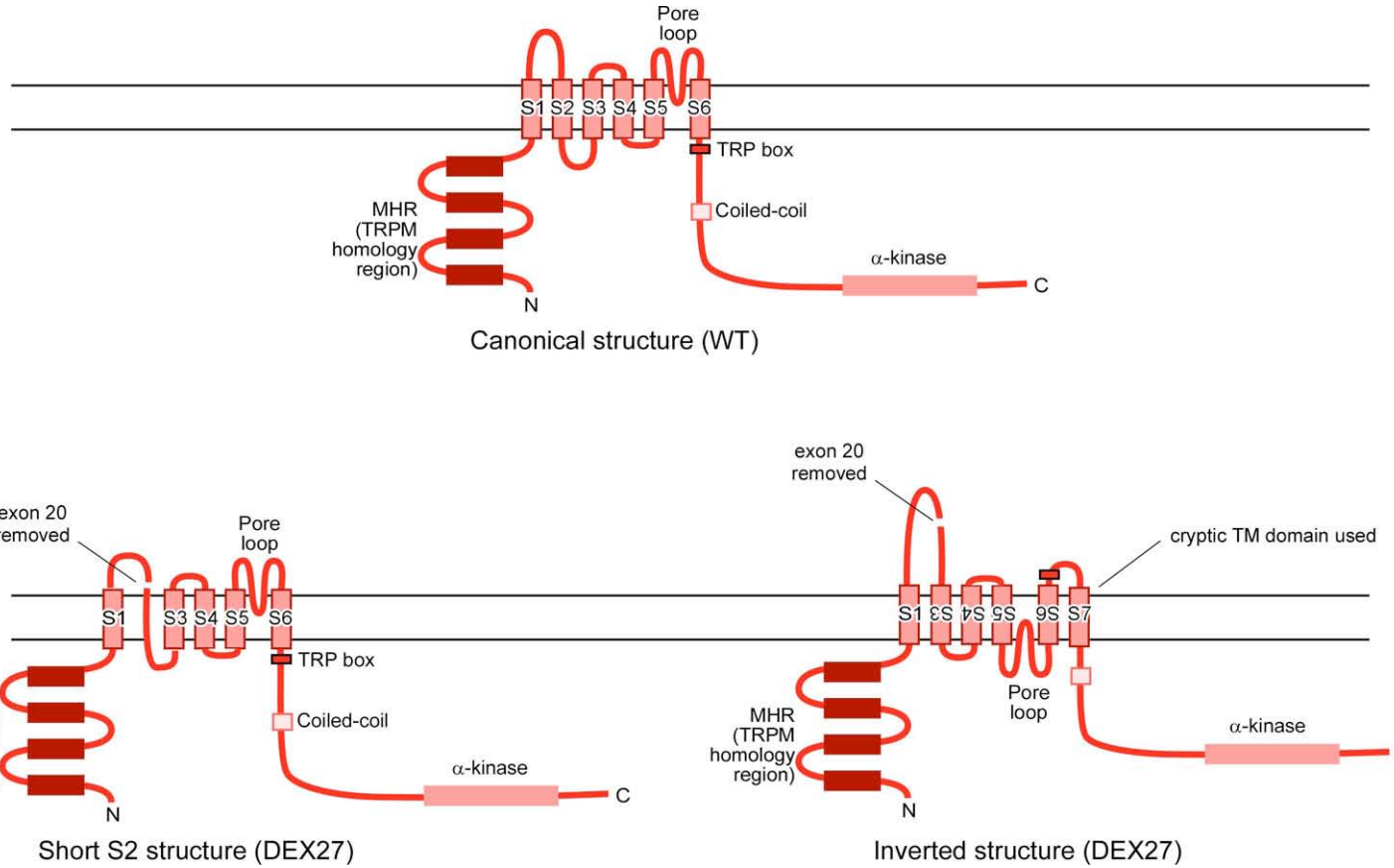
Pore
loop
S1 S2 S3 S4 S5 S6
TRP box
MHR
(TRPM
homology
region)
Coiled-coil
α-kinase
N
C
Canonical structure (WT)
exon 20
removed
Pore
loop
S1 S3 S4 S5 S6
TRP box
MHR
(TRPM
homology
region)
Coiled-coil
α-kinase
N
C
Short S2 structure (DEX27)
exon 20
removed
cryptic TM domain used
S1 S3 S4 S5 S6 S7
Pore
loop
MHR
(TRPM
homology
region)
α-kinase
N
C
Inverted structure (DEX27)

Figure 4.6 – Predicted topology of canonical TRPM7 and DEX27 protein. The inverted structure of DEX27 was predicted by TOPCONs SCAMPI-msa model (TOPCONS; http://topcons.net/index.php). The Short S2 structure of DEX27 was based on the idea that a subsequent transmembrane segment (S3, for example) could have a dominant effect, i.e., it may want to stay in the membrane in the same orientation (Lu et al., 1998; Sakaguchi, 2002; Xiong et al., 1997).

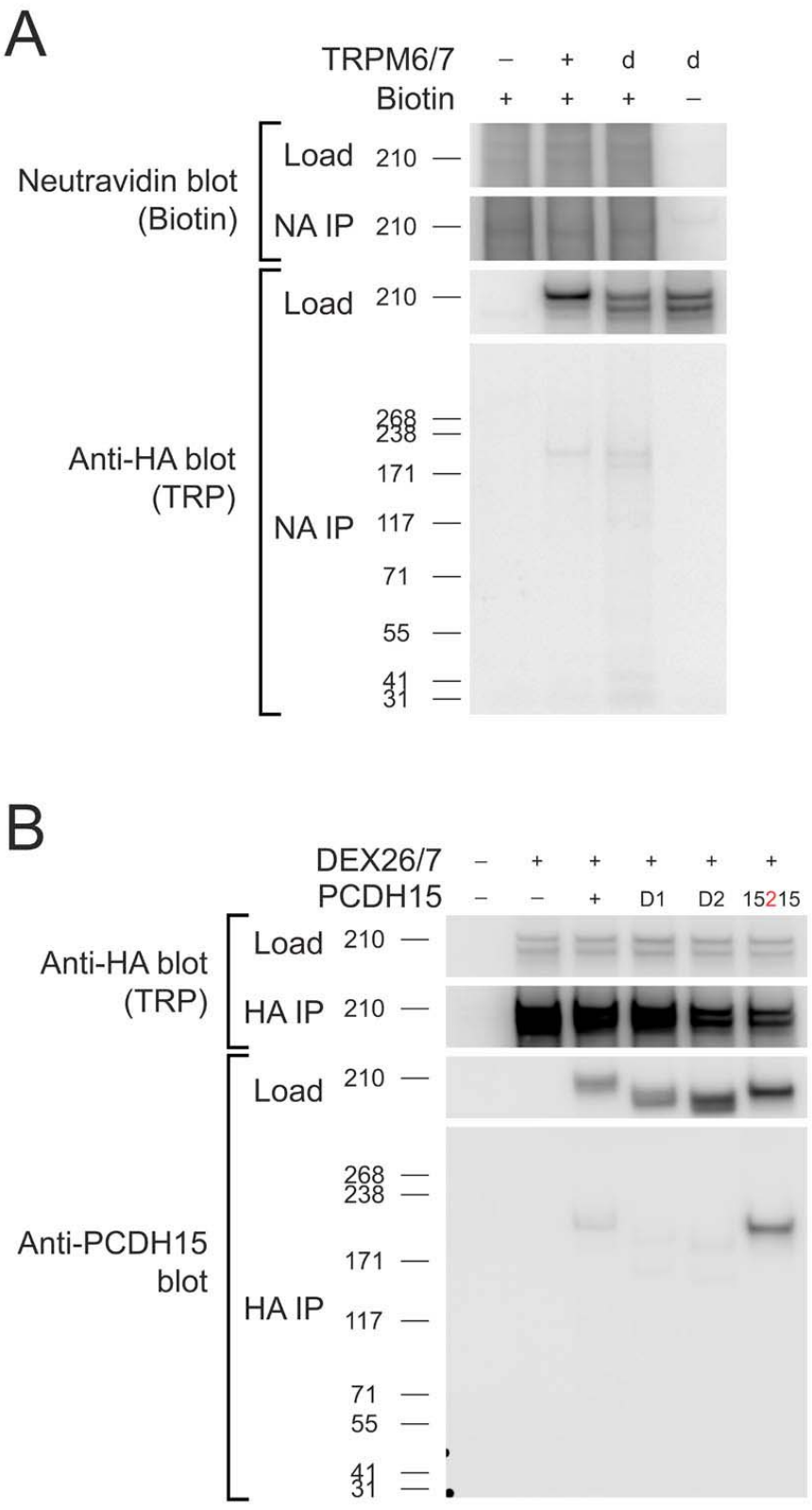
A
TRPM6/7 – + d d
Biotin + + + –
Neutravidin blot (Biotin)
Load
NA IP
210
Anti-HA blot (TRP)
Load
NA IP
268
238
171
117
71
55
41
31
B
DEX26/7 – + + + + +
PCDH15 – – + D1 D2 15215
Anti-HA blot (TRP)
Load
HA IP
210
Anti-PCDH15 blot
Load
HA IP
268
238
171
117
71
55
41
31

Figure 4.7 – DEX26/7 protein behaves similarly to TRPM6/7.
A, both TRPM6/7 and DEX26/7 protein were expressed and go to cell surface. HEK293T cells were transfected with TRPM6/7 or DEX26/7 (“d”). Before harvest, the cells were surface biotinylated. Cell lysates were then immunoprecipitated with neutravin-agarose, then probed with anti-HA antibody. B, DEX26/7 interacted with PCDH15 in a similar fashion with TRPM6/7.

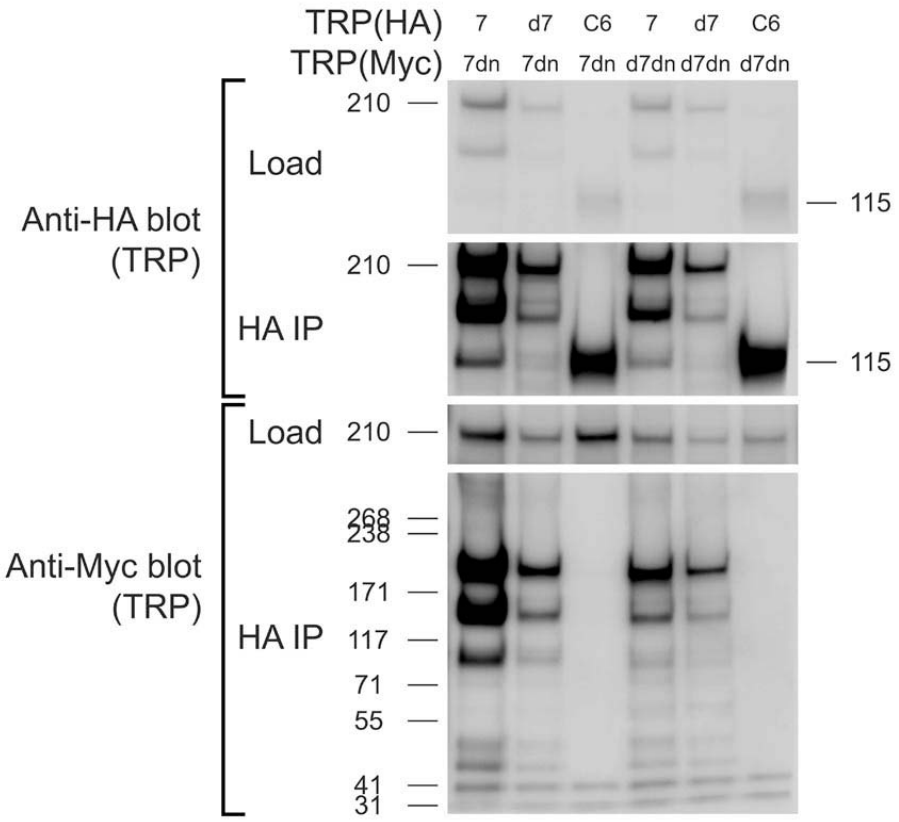

Figure 4.8 – Dominant negative versions of TRPM7 and DEX27 interact with wild type channels

HA and 3X myc tagged versions of TRPM7 (7), dnTRPM7 (7dn), DEX27 (d7), and dnDEX27 (d7dn) were transfected into HEK293T cells. HA tagged TRPC6 (C6) was used as a control. Lysates were immunoprecipitated with anti-HA agarose and probed with anti-myc antibody.

A

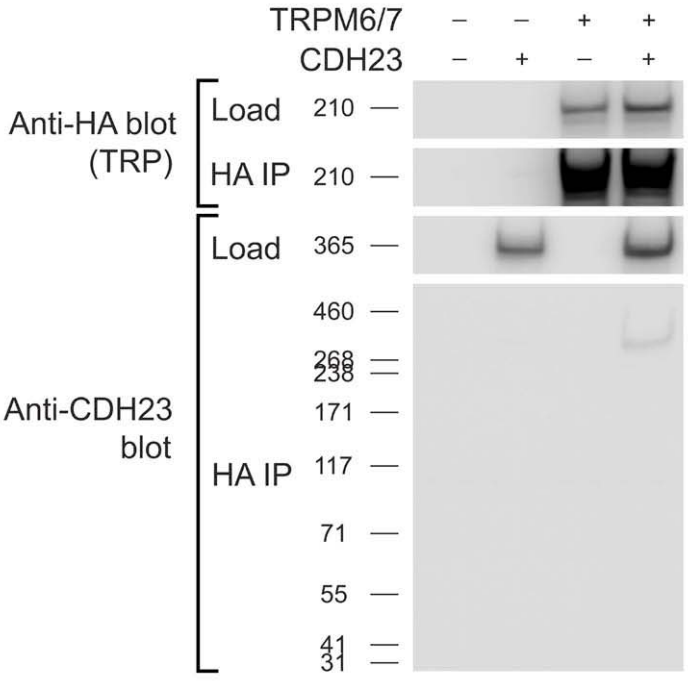
TRPM6/7 – – + +
CDH23 – + – +
Anti-HA blot (TRP)
Load
HA IP
210
210
Anti-CDH23 blot
Load
365
460
268
238
171
HA IP
117
71
55
41
31

B

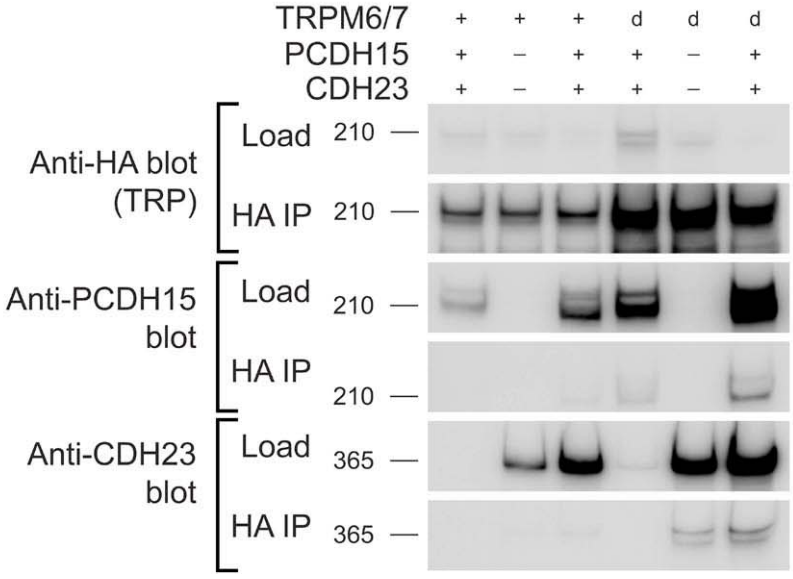
TRPM6/7 + + + d d d
PCDH15 + – + + – +
CDH23 + – + + – +
Anti-HA blot (TRP)
Load
HA IP
210
210
Anti-PCDH15 blot
Load
HA IP
210
210
Anti-CDH23 blot
Load
HA IP
365
365

Figure 4.9 – CDH23 co-immunoprecipitates with TRPM6/7 and DEX26/7.
A, CDH23 interacts with TRPM6/7 in HEK293T cells. B, CDH23 co-immunoprecipitated with TRPM6/7 and DEX26/7 (d) independent of PCDH15.

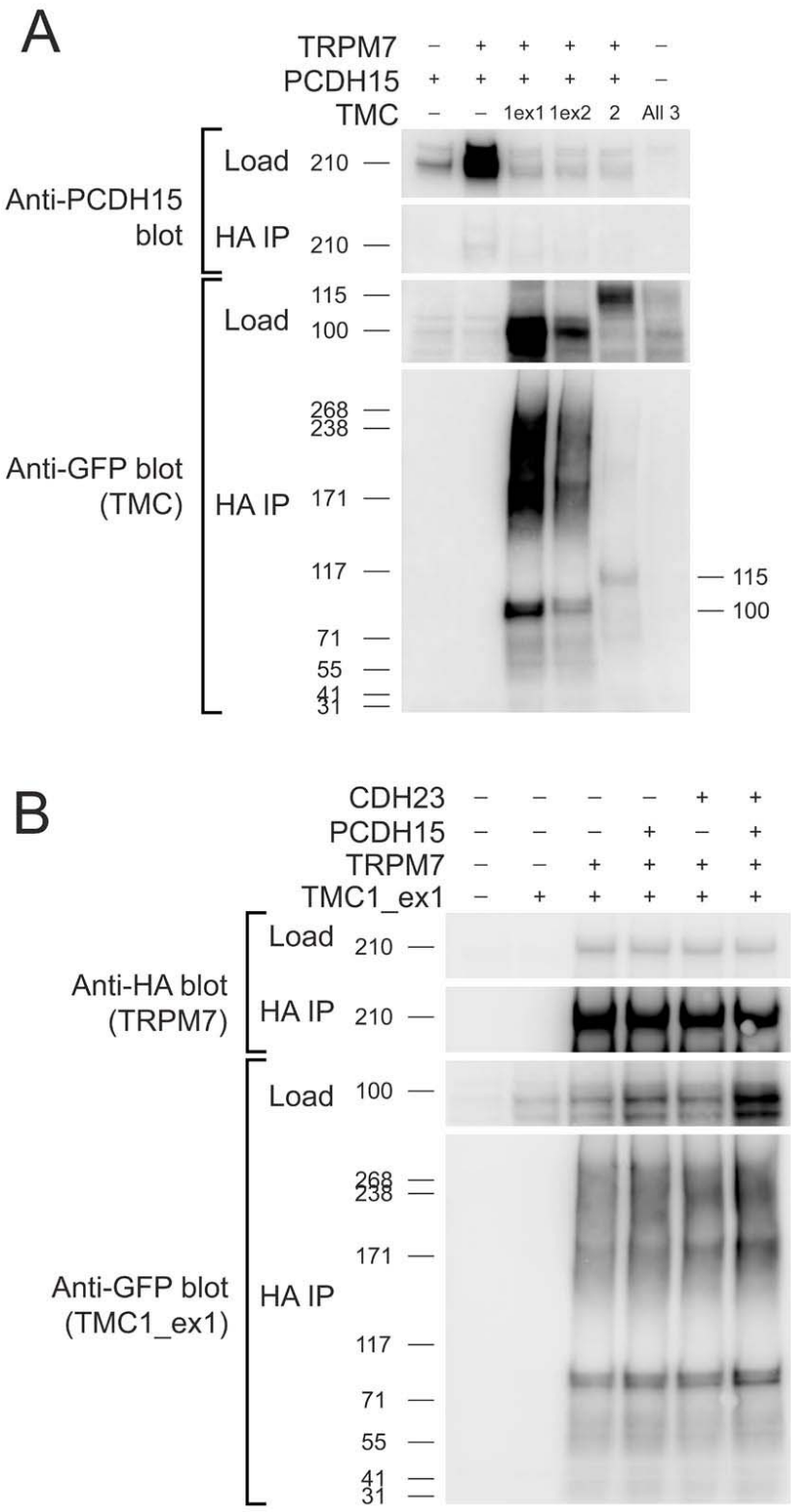

Figure 4.10 – TMCs co-immunoprecipitate with TRPM7 and PCDH15.

TMC1_ex1(1ex1), TMC1_ex2(1ex2), and TMC2 were all tagged with AcGFP on the C terminal end. A, lysates were immunoprecipitated with anti-HA agarose and probed with anti-GFP antibody. All three forms of TMC co-immunoprecipitated with TRPM7/PCDH15 complex. B, TMC1_ex1 co-immunoprecipitated with TRPM7, independent of PCDH15 or CDH23.

A

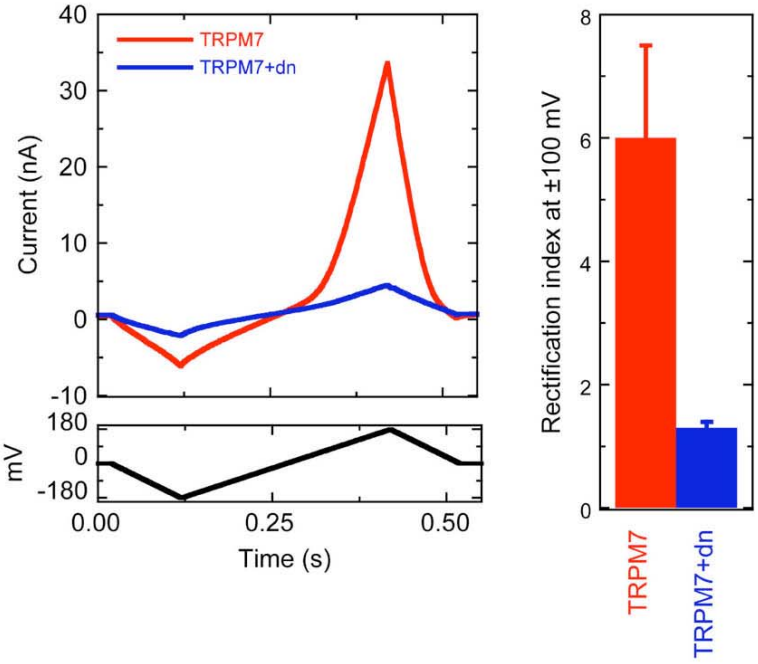
TRPM7
TRPM7+dn
Current (nA)
40
30
20
10
0
-10
mV
180
0
-180
0.00
0.25
0.50
Time (s)
Rectification index at ±100 mV
8
6
4
2
0
TRPM7
TRPM7+dn

B

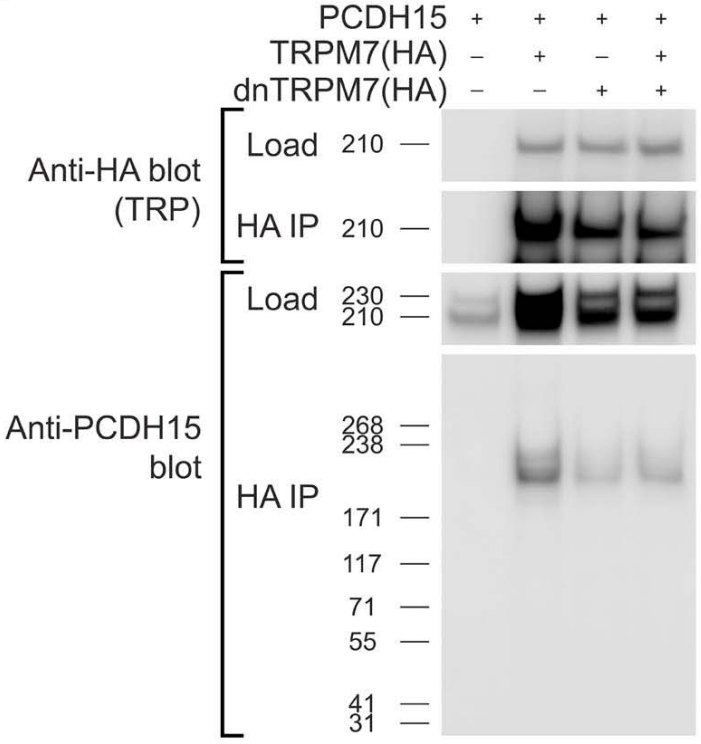
PCDH15 + + + +
TRPM7(HA) – + – +
dnTRPM7(HA) – – + +
Anti-HA blot (TRP)
Load 210
HA IP 210
Load 230 210
Anti-PCDH15 blot
HA IP
268
238
171
117
71
55
41
31

Figure 4.11 –dnTRPM7 inhibit wild type TRPM7 current and interacts with PCDH15. A, dnTRPM7 inhibited current from wild type TRPM7 in HEK293T cells. Whole cell currents were recorded on HEK293T cells transfected with TRPM7 only, or TRPM7 + dnTRPM7 (3X DNA was used for dnTRPM7 than wild type TRPM7). A voltage ramp from -180 mV to +180 mV was applied to the cells and currents recorded (left); rectification index is shown on the right. B, dnTRPM7 co-immunoprecipitated with PCDH15, similar to wild type TRPM7.

A

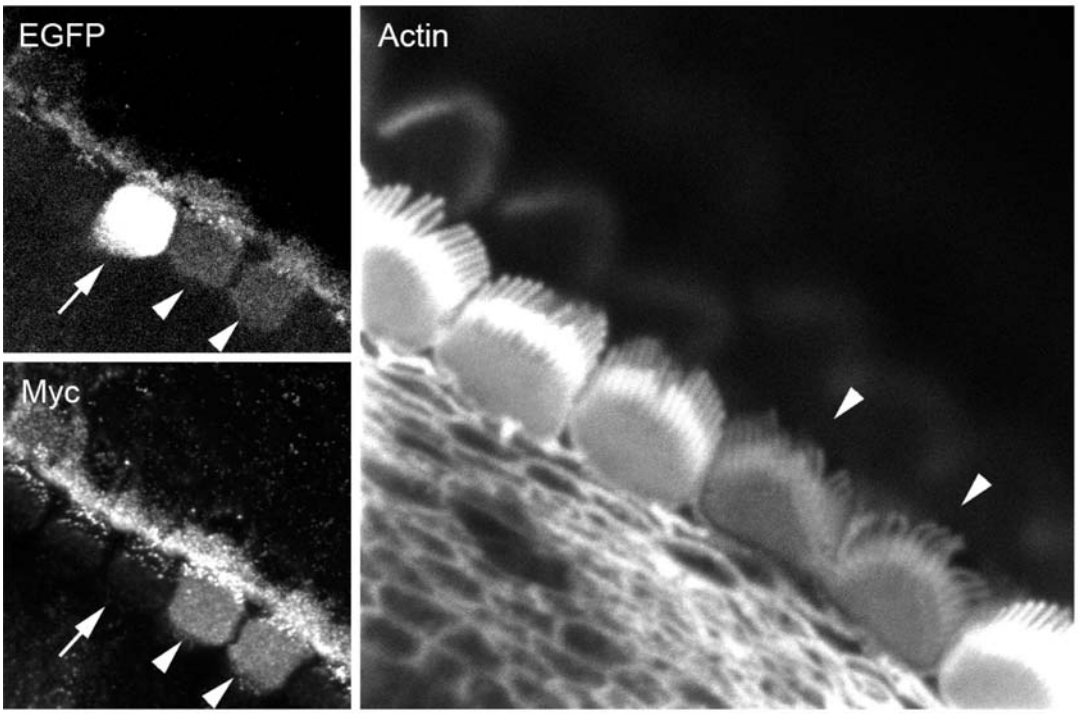

B

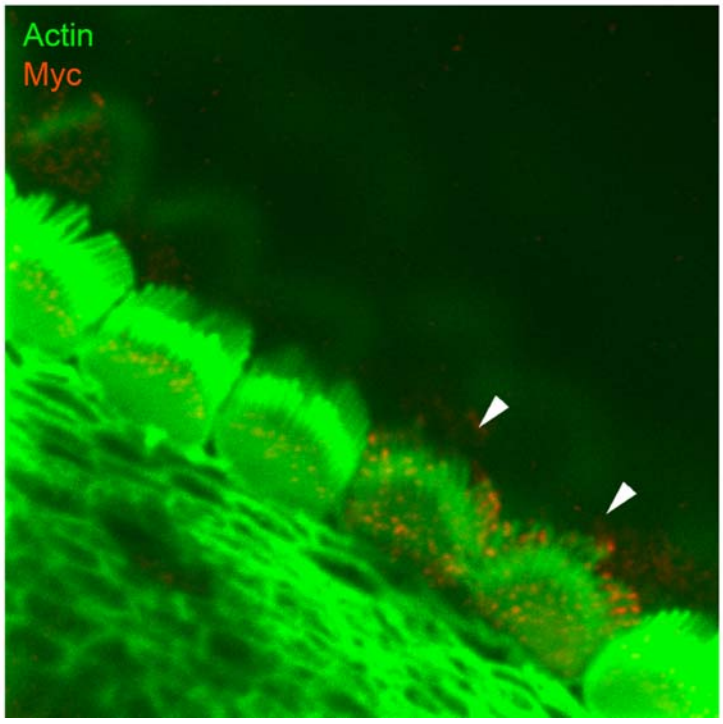

Figure 4.12 – dnTRPM7_3Xmyc transfected hair cells have thinner stereocilia
Mouse hair cell progenitors were transfected with EGFP and dnTRPM7_3Xmyc using in utero electroporation at E12.5. At P6.5, organ of Corti were dissected, stained with anti-myc antibody, and imaged. A, upper left: EGFP; lower left, myc staining; right: TRITC-phalloidin stain of the same area in a bigger view. Arrows point to an inner hair cell with strong EGFP expression. This cell is not myc positive. Arrowheads point to the two neighboring cells, which have weak EGFP expression, but are myc positive. In the phalloidin stain panel on the right, note the thinner and bent stereocilia of the two cells that are also myc positive (lower left). B, the right panel in A, pseudo-colored. Actin is shown in green and myc staining in shown in red. Note the myc staining at the tips of some stereocilia.

Chapter 5 – Conclusions and future directions

General summary

The work presented in this thesis provides new information on the molecular components of the hair bundle and their interactions, as well as an improved method for the studying the localization of hair bundle proteins. Chapter 2 describes an improved gene gun method for transiently transfect hair cells in frog, chicken, and mouse. By modifying the Bio-Rad Helios gene gun and adding a sample chamber that helps to reduce the damaging effect, we report improved transfection efficiency and reduced damage to the hair bundle. In Chapter 3, I characterize the lipid components of the hair bundle, and describe large membrane domains in hair bundles. These large membrane domains are responsible for activation of radixin, an important protein in the hair bundle, in a spatially constricted manner. Chapter 4 characterizes the interaction between PCDH15, a tip link component, and TRPM7, a MET channel candidate.

Chapter 2 conclusions and future directions

In chapter 2, we modified the Helios Gene Gun and developed a protocol that resulted in increased transfection efficiency with minimal damage to hair cells. The combination of increased penetration power and reduced shockwave will be of general applicability for transfection of many other cell types and tissues. The improved gene-gun transfection method should facilitate studies examining protein localization, interaction, and function in hair cells and many other cell types.

In particular, we used the improved method to transfect mouse cochlea hair cells through the basilar membrane, thus minimizing damage to the hair bundle. We speculate that with this method, tip links and mechanotransduction of the transfected hair cell could be preserved. Patch clamp experiments that measure the MET current and adaptation are necessary to test this hypothesis. If the MET transduction of the transfected hair cells are indeed unaffected, this method could offer a quick and easy way to study the localization and function of proteins in the tip link complex, including the MET channel candidates. So far, we have only transfected cochlea of CD1 mice at age P4. However, based on the comparison between cochlea from CD1 mice and C57BL6 mice, we suspect that cochlea from C57BL6 could be transfected with this method from P0 to P8 (for older mice, dissection of the cochlea becomes very difficult), spanning most of the period in which the MET channel complex matures (Lelli et al., 2009). Further experiments to optimize the transfection conditions of mouse cochlea at these different ages may be necessary. Variables in the transfection conditions include gold particle size, helium burst pressure, and diffuser membranes of different pore sizes.

Chapter 3 conclusions and future directions

In chapter 3, I described one functional role of the large membrane domains in hair bundles: spatial constricted activation of radixin. Membrane domains in the hair bundle could play important roles in other aspects of the hair bundle function, including mechnotransduction. For example, cholesterol has been shown to be a major component of hair cell stereocilia (Forge, 1991; Jacobs and Hudspeth, 1990). These observations were confirmed by our lipid mass spectrometry results in chapter 3.

Cholesterol has been implicated in mechanotransduction in *C. elegans*: MEC-2, one of the DEG/ENaC channels that underlie touch sensation, binds cholesterol and mutations that disrupt touch sensation also disrupt cholesterol binding (Huber et al., 2006). In addition, a group found that cholesterol may play an important role in osteoblastic cell mechanotransduction (Xing et al., 2011). In vertebrate hair cells, PIP_2 is required for mechanotransduction (Hirono et al., 2004). We found that cholesterol is concentrated near the stereocilia tips in isolated bullfrog hair cells (Figure 5.1, H), and cyclodextrins, reagents that bind and extract cholesterol from the cellular membranes, modulate MET current in transepithelial assays using bullfrog sacculus (Figure 5.1, A-G). When isolated hair cells were treated with these cyclodextrins for longer periods of time (30 – 120 min), localizations of PMCA2 and PTPRQ in the hair bundle were changed significantly (data not shown). Furthermore, cholesterol loading also changed the localization pattern of PMCA2 and PTPRQ (data not shown).

Collectively, these results suggest that lipid domains may play important roles in protein localization and function in the hair bundle. To further investigate the roles lipid and membrane domains play in hair bundle protein localization and mechanotransduction, transient transfection experiments, using the improved gene gun method described in chapter 2, could be performed. For example, to study the role PIP_2 plays in protein localization, one could transiently express the phospholipase C (PLC)-δ1 pleckstrin homology (PH) domain fused to green fluorescent protein (GFP). This PH domain binds specifically and with high affinity to PIP_2, such that the localization of PIP_2 could be monitored by live confocal imaging (Micheva et al., 2001). Co-transfection of a

hair bundle protein together with the PLC-δ1 PH domain could provide useful information about the regulatory role PIP_2 plays in the localization of the particular protein. Also, GPI-anchored proteins have been used in transient transfection experiments to study the role of lipid rafts (Xing et al., 2011). This method could be used together with the improved gene gun method described in chapter 2, to study the role of lipid domains in localizing hair bundle proteins.

Chapter 4 conclusions and future directions

In order to obtain candidates for the MET channel, Clive Morgan, a postdoc in the Gillespie lab, homogenized thousands of chicken ears and subjected them to a sophisticated purification procedure. In his procedure, G19, a monoclonal antibody against PCDH15, was used in an affinity purification step. At the end of the purification procedure, the protein affinity purification eluate was examined by mass spectrometry. TRPM7 was identified as one of the ion channels in the complex. This result suggests that PCDH15 and TRPM7 are in the same complex in the chicken ear, through direct or indirect interactions. This result also suggests that TRPM7 could be the MET channel. In chapter 3, we characterized the interaction between PCDH15 and TRPM7. Because TRPM6 is a close family member of TRPM7 and frequently forms heteromeric channels with TRPM7 (Fonfria et al., 2006; Li et al., 2006), we also included TRPM6 in the study. The interaction studies were done in HEK293T cells, a heterologous system, in which the proteins were transiently expressed. Through these experiments, we concluded that PCDH15 interacts with TRPM6/7, probably through its extracellular domains. Also, TMCs, newly proposed candidates of MET channel, interact with TRPM6/7 and PCDH15

in similar immunoprecipitation experiments. Although we performed many control experiments, we understand that these immunoprecipitation results should be interpreted with caution.

The more significant questions are: A. Do TRPM6/7 proteins localize near the tip of the stereocilia (where MET channel locates)? B. Do TRPM6/7 proteins interact with PCDH15 in hair cells, near the tip of the stereocilia? We do not have answers to the second question; regarding the first question, our in utero electroporation experiments suggest that dnTRPM7_3Xmyc, which behaves similarly to wild type TRPM7, localize near the stereocilia tips in mouse hair cells. However, we did not observe any myc positive hair cells when we introduced TRPM7_3Xmyc into hair cells by electroporation. This could result from the possibility that wild type TRPM7 is toxic to the hair cells or is selectively inhibited by the hair cells, as previously discussed in chapter 4. To address this, we are doing short-harvest experiments with TRPM7, and we will use TRPM8, another member of the TRPM family, as an alternative control to the dnTRPM7.

Another factor at work is the low frequency of transfected cochleas and small number of transfected hair cells we observed. We have noticed that in the in utero electroporation technique, as the plasmid size increases, transfection efficiency decreases dramatically, as plasmids over 10KB result in very low transfection efficiency (John V. Brigande, unpublished observations). One strategy to reduce the size of the plasmids and increase the transfection efficiency is the use of minicircle DNA vector, which is a circular expression cassette without the bacterial plasmid DNA backbone. These vectors have been shown to have 10- to 1,000-fold enhancement compared with

regular plasmids in long-term transgene expression in vivo and in vitro (Chen et al., 2003; Huang et al., 2009; Jia et al., 2010). We produced minicircle versions of TRPM7_3Xmyc and dnTRPM7_3Xmyc and are in the process of testing them in the in utero electroporation experiments. Another strategy is to increase the transfection efficiency of electroporation through a dual-pulse electroporation paradigm, which was shown to increase transfection efficiency and reduce damage during electroporation in vitro (Stroh et al., 2010; Yockell-Lelievre et al., 2009) and could improve transfection efficiency in vivo (Andre et al., 2008; Hojman et al., 2008). We are in the process of testing this new approach. Alternatively, the improved gene gun method described in chapter 2 could be used to study the localization of TRPM6/7 channel proteins.

The localization of dnTRPM7_3Xmyc near stereocilia tips were based on antibody staining. Because different antibodies could stain the stereocilia tips non-specifically (Gillespie lab, unpublished observations), we have generated N and C terminal TdTomato fusion constructs of TRPM7 and dnTRPM7, which could be transfected into muse hair cells using in utero electroporation or gene gun transfection.

Aside from proper localization, the MET channel candidate's functional importance has to be demonstrated. One strategy to show functional importance is knocking out the protein using transgenic mice. Since global knockout of either TRPM6 and TRPM7 results in embryonic lethality (Jin et al., 2008; Woudenberg-Vrenken et al., 2011), conditional knockouts of TRPM6 and TRPM7 that are restricted to hair cells are necessary. We are in the process of testing a hair cell specific TRPM7 conditional knockout, in collaboration of Dr. Uli Mueller. Preliminary hearing tests on these TRPM7

conditional knockout mice, using click auditory brainstem response (click ABR, a hearing test with a multiple-frequency sound, the “click”), revealed no apparent hearing deficit.

The tonotopic conductance differences of the MET channel suggest that the channel might consist of several distinct subunits with variations in subunit composition from the base to the apex of the cochlea (Beurg et al., 2006; Ricci et al., 2003). The potential existence of several subunits raises the possibility of compensation among them in genetic knockout studies. This has been the challenge in defining the role of DEG/ENaC proteins in mammalian mechanotransduction (Drew et al., 2004; Drummond et al., 2000; Fricke et al., 2000; Garcia-Anoveros et al., 2001; Price et al., 2000). If the MET channels are composed of multiple members of the TRPM family, and they can compensate for each other functionally, conditionally knocking out one member could have normal hearing and mechanotransduction. In zebrafish, when TRPM6 was knocked down with antisense morpholino oligos on a TRPM7 mutant background, reduced number of hair cells, as well as reduced FM1-43 uptake into hair cells (per hair cell) were observed (Teresa Nicolson, unpublished observation). In these fish, mRNA levels of TRPM1, TRPM3, and TRPM7 were all up-regulated, suggesting compensation of TRPM6 from the other three members of the TRPM family. This observation is consistent with the previous finding that TRPM1, TRPM3, TRPM6, and TRPM7 could form a subgroup within the TRPM family (Fujiwara and Minor, 2008). In this regard, the dnTRPM7 approach may be of advantage over the knockout of any single member, because it may inhibit current not only from TRPM7, but also those from other heteromeric channels

containing TRPM7 subunits. Indeed, in HEK293T cells, dnTRPM7 inhibited current of co-expressed TRPM6 and TRPM7 (Gillespie lab, unpublished results).

Pure-tone ABR tests on the TRPM7 conditional knockout mice might provide more information regarding the roles TRPM7 play in hearing and hair cell function. Alternatively, conditionally knocking out multiple members of the TRPM family (within the sub-group of TRPM1, 3, 6 and 7, for example) may provide more insight. These experiments are expensive and time-consuming, which highlights the challenging nature of hearing research.

Concluding remarks

New tools that emerge from this thesis include improved transient transfection of hair cells using gene gun, which enhances our ability to deeply investigate the localization, interaction, and function of hair bundle proteins. The characterizations of lipid components in the hair bundle, as well as discovery of functional lipid domains, provide more insight into the molecular composition and functional mechanisms of hair cells. Finally, characterizing the PCDH15-TRPM6/7 interactions provide more information that may help to identify the MET channels. Together, these tools and discoveries open new doors further investigate the molecular mechanisms hair bundle function, particularly mechanotransduction.

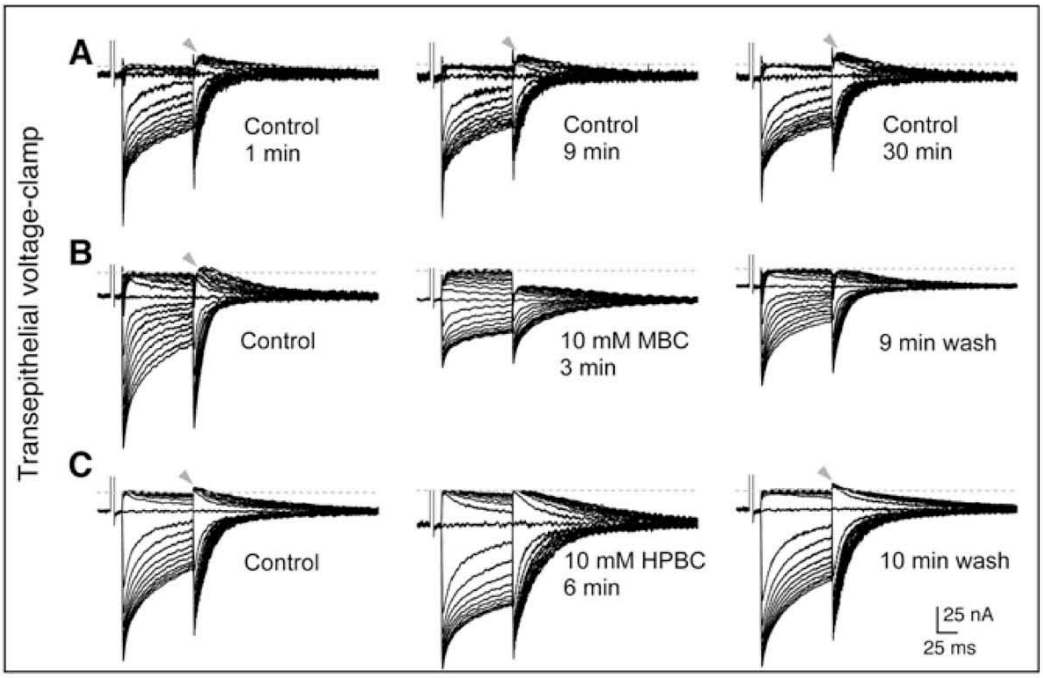
A
Control
1 min
Control
9 min
Control
30 min
B
Control
10 mM MBC
3 min
9 min wash
C
Control
10 mM HPBC
6 min
10 min wash
25 nA
25 ms
Transepithelial voltage-clamp

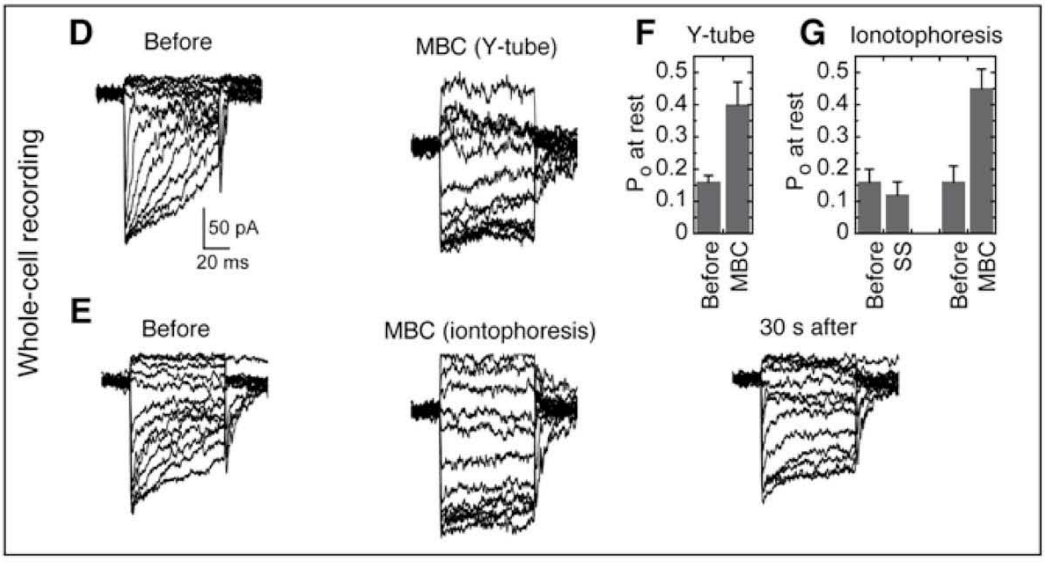
D
Before
MBC (Y-tube)
50 pA
20 ms
E
Before
MBC (iontophoresis)
30 s after
F
Y-tube
G
Iontophoresis
P_o at rest
0.5
0.4
0.3
0.2
0.1
0
Before
MBC
Before
SS
Before
MBC
Whole-cell recording

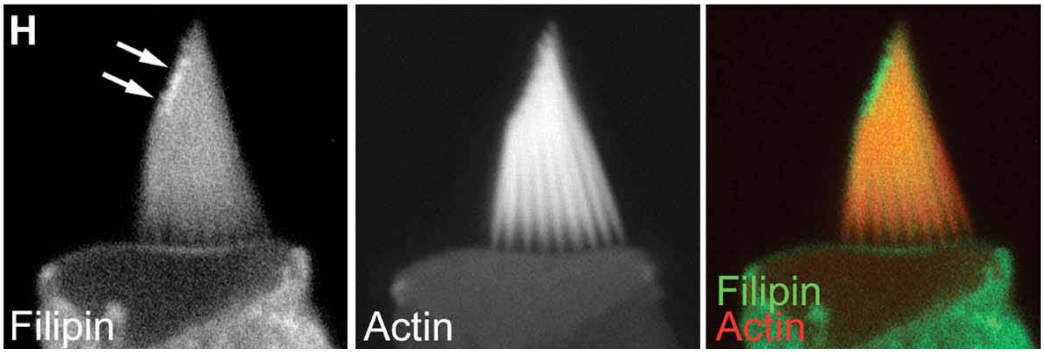
H
Filipin
Actin
Filipin
Actin

Figure 5.1 - Alteration of mechanotransduction by cyclodextrins.

A-C, Transepithelial voltage-clamp assay; cyclodextrins added to apical (hair bundle) compartment. Many hair cells are activated and measured simultaneously. Downward current corresponds to transduction-channel activation; transient before mechanical step is response to voltage pulse to test transepithelial resistance. A, Control. B, MBC decreased total current and increases resting Po. Po returned to normal after wash-out. C, HPBC also increased resting Po but did not affect total current. D-G, Whole-cell recording from single hair cells. D, MBC applied through a Y-tube (10 mM) to bundle region. Po increased substantially. E, MBC applied locally near stereocilia tips through "ionotophoresis" (actually electro-osmosis, as MBC is not charged) also increased Po, which reversed after iontophoretic current stopped. F, Y-tube summary (n=5; mean ± SEM). Difference is significant at $p<0.01$ by t-test. G, Iontophoresis summary; "SS" is standard saline control (n=3 for SS and n=4 for MBC). Difference for MBC is significant at $p<0.05$ by t-test. Stimuli for A-C were -2000 nm to +2000 nm in 200 nm increments; stimuli for D-E were -400 nm to +800 nm in 100 nm increments. H, cholesterol localization in the hair bundle. Filipin was used to stain cholesterol. Note the elevated staining near the stereocilia tips (arrows).

References

Andre, F.M., Gehl, J., Sersa, G., Preat, V., Hojman, P., Eriksen, J., Golzio, M., Cemazar, M., Pavselj, N., Rols, M.P.*, et al.* (2008). Efficiency of high- and low-voltage pulse combinations for gene electrotransfer in muscle, liver, tumor, and skin. Hum Gene Ther *19*, 1261-1271.

Babiychuk, E.B., Monastyrskaya, K., Burkhard, F.C., Wray, S., and Draeger, A. (2002). Modulating signaling events in smooth muscle: cleavage of annexin 2 abolishes its binding to lipid rafts. Faseb J *16*, 1177-1184.

Babiychuk, E.B., Monastyrskaya, K., and Draeger, A. (2008). Fluorescent annexin A1 reveals dynamics of ceramide platforms in living cells. Traffic (Copenhagen, Denmark) *9*, 1757-1775.

Bahloul, A., Michel, V., Hardelin, J., Nouaille, S., Hoos, S., Houdusse, A., England, P., and Petit, C. (2010). Cadherin-23, myosin VIIa and harmonin, encoded by Usher syndrome type I genes, form a ternary complex and interact with membrane phospholipids. Hum Mol Genet *19*, 3557-3565.

Baird, D., Stefan, C., Audhya, A., Weys, S., and Emr, S. (2008). Assembly of the PtdIns 4-kinase Stt4 complex at the plasma membrane requires Ypp1 and Efr3. The Journal of cell biology *183*, 1061-1074.

Bali, R., Savino, L., Ramirez, D.A., Tsvetkova, N.M., Bagatolli, L., Tablin, F., Crowe, J.H., and Leidy, C. (2009). Macroscopic domain formation during cooling in the platelet

plasma membrane: an issue of low cholesterol content. Biochimica et biophysica acta *1788*, 1229-1237.

Bates-Withers, C., Sah, R., and Clapham, D.E. (2011). TRPM7, the Mg(2+) inhibited channel and kinase. Adv Exp Med Biol *704*, 173-183.

Bedrosian, J., Gratton, M., Brigande, J., Tang, W., Landau, J., and Bennett, J. (2006). In vivo delivery of recombinant viruses to the fetal murine cochlea: transduction characteristics and long-term effects on auditory function. Mol Ther *14*, 328-335.

Belyantseva, I., Boger, E., and Friedman, T. (2003). Myosin XVa localizes to the tips of inner ear sensory cell stereocilia and is essential for staircase formation of the hair bundle. Proc. Natl. Acad. Sci. USA *100*, 13958-13963.

Belyantseva, I.A. (2009). Helios Gene Gun-mediated transfection of the inner ear sensory epithelium. Methods Mol Biol *493*, 103-123.

Ben-David, O., and Futerman, A. (2010). The role of the ceramide acyl chain length in neurodegeneration: involvement of ceramide synthases. Neuromolecular Med *12*, 341-350.

Beurg, M., Evans, M., Hackney, C., and Fettiplace, R. (2006). A large-conductance calcium-selective mechanotransducer channel in mammalian cochlear hair cells. J Neurosci *26*, 10992-11000.

Beurg, M., Fettiplace, R., Nam, J.H., and Ricci, A.J. (2009). Localization of inner hair cell mechanotransducer channels using high-speed calcium imaging. Nat Neurosci *12*, 553-558.

Bligh, E.G., and Dyer, W.J. (1959). A rapid method of total lipid extraction and purification. Can. J. Biochem. Physiol. *37*, 911-917.

Boeda, B., El-Amraoui, A., Bahloul, A., Goodyear, R., Daviet, L., Blanchard, S., Perfettini, I., Fath, K., Shorte, S., Reiners, J.*, et al.* (2002). Myosin VIIa, harmonin and cadherin 23, three Usher I gene products that cooperate to shape the sensory hair cell bundle. EMBO J *21*, 6689-6699.

Bornig, H., and Geyer, G. (1974). Staining of cholesterol with the fluorescent antibiotic "filipin". Acta Histochem *50*, 110-115.

Boulgaropoulos, B., Arsov, Z., Laggner, P., and Pabst, G. (2011). Stable and unstable lipid domains in ceramide-containing membranes. Biophysical journal *100*, 2160-2168.

Boussif, O., Lezoualc'h, F., Zanta, M., Mergny, M., Scherman, D., Demeneix, B., and Behr, J. (1995). A versatile vector for gene and oligonucleotide transfer into cells in culture and in vivo: polyethylenimine. Proceedings of the National Academy of Sciences of the United States of America *92*, 7297-7301.

Brown, S.D., Hardisty-Hughes, R.E., and Mburu, P. (2008). Quiet as a mouse: dissecting the molecular and genetic basis of hearing. Nat Rev Genet *9*, 277-290.

Brügger, B., Glass, B., Haberkant, P., Leibrecht, I., Wieland, F., and Krausslich, H. (2006). The HIV lipidome: a raft with an unusual composition. Proceedings of the National Academy of Sciences of the United States of America *103*, 2641-2646.

Caberlotto, E., Michel, V., de Monvel, J.B., and Petit, C. (2011). Coupling of the mechanotransduction machinery and F-actin polymerization in the cochlear hair bundles. Bioarchitecture *1*, 169-174.

Canals, D., Jenkins, R., Roddy, P., Hernandez-Corbacho, M., Obeid, L., and Hannun, Y. (2010). Differential effects of ceramide and sphingosine 1-phosphate on ERM phosphorylation: probing sphingolipid signaling at the outer plasma membrane. The Journal of biological chemistry *285*, 32476-32485.

Castro, B.M., Silva, L.C., Fedorov, A., de Almeida, R.F., and Prieto, M. (2009). Cholesterol-rich fluid membranes solubilize ceramide domains: implications for the structure and dynamics of mammalian intracellular and plasma membranes. The Journal of biological chemistry *284*, 22978-22987.

Caterina, M.J., Rosen, T.A., Tominaga, M., Brake, A.J., and Julius, D. (1999). A capsaicin-receptor homologue with a high threshold for noxious heat. Nature *398*, 436-441.

Chalfie, M. (2009). Neurosensory mechanotransduction. Nat Rev Mol Cell Biol *10*, 44-52.

Chatterjee, S., and Mayor, S. (2001). The GPI-anchor and protein sorting. Cell Mol Life Sci *58*, 1969-1987.

Chen, Z.Y., He, C.Y., Ehrhardt, A., and Kay, M.A. (2003). Minicircle DNA vectors devoid of bacterial DNA result in persistent and high-level transgene expression in vivo. Mol Ther *8*, 495-500.

Cherny, V.V., Henderson, L.M., and DeCoursey, T.E. (1997). Proton and chloride currents in Chinese hamster ovary cells. Membr Cell Biol *11*, 337-347.

Chubanov, V., Waldegger, S., Mederos y Schnitzler, M., Vitzthum, H., Sassen, M.C., Seyberth, H.W., Konrad, M., and Gudermann, T. (2004). Disruption of TRPM6/TRPM7 complex formation by a mutation in the TRPM6 gene causes hypomagnesemia with

secondary hypocalcemia. Proceedings of the National Academy of Sciences of the United States of America *101*, 2894-2899.

Corey, D., Garcia-Anoveros, J., Holt, J., Kwan, K., Lin, S., Vollrath, M., Amalfitano, A., Cheung, E., Derfler, B., Duggan, A.*, et al.* (2004). TRPA1 is a candidate for the mechanosensitive transduction channel of vertebrate hair cells. Nature *432*, 723-730.

Corey, D.P. (2006). What is the hair cell transduction channel? The Journal of physiology *576*, 23-28.

Corey, D.P., and Hudspeth, A.J. (1979a). Ionic basis of the receptor potential in a vertebrate hair cell. Nature *281*, 675-677.

Corey, D.P., and Hudspeth, A.J. (1979b). Response latency of vertebrate hair cells. Biophys. J. *26*, 499-506.

Cremesti, A., Paris, F., Grassme, H., Holler, N., Tschopp, J., Fuks, Z., Gulbins, E., and Kolesnick, R. (2001). Ceramide enables fas to cap and kill. The Journal of biological chemistry *276*, 23954-23961.

Cueva, J., Mulholland, A., and Goodman, M. (2007). Nanoscale organization of the MEC-4 DEG/ENaC sensory mechanotransduction channel in Caenorhabditis elegans touch receptor neurons. J Neurosci *27*, 14089-14098.

Dalluge, R., Haberland, A., Zaitsev, S., Schneider, M., Zastrow, H., Sukhorukov, G., and Bottger, M. (2002). Characterization of structure and mechanism of transfection-active peptide-DNA complexes. Biochimica et biophysica acta *1576*, 45-52.

Dazert, S., Aletsee, C., Brors, D., Gravel, C., Sendtner, M., and Ryan, A. (2001). In vivo adenoviral transduction of the neonatal rat cochlea and middle ear. Hearing research *151*, 30-40.

Denk, W., Holt, J.R., Shepherd, G.M., and Corey, D.P. (1995). Calcium imaging of single stereocilia in hair cells: localization of transduction channels at both ends of tip links. Neuron *15*, 1311-1321.

Diebold, S., Cotten, M., Koch, N., and Zenke, M. (2001). MHC class II presentation of endogenously expressed antigens by transfected dendritic cells. Gene Ther *8*, 487-493.

Dietrich, A., Kalwa, H., Fuchs, B., Grimminger, F., Weissmann, N., and Gudermann, T. (2007). In vivo TRPC functions in the cardiopulmonary vasculature. Cell Calcium *42*, 233-244.

Driver, E., and Kelley, M. (2010). Transfection of mouse cochlear explants by electroporation. Curr Protoc Neurosci *Chapter 4*, Unit 4.34.31-10.

Dumont, R.A., Lins, U., Filoteo, A.G., Penniston, J.T., Kachar, B., and Gillespie, P.G. (2001). Plasma membrane Ca2+-ATPase isoform 2a is the PMCA of hair bundles. J Neurosci *21*, 5066-5078.

Eatock, R.A., Corey, D.P., and Hudspeth, A.J. (1987). Adaptation of mechanoelectrical transduction in hair cells of the bullfrog's sacculus. J. Neurosci. *7*, 2821-2836.

Eberl, D.F., Duyk, G.M., and Perrimon, N. (1997). A genetic screen for mutations that disrupt an auditory response in Drosophila melanogaster. Proceedings of the National Academy of Sciences of the United States of America *94*, 14837-14842.

Edidin, M. (2003). The state of lipid rafts: from model membranes to cells. Annu. Rev. Biophys. Biomol. Struct. *32*, 257-283.

Fain, G.L. (2003). Sensory Transduction (Sunderland, MA: Sinauer).

Farooqi, A.A., Javeed, M.K., Javed, Z., Riaz, A.M., Mukhtar, S., Minhaj, S., Abbas, S., and Bhatti, S. (2011). TRPM channels: same ballpark, different players, and different rules in immunogenetics. Immunogenetics *63*, 773-787.

Farris, H., LeBlanc, C., Goswami, J., and Ricci, A. (2004). Probing the pore of the auditory hair cell mechanotransducer channel in turtle. The Journal of physiology *558*, 769-792.

Fehon, R., McClatchey, A., and Bretscher, A. (2010). Organizing the cell cortex: the role of ERM proteins. Nat Rev Mol Cell Biol *11*, 276-287.

Feigenson, G.W. (2007). Phase boundaries and biological membranes. Annu Rev Biophys Biomol Struct *36*, 63-77.

Feigenson, G.W., and Buboltz, J.T. (2001). Ternary phase diagram of dipalmitoyl-PC/dilauroyl-PC/cholesterol: nanoscopic domain formation driven by cholesterol. Biophysical journal *80*, 2775-2788.

Ferraretto, A., Pitto, M., Palestini, P., and Masserini, M. (1997). Lipid domains in the membrane: thermotropic properties of sphingomyelin vesicles containing GM1 ganglioside and cholesterol. Biochemistry *36*, 9232-9236.

Finsinger, D., Remy, J., Erbacher, P., Koch, C., and Plank, C. (2000). Protective copolymers for nonviral gene vectors: synthesis, vector characterization and application in gene delivery. Gene Ther *7*, 1183-1192.

Fleig, A., and Penner, R. (2004). The TRPM ion channel subfamily: molecular, biophysical and functional features. Trends Pharmacol Sci *25*, 633-639.

Fonfria, E., Murdock, P.R., Cusdin, F.S., Benham, C.D., Kelsell, R.E., and McNulty, S. (2006). Tissue distribution profiles of the human TRPM cation channel family. J Recept Signal Transduct Res *26*, 159-178.

Forge, A. (1991). Structural features of the lateral walls in mammalian cochlear outer hair cells. Cell Tissue Res *265*, 473-483.

Fra, A., Williamson, E., Simons, K., and Parton, R. (1994). Detergent-insoluble glycolipid microdomains in lymphocytes in the absence of caveolae. The Journal of biological chemistry *269*, 30745-30748.

Friedman, L.M., Dror, A.A., and Avraham, K.B. (2007). Mouse models to study inner ear development and hereditary hearing loss. Int J Dev Biol *51*, 609-631.

Fujiwara, Y., and Minor, D.L., Jr. (2008). X-ray crystal structure of a TRPM assembly domain reveals an antiparallel four-stranded coiled-coil. J Mol Biol *383*, 854-870.

Furness, D.N., and Hackney, C.M. (1985). Cross-links between stereocilia in the guinea pig cochlea. Hearing Res. *18*, 177-188.

Gaus, K., Gratton, E., Kable, E.P., Jones, A.S., Gelissen, I., Kritharides, L., and Jessup, W. (2003). Visualizing lipid structure and raft domains in living cells with two-photon microscopy. Proceedings of the National Academy of Sciences of the United States of America *100*, 15554-15559.

Gillespie, P., and Müller, U. (2009). Mechanotransduction by hair cells: models, molecules, and mechanisms. Cell *139*, 33-44.

Gillespie, P.G., and Hudspeth, A.J. (1991). High-purity isolation of bullfrog hair bundles and subcellular and topological localization of constituent proteins. The Journal of cell biology *112*, 625-640.

Gomez-Mouton, C., Abad, J.L., Mira, E., Lacalle, R.A., Gallardo, E., Jimenez-Baranda, S., Illa, I., Bernad, A., Manes, S., and Martinez, A.C. (2001). Segregation of leading-edge and uropod components into specific lipid rafts during T cell polarization. Proceedings of the National Academy of Sciences of the United States of America *98*, 9642-9647.

Gong, Z., Son, W., Chung, Y., Kim, J., Shin, D., McClung, C., Lee, Y., Lee, H., Chang, D., Kaang, B.*, et al.* (2004). Two interdependent TRPV channel subunits, inactive and Nanchung, mediate hearing in Drosophila. J Neurosci *24*, 9059-9066.

Goodyear, R., Gale, J., Ranatunga, K., Kros, C., and Richardson, G. (2008). Aminoglycoside-induced phosphatidylserine externalization in sensory hair cells is regionally restricted, rapid, and reversible. J Neurosci *28*, 9939-9952.

Goodyear, R., Legan, P., Wright, M., Marcotti, W., Oganesian, A., Coats, S., Booth, C., Kros, C., Seifert, R., Bowen-Pope, D., and Richardson, G. (2003). A receptor-like inositol lipid phosphatase is required for the maturation of developing cochlear hair bundles. J. Neurosci. *23*, 9208-9219.

Granato, M., van Eeden, F.J., Schach, U., Trowe, T., Brand, M., Furutani-Seiki, M., Haffter, P., Hammerschmidt, M., Heisenberg, C.P., Jiang, Y.J.*, et al.* (1996). Genes controlling and mediating locomotion behavior of the zebrafish embryo and larva. Development *123*, 399-413.

Grillet, N., Xiong, W., Reynolds, A., Kazmierczak, P., Sato, T., Lillo, C., Dumont, R., Hintermann, E., Sczaniecka, A., Schwander, M*., et al.* (2009). Harmonin mutations cause mechanotransduction defects in cochlear hair cells. Neuron *62*, 375-387.

Gubbels, S., Woessner, D., Mitchell, J., Ricci, A., and Brigande, J. (2008). Functional auditory hair cells produced in the mammalian cochlea by in utero gene transfer. Nature *455*, 537-541.

Hakomori, S. (2004). Glycosynapses: microdomains controlling carbohydrate-dependent cell adhesion and signaling. An Acad Bras Cienc *76*, 553-572.

Hanono, A., Garbett, D., Reczek, D., Chambers, D., and Bretscher, A. (2006). EPI64 regulates microvillar subdomains and structure. The Journal of cell biology *175*, 803-813.

Harder, T., Scheiffele, P., Verkade, P., and Simons, K. (1998). Lipid domain structure of the plasma membrane revealed by patching of membrane components. The Journal of cell biology *141*, 929-942.

Hart, A.C., Sims, S., and Kaplan, J.M. (1995). Synaptic code for sensory modalities revealed by C. elegans GLR-1 glutamate receptor. Nature *378*, 82-85.

Hasson, T., Gillespie, P.G., Garcia, J.A., MacDonald, R.B., Zhao, Y., Yee, A.G., Mooseker, M.S., and Corey, D.P. (1997). Unconventional myosins in inner-ear sensory epithelia. J. Cell Biol. *137*, 1287-1307.

Hilgemann, D., Feng, S., and Nasuhoglu, C. (2001). The complex and intriguing lives of PIP_2 with ion channels and transporters. Sci. STKE *2001*, RE19.

Hill, J., Brett, C., Chyou, A., Kallay, L., Sakaguchi, M., Rao, R., and Gillespie, P. (2006a). Vestibular hair bundles control pH with (Na^+, K^+)/H^+ exchangers NHE6 and NHE9. J Neurosci *26*, 9944-9955.

Hill, J., Williams, D., LeMasurier, M., Dumont, R., Strehler, E., and Gillespie, P. (2006b). Splice-site A choice targets plasma-membrane Ca2+-ATPase isoform 2 to hair bundles. J Neurosci *26*, 6172-6180.

Hirono, M., Denis, C.S., Richardson, G.P., and Gillespie, P.G. (2004). Hair cells require phosphatidylinositol 4,5-bisphosphate for mechanical transduction and adaptation. Neuron *44*, 309-320.

Hojman, P., Gissel, H., Andre, F.M., Cournil-Henrionnet, C., Eriksen, J., Gehl, J., and Mir, L.M. (2008). Physiological effects of high- and low-voltage pulse combinations for gene electrotransfer in muscle. Hum Gene Ther *19*, 1249-1260.

Holopainen, J., Brockman, H., Brown, R., and Kinnunen, P. (2001). Interfacial interactions of ceramide with dimyristoylphosphatidylcholine: impact of the N-acyl chain. Biophysical journal *80*, 765-775.

Holt, J. (2002). Viral-mediated gene transfer to study the molecular physiology of the Mammalian inner ear. Audiol Neurootol *7*, 157-160.

Howard, J., and Hudspeth, A.J. (1988). Compliance of the hair bundle associated with gating of mechanoelectrical transduction channels in the bullfrog's saccular hair cell. Neuron *1*, 189-199.

Huang, M., Chen, Z., Hu, S., Jia, F., Li, Z., Hoyt, G., Robbins, R.C., Kay, M.A., and Wu, J.C. (2009). Novel minicircle vector for gene therapy in murine myocardial infarction. Circulation *120*, S230-237.

Huber, T.B., Schermer, B., Muller, R.U., Hohne, M., Bartram, M., Calixto, A., Hagmann, H., Reinhardt, C., Koos, F., Kunzelmann, K.*, et al.* (2006). Podocin and MEC-2 bind cholesterol to regulate the activity of associated ion channels. Proceedings of the National Academy of Sciences of the United States of America *103*, 17079-17086.

Hudspeth, A.J. (1989). How the ear's works work. Nature *341*, 397-404.

Hudspeth, A.J., and Jacobs, R. (1979). Stereocilia mediate transduction in vertebrate hair cells (auditory system/cilium/vestibular system). Proc. Natl. Acad. Sci. USA *76*, 1506-1509.

Ishimoto, S., Kawamoto, K., Kanzaki, S., and Raphael, Y. (2002). Gene transfer into supporting cells of the organ of Corti. Hearing research *173*, 187-197.

Jacobs, R.A., and Hudspeth, A.J. (1990). Ultrastructural correlates of mechanoelectrical transduction in hair cells of the bullfrog's internal ear. Cold Spring Harbor symposia on quantitative biology *55*, 547-561.

Jia, F., Wilson, K.D., Sun, N., Gupta, D.M., Huang, M., Li, Z., Panetta, N.J., Chen, Z.Y., Robbins, R.C., Kay, M.A.*, et al.* (2010). A nonviral minicircle vector for deriving human iPS cells. Nat Methods *7*, 197-199.

Jin, J., Desai, B.N., Navarro, B., Donovan, A., Andrews, N.C., and Clapham, D.E. (2008). Deletion of Trpm7 disrupts embryonic development and thymopoiesis without altering Mg2+ homeostasis. Science (New York, N.Y *322*, 756-760.

Jin, J., Wu, L.J., Jun, J., Cheng, X., Xu, H., Andrews, N.C., and Clapham, D.E. (2012). The channel kinase, TRPM7, is required for early embryonic development. Proceedings of the National Academy of Sciences of the United States of America *109*, E225-233.

Kachar, B., Battaglia, A., and Fex, J. (1997). Compartmentalized vesicular traffic around the hair cell cuticular plate. Hearing research *107*, 102-112.

Karavitaki, K.D., and Corey, D.P. (2010). Sliding adhesion confers coherent motion to hair cell stereocilia and parallel gating to transduction channels. J Neurosci *30*, 9051-9063.

Karra, D., and Dahm, R. (2010). Transfection techniques for neuronal cells. J Neurosci *30*, 6171-6177.

Kawashima, Y., Geleoc, G.S., Kurima, K., Labay, V., Lelli, A., Asai, Y., Makishima, T., Wu, D.K., Della Santina, C.C., Holt, J.R., and Griffith, A.J. (2011). Mechanotransduction in mouse inner ear hair cells requires transmembrane channel-like genes. J Clin Invest *121*, 4796-4809.

Kazmierczak, P., Sakaguchi, H., Tokita, J., Wilson-Kubalek, E., Milligan, R., Müller, U., and Kachar, B. (2007). Cadherin 23 and protocadherin 15 interact to form tip-link filaments in sensory hair cells. Nature *449*, 87-91.

Kellenberger, S., and Schild, L. (2002). Epithelial sodium channel/degenerin family of ion channels: a variety of functions for a shared structure. Physiol Rev *82*, 735-767.

Kelley, M.W., Ochiai, C.K., and Corwin, J.T. (1992). Maturation of kinocilia in amphibian hair cells: growth and shortening related to kinociliary bulb formation. Hearing research *59*, 108-115.

Kernan, M., Cowan, D., and Zuker, C. (1994). Genetic dissection of mechanosensory transduction: mechanoreception- defective mutations of Drosophila. Neuron *12*, 1195-1206.

Khan, S., Ahmed, Z., Shabbir, M., Kitajiri, S., Kalsoom, S., Tasneem, S., Shayiq, S., Ramesh, A., Srisailpathy, S., Khan, S*., et al.* (2007). Mutations of the RDX gene cause nonsyndromic hearing loss at the DFNB24 locus. Hum Mutat *28*, 417-423.

Kitajiri, S., Fukumoto, K., Hata, M., Sasaki, H., Katsuno, T., Nakagawa, T., Ito, J., Tsukita, S., and Tsukita, S. (2004). Radixin deficiency causes deafness associated with progressive degeneration of cochlear stereocilia. The Journal of cell biology *166*, 559-570.

Klausner, R., Kleinfeld, A., Hoover, R., and Karnovsky, M. (1980). Lipid domains in membranes. Evidence derived from structural perturbations induced by free fatty acids and lifetime heterogeneity analysis. The Journal of biological chemistry *255*, 1286-1295.

Klimaschewski, L., Nindl, W., Pimpl, M., Waltinger, P., and Pfaller, K. (2002). Biolistic transfection and morphological analysis of cultured sympathetic neurons. J Neurosci Methods *113*, 63-71.

Konyakhina, T.M., Goh, S.L., Amazon, J., Heberle, F.A., Wu, J., and Feigenson, G.W. (2011). Control of a nanoscopic-to-macroscopic transition: modulated phases in four-component DSPC/DOPC/POPC/Chol giant unilamellar vesicles. Biophysical journal *101*, L8-10.

Kozak, J.A., and Cahalan, M.D. (2003). MIC channels are inhibited by internal divalent cations but not ATP. Biophysical journal *84*, 922-927.

Krapivinsky, G., Mochida, S., Krapivinsky, L., Cibulsky, S.M., and Clapham, D.E. (2006). The TRPM7 ion channel functions in cholinergic synaptic vesicles and affects transmitter release. Neuron *52*, 485-496.

Kung, C., Martinac, B., and Sukharev, S. (2010). Mechanosensitive channels in microbes. Annu Rev Microbiol *64*, 313-329.

Kurzchalia, T.V., and Parton, R.G. (1999). Membrane microdomains and caveolae. Current opinion in cell biology *11*, 424-431.

Kuziemko, G., Stroh, M., and Stevens, R. (1996). Cholera toxin binding affinity and specificity for gangliosides determined by surface plasmon resonance. Biochemistry *35*, 6375-6384.

Kwan, K., Allchorne, A., Vollrath, M., Christensen, A., Zhang, D., Woolf, C., and Corey, D. (2006). TRPA1 contributes to cold, mechanical, and chemical nociception but is not essential for hair-cell transduction. Neuron *50*, 277-289.

Lajoie, P., Goetz, J.G., Dennis, J.W., and Nabi, I.R. (2009). Lattices, rafts, and scaffolds: domain regulation of receptor signaling at the plasma membrane. The Journal of cell biology *185*, 381-385.

Lelli, A., Asai, Y., Forge, A., Holt, J., and Geleoc, G. (2009). Tonotopic gradient in the developmental acquisition of sensory transduction in outer hair cells of the mouse cochlea. J Neurophysiol *101*, 2961-2973.

Li, M., Jiang, J., and Yue, L. (2006). Functional characterization of homo- and heteromeric channel kinases TRPM6 and TRPM7. J Gen Physiol *127*, 525-537.

Liebisch, G., Binder, M., Schifferer, R., Langmann, T., Schulz, B., and Schmitz, G. (2006). High throughput quantification of cholesterol and cholesteryl ester by electrospray ionization tandem mass spectrometry (ESI-MS/MS). Biochimica et biophysica acta *1761*, 121-128.

Liedtke, W., Tobin, D.M., Bargmann, C.I., and Friedman, J.M. (2003). Mammalian TRPV4 (VR-OAC) directs behavioral responses to osmotic and mechanical stimuli in Caenorhabditis elegans. Proceedings of the National Academy of Sciences of the United States of America *100 Suppl 2*, 14531-14536.

Lingwood, D., Ries, J., Schwille, P., and Simons, K. (2008). Plasma membranes are poised for activation of raft phase coalescence at physiological temperature. Proceedings of the National Academy of Sciences of the United States of America *105*, 10005-10010.

Liu, Y., Okada, T., Sheykholeslami, K., Shimazaki, K., Nomoto, T., Muramatsu, S., Kanazawa, T., Takeuchi, K., Ajalli, R., Mizukami, H.*, et al.* (2005). Specific and efficient transduction of Cochlear inner hair cells with recombinant adeno-associated virus type 3 vector. Mol Ther *12*, 725-733.

Lu, Y., Xiong, X., Helm, A., Kimani, K., Bragin, A., and Skach, W.R. (1998). Co- and posttranslational translocation mechanisms direct cystic fibrosis transmembrane conductance regulator N terminus transmembrane assembly. The Journal of biological chemistry *273*, 568-576.

Luebke, A., Foster, P., Muller, C., and Peel, A. (2001). Cochlear function and transgene expression in the guinea pig cochlea, using adenovirus- and adeno-associated virus-directed gene transfer. Hum Gene Ther *12*, 773-781.

Lumpkin, E.A., and Hudspeth, A.J. (1998). Regulation of free Ca^{2+} concentration in hair-cell stereocilia. J. Neurosci. *18*, 6300-6318.

Ma, B., Zhang, S., Jiang, H., Zhao, B., and Lv, H. (2007). Lipoplex morphologies and their influences on transfection efficiency in gene delivery. J Control Release *123*, 184-194.

Marmo, F., Balsamo, G., and Franco, E. (1983). Calcite in the statoconia of amphibians: a detailed analysis in the frog Rana esculenta. Cell Tissue Res *233*, 35-43.

Masserini, M., and Ravasi, D. (2001). Role of sphingolipids in the biogenesis of membrane domains. Biochimica et biophysica acta *1532*, 149-161.

McLaughlin, S., Wang, J., Gambhir, A., and Murray, D. (2002). PIP(2) and proteins: interactions, organization, and information flow. Annu. Rev. Biophys. Biomol. Struct. *31*, 151-175.

Meyers, J., MacDonald, R., Duggan, A., Lenzi, D., Standaert, D., Corwin, J., and Corey, D. (2003). Lighting up the senses: FM1-43 loading of sensory cells through nonselective ion channels. J Neurosci *23*, 4054-4065.

Micheva, K.D., Holz, R.W., and Smith, S.J. (2001). Regulation of presynaptic phosphatidylinositol 4,5-biphosphate by neuronal activity. The Journal of cell biology *154*, 355-368.

Montcouquiol, M., Rachel, R.A., Lanford, P.J., Copeland, N.G., Jenkins, N.A., and Kelley, M.W. (2003). Identification of Vangl2 and Scrb1 as planar polarity genes in mammals. Nature *423*, 173-177.

Mossman, K.D., Campi, G., Groves, J.T., and Dustin, M.L. (2005). Altered TCR signaling from geometrically repatterned immunological synapses. Science (New York, N.Y *310*, 1191-1193.

Neisch, A., and Fehon, R. (2011). Ezrin, Radixin and Moesin: key regulators of membrane-cortex interactions and signaling. Current opinion in cell biology *23*, 377-382.

Nicolson, T., Rusch, A., Friedrich, R., Granato, M., Ruppersberg, J., and Nusslein-Volhard, C. (1998). Genetic analysis of vertebrate sensory hair cell mechanosensation: the zebrafish circler mutants. Neuron *20*, 271-283.

Numata, T., and Okada, Y. (2008). Proton conductivity through the human TRPM7 channel and its molecular determinants. The Journal of biological chemistry *283*, 15097-15103.

O'Brien, J., Holt, M., Whiteside, G., Lummis, S., and Hastings, M. (2001). Modifications to the hand-held Gene Gun: improvements for in vitro biolistic transfection of organotypic neuronal tissue. J Neurosci Methods *112*, 57-64.

Oberwinkler, J., Lis, A., Giehl, K.M., Flockerzi, V., and Philipp, S.E. (2005). Alternative splicing switches the divalent cation selectivity of TRPM3 channels. The Journal of biological chemistry *280*, 22540-22548.

Oganesian, A., Poot, M., Daum, G., Coats, S., Wright, M., Seifert, R., and Bowen-Pope, D. (2003). Protein tyrosine phosphatase RQ is a phosphatidylinositol phosphatase that can regulate cell survival and proliferation. Proc. Natl. Acad. Sci. U S A *100*, 7563-7568.

Ogris, M., Steinlein, P., Kursa, M., Mechtler, K., Kircheis, R., and Wagner, E. (1998). The size of DNA/transferrin-PEI complexes is an important factor for gene expression in cultured cells. Gene Ther *5*, 1425-1433.

Ohmori, H. (1985). Mechano-electrical transduction currents in isolated vestibular hair cells of the chick. The Journal of physiology *359*, 189-217.

Pataky, F., Pironkova, R., and Hudspeth, A. (2004). Radixin is a constituent of stereocilia in hair cells. Proceedings of the National Academy of Sciences of the United States of America *101*, 2601-2606.

Petit, C. (2006). From deafness genes to hearing mechanisms: harmony and counterpoint. Trends Mol Med *12*, 57-64.

Prober, D.A., Zimmerman, S., Myers, B.R., McDermott, B.M., Jr., Kim, S.H., Caron, S., Rihel, J., Solnica-Krezel, L., Julius, D., Hudspeth, A.J., and Schier, A.F. (2008). Zebrafish TRPA1 channels are required for chemosensation but not for thermosensation or mechanosensory hair cell function. J Neurosci *28*, 10102-10110.

Rajendran, L., Masilamani, M., Solomon, S., Tikkanen, R., Stuermer, C.A., Plattner, H., and Illges, H. (2003). Asymmetric localization of flotillins/reggies in preassembled platforms confers inherent polarity to hematopoietic cells. Proceedings of the National Academy of Sciences of the United States of America *100*, 8241-8246.

Rajendran, L., and Simons, K. (2005). Lipid rafts and membrane dynamics. J Cell Sci *118*, 1099-1102.

Raju, P., McSloy, N., Truong, N., and Kendall, M. (2006). Assessment of epidermal cell viability by near infrared multi-photon microscopy following ballistic delivery of gold micro-particles. Vaccine *24*, 4644-4647.

Rauvala, H. (1979). Monomer-micelle transition of the ganglioside GM1 and the hydrolysis by Clostridium perfringens neuraminidase. European journal of biochemistry / FEBS *97*, 555-564.

Reczek, D., Berryman, M., and Bretscher, A. (1997). Identification of EBP50: A PDZ-containing phosphoprotein that associates with members of the ezrin-radixin-moesin family. The Journal of cell biology *139*, 169-179.

Reiners, J., Reidel, B., El-Amraoui, A., Boeda, B., Huber, I., Petit, C., and Wolfrum, U. (2003). Differential distribution of harmonin isoforms and their possible role in Usher-1 protein complexes in mammalian photoreceptor cells. Invest Ophthalmol Vis Sci *44*, 5006-5015.

Ricci, A., Crawford, A., and Fettiplace, R. (2003). Tonotopic variation in the conductance of the hair cell mechanotransducer channel. Neuron *40*, 983-990.

Ross, P., and Hui, S. (1999). Lipoplex size is a major determinant of in vitro lipofection efficiency. Gene Ther *6*, 651-659.

Runnels, L.W., Yue, L., and Clapham, D.E. (2001). TRP-PLIK, a bifunctional protein with kinase and ion channel activities. Science (New York, N.Y *291*, 1043-1047.

Runnels, L.W., Yue, L., and Clapham, D.E. (2002). The TRPM7 channel is inactivated by PIP(2) hydrolysis. Nat Cell Biol *4*, 329-336.

Ruvkun, G., and Hobert, O. (1998). The taxonomy of developmental control in Caenorhabditis elegans. Science (New York, N.Y *282*, 2033-2041.

Rzadzinska, A., Schneider, M., Davies, C., Riordan, G., and Kachar, B. (2004). An actin molecular treadmill and myosins maintain stereocilia functional architecture and self-renewal. J. Cell Biol. *164*, 887-897.

Sakaguchi, H., Tokita, J., Muller, U., and Kachar, B. (2009). Tip links in hair cells: molecular composition and role in hearing loss. Curr Opin Otolaryngol Head Neck Surg *17*, 388-393.

Sakaguchi, H., Tokita, J., Naoz, M., Bowen-Pope, D., Gov, N., and Kachar, B. (2008). Dynamic compartmentalization of protein tyrosine phosphatase receptor Q at the proximal end of stereocilia: implication of myosin VI-based transport. Cell motility and the cytoskeleton *65*, 528-538.

Sakaguchi, M. (2002). Autonomous and heteronomous positioning of transmembrane segments in multispanning membrane protein. Biochem Biophys Res Commun *296*, 1-4.

Sampaio, J., Gerl, M., Klose, C., Ejsing, C., Beug, H., Simons, K., and Shevchenko, A. (2011). Membrane lipidome of an epithelial cell line. Proceedings of the National Academy of Sciences of the United States of America *108*, 1903-1907.

Schlingmann, K.P., Weber, S., Peters, M., Niemann Nejsum, L., Vitzthum, H., Klingel, K., Kratz, M., Haddad, E., Ristoff, E., Dinour, D.*, et al.* (2002). Hypomagnesemia with secondary hypocalcemia is caused by mutations in TRPM6, a new member of the TRPM gene family. Nature genetics *31*, 166-170.

Selvaraj, V., Asano, A., Buttke, D.E., McElwee, J.L., Nelson, J.L., Wolff, C.A., Merdiushev, T., Fornes, M.W., Cohen, A.W., Lisanti, M.P.*, et al.* (2006). Segregation of micron-scale membrane sub-domains in live murine sperm. J Cell Physiol *206*, 636-646.

Seppala, S., Slusky, J.S., Lloris-Garcera, P., Rapp, M., and von Heijne, G. (2010). Control of membrane protein topology by a single C-terminal residue. Science (New York, N.Y *328*, 1698-1700.

Shi, X., and Nuttall, A. (2007). Expression of adhesion molecular proteins in the cochlear lateral wall of normal and PARP-1 mutant mice. Hearing research *224*, 1-14.

Shin, J.B., Martinez-Salgado, C., Heppenstall, P.A., and Lewin, G.R. (2003). A T-type calcium channel required for normal function of a mammalian mechanoreceptor. Nat Neurosci *6*, 724-730.

Shin, J.B., Streijger, F., Beynon, A., Peters, T., Gadzala, L., McMillen, D., Bystrom, C., Van der Zee, C.E., Wallimann, T., and Gillespie, P.G. (2007). Hair bundles are specialized for ATP delivery via creatine kinase. Neuron *53*, 371-386.

Shotwell, S., Jacobs, R., and Hudspeth, A. (1981). Directional sensitivity of individual vertebrate hair cells to controlled deflection of their hair bundles. Ann N Y Acad Sci *374*, 1-10.

Sidi, S., Friedrich, R., and Nicolson, T. (2003). NompC TRP channel required for vertebrate sensory hair cell mechanotransduction. Science (New York, N.Y *301*, 96-99.

Siemens, J., Kazmierczak, P., Reynolds, A., Sticker, M., Littlewood-Evans, A., and Müller, U. (2002). The Usher syndrome proteins cadherin 23 and harmonin form a complex by

means of PDZ-domain interactions. Proceedings of the National Academy of Sciences of the United States of America *99*, 14946-14951.

Siemens, J., Lillo, C., Dumont, R., Reynolds, A., Williams, D., Gillespie, P., and Müller, U. (2004). Cadherin 23 is a component of the tip link in hair-cell stereocilia. Nature *428*, 950-955.

Simons, K., and Sampaio, J. (2011). Membrane organization and lipid rafts. Cold Spring Harb Perspect Biol *3*, a004697.

Simons, K., and Toomre, D. (2000). Lipid rafts and signal transduction. Nat Rev Mol Cell Biol *1*, 31-39.

Simons, K., and Vaz, W.L. (2004). Model systems, lipid rafts, and cell membranes. Annu Rev Biophys Biomol Struct *33*, 269-295.

Singer, S., and Nicolson, G. (1972). The fluid mosaic model of the structure of cell membranes. Science (New York, N.Y *175*, 720-731.

Sonnino, S., Mauri, L., Chigorno, V., and Prinetti, A. (2007). Gangliosides as components of lipid membrane domains. Glycobiology *17*, 1R-13R.

Spinelli, K.J., Klimek, J.E., Wilmarth, P.A., Shin, J.B., Choi, D., David, L.L., and Gillespie, P.G. Distinct energy metabolism of auditory and vestibular sensory epithelia revealed by quantitative mass spectrometry using MS2 intensity.

Stapelbroek, J., Peters, T., van Beurden, D., Curfs, J., Joosten, A., Beynon, A., van Leeuwen, B., van der Velden, L., Bull, L., Oude Elferink, R.*, et al.* (2009). ATP8B1 is essential for maintaining normal hearing. Proceedings of the National Academy of Sciences of the United States of America *106*, 9709-9714.

Stroh, T., Erben, U., Kuhl, A.A., Zeitz, M., and Siegmund, B. (2010). Combined pulse electroporation--a novel strategy for highly efficient transfection of human and mouse cells. PLoS One *5*, e9488.

Takezawa, R., Schmitz, C., Demeuse, P., Scharenberg, A.M., Penner, R., and Fleig, A. (2004). Receptor-mediated regulation of the TRPM7 channel through its endogenous protein kinase domain. Proceedings of the National Academy of Sciences of the United States of America *101*, 6009-6014.

Thomas, J., Bardou, J., L'hoste, S., Mauchamp, B., and Chavancy, G. (2001). A helium burst biolistic device adapted to penetrate fragile insect tissues. Journal of insect science (Online) *1*, 9.

Tobin, D., Madsen, D., Kahn-Kirby, A., Peckol, E., Moulder, G., Barstead, R., Maricq, A., and Bargmann, C. (2002). Combinatorial expression of TRPV channel proteins defines their sensory functions and subcellular localization in C. elegans neurons. Neuron *35*, 307-318.

Tracey, W.D., Jr., Wilson, R.I., Laurent, G., and Benzer, S. (2003). painless, a Drosophila gene essential for nociception. Cell *113*, 261-273.

Trzeciakiewicz, A., Opolski, A., and Mazur, A. (2005). [TRPM7: a protein responsible for magnesium homeostasis in a cell]. Postepy Hig Med Dosw (Online) *59*, 496-502.

van Meer, G., Voelker, D.R., and Feigenson, G.W. (2008). Membrane lipids: where they are and how they behave. Nat Rev Mol Cell Biol *9*, 112-124.

Veatch, S.L., and Keller, S.L. (2003). Separation of liquid phases in giant vesicles of ternary mixtures of phospholipids and cholesterol. Biophysical journal *85*, 3074-3083.

Veatch, S.L., Polozov, I.V., Gawrisch, K., and Keller, S.L. (2004). Liquid domains in vesicles investigated by NMR and fluorescence microscopy. Biophysical journal *86*, 2910-2922.

Voets, T., Nilius, B., Hoefs, S., van der Kemp, A.W., Droogmans, G., Bindels, R.J., and Hoenderop, J.G. (2004). TRPM6 forms the Mg2+ influx channel involved in intestinal and renal Mg2+ absorption. The Journal of biological chemistry *279*, 19-25.

Walker, R.G., Willingham, A.T., and Zuker, C.S. (2000). A Drosophila mechanosensory transduction channel. Science (New York, N.Y *287*, 2229-2234.

Wang, H., Murphy, R., Taaffe, D., Yin, S., Xia, L., Hauswirth, W., Bance, M., Robertson, G., and Wang, J. (2011). Efficient cochlear gene transfection in guinea-pigs with adeno-associated viral vectors by partial digestion of round window membrane. Gene Ther.

Webb, S.W., Grillet, N., Andrade, L.R., Xiong, W., Swarthout, L., Della Santina, C.C., Kachar, B., and Muller, U. (2011). Regulation of PCDH15 function in mechanosensory hair cells by alternative splicing of the cytoplasmic domain. Development *138*, 1607-1617.

Woudenberg-Vrenken, T.E., Sukinta, A., van der Kemp, A.W., Bindels, R.J., and Hoenderop, J.G. (2011). Transient receptor potential melastatin 6 knockout mice are lethal whereas heterozygous deletion results in mild hypomagnesemia. Nephron Physiol *117*, p11-19.

Xing, Y., Gu, Y., Xu, L.C., Siedlecki, C.A., Donahue, H.J., and You, J. (2011). Effects of membrane cholesterol depletion and GPI-anchored protein reduction on osteoblastic mechanotransduction. J Cell Physiol *226*, 2350-2359.

Xiong, X., Bragin, A., Widdicombe, J.H., Cohn, J., and Skach, W.R. (1997). Structural cues involved in endoplasmic reticulum degradation of G85E and G91R mutant cystic fibrosis transmembrane conductance regulator. J Clin Invest *100*, 1079-1088.

Yamoah, E.N., Lumpkin, E.A., Dumont, R.A., Smith, P.J., Hudspeth, A.J., and Gillespie, P.G. (1998). Plasma membrane Ca2+-ATPase extrudes Ca2+ from hair cell stereocilia. J Neurosci *18*, 610-624.

Yockell-Lelievre, J., Riendeau, V., Gagnon, S.N., Garenc, C., and Audette, M. (2009). Efficient transfection of endothelial cells by a double-pulse electroporation method. DNA Cell Biol *28*, 561-566.

Yoshikawa, M., Go, S., Takasaki, K., Kakazu, Y., Ohashi, M., Nagafuku, M., Kabayama, K., Sekimoto, J., Suzuki, S., Takaiwa, K.*, et al.* (2009). Mice lacking ganglioside GM3 synthase exhibit complete hearing loss due to selective degeneration of the organ of Corti. Proceedings of the National Academy of Sciences of the United States of America *106*, 9483-9488.

Zheng, J., and Gao, W. (2000). Overexpression of Math1 induces robust production of extra hair cells in postnatal rat inner ears. Nat Neurosci *3*, 580-586.

Zhou, X.L., Batiza, A.F., Loukin, S.H., Palmer, C.P., Kung, C., and Saimi, Y. (2003). The transient receptor potential channel on the yeast vacuole is mechanosensitive. Proceedings of the National Academy of Sciences of the United States of America *100*, 7105-7110.

Zuidam, N., and Barenholz, Y. (1999). Characterization of DNA-lipid complexes commonly used for gene delivery. Int J Pharm *183*, 43-46.